Mathematical Models of Kidney Function: Effects of Hypertension and Circadian Rhythm

by

Kaixin Zheng

A thesis
presented to the University of Waterloo
in fulfillment of the
thesis requirement for the degree of
Master of Mathematics
in
Applied Mathematics

Waterloo, Ontario, Canada, 2024

© Kaixin Zheng 2024

Author's Declaration

I hereby declare that I am the sole author of this thesis. This is a true copy of the thesis, including any required final revisions, as accepted by my examiners.

I understand that my thesis may be made electronically available to the public.

Abstract

Hypertension induced by chronic angiotensin II (Ang II) infusion serves as a valuable experimental model for studying blood pressure regulation and the kidney's role in electrolyte and fluid homeostasis. The kidney's function is modulated by the renin-angiotensin-aldosterone system (RAAS) and circadian rhythms, with notable differences observed between males and females in the former. Under normotensive conditions, female rat nephrons exhibit lower Na^+/H^+ exchanger 3 (NHE3) activity in the proximal tubule but higher Na^+ transporter activities along distal segments compared to males. Chronic Ang II infusion reduces NHE3 activity, shifts Na^+ transport downstream, and promotes vasoconstriction, anti-natriuresis, and hypertension. These effects are further influenced by diurnal oscillations in glomerular filtration, electrolyte transport, and renal transporter regulation by circadian clock genes.

Using computational models of kidney function, this thesis explores two key areas: (i) the impact of Ang II infusion on segmental electrolyte transport and diuretic responses in male and female rat nephrons, and (ii) the influence of diurnal rhythms on the natriuretic and diuretic effects of loop, thiazide, and K^+-sparing diuretics under normotensive and hypertensive conditions in male rats. Simulations suggest that NHE3 downregulation in the proximal tubule is a primary driver of natriuresis and diuresis, with stronger effects in males. In hypertension, the downstream shift in Na^+ transport load amplifies the effects of diuretics, with hypertensive females exhibiting larger relative increases in Na^+ excretion due to their higher distal transport load. Additionally, diuretic responses vary by time of day, with qualitatively similar diurnal oscillations observed in normotensive and hypertensive kidneys. These findings provide insights into sex-specific and time-dependent responses to hypertension and diuretic therapies, emphasizing the need to consider both physiological context and administration timing in treatment strategies.

Acknowledgements

I would like to express my heartfelt gratitude to my supervisor, Dr. Anita Layton, for her unwavering support, insightful guidance, and for providing me with the opportunity to engage in meaningful research. Her mentorship has been invaluable throughout this journey. Dr. Layton is not only an exceptional researcher and responsible leader but also a supportive supervisor and a kind individual, and I am deeply appreciative of her influence on my academic growth.

I am also deeply grateful to my thesis committee members, Dr. Sue Ann Campbell and Dr. Matthew Scott, for their thoughtful reviews of my thesis and for attending my dissertation. Their insightful feedback has greatly enriched my work.

I would like to extend my thanks to my lab mates: Shervin Hakimi, Mehrshad Sadria, Dr. Pritha Dutta, Dr. Stéphanie Abo, Melissa Stadt, Christopher West, Dr. Belal Abuelnasr, Jessica Zhu, Bing Hu, Zaheer Mohideen, Dr. Gordon McNicol, and Matt Wiens for their kindness and support, especially during my early days in the lab. Their assistance and camaraderie have made a significant difference.

I would also like to express my appreciation to Dr. Mohammad Kohandel, Dr. Marek Stastna, Dr. Brian Ingalls, and Dr. Hans De Sterck for their invaluable support in helping me build a solid foundation through their courses on various topics.

Lastly, I am truly thankful to the many friends I made in the Applied Mathematics department, including Haocheng Chang, Dongze Li, Ruikun Zhou, Thanin Quartz and Zhexuan Zeng for their support during challenging times. Your encouragement kept me going when I needed it the most.

Dedication

This thesis is dedicated to my parents, Yijiao Bao and Qitian Zheng, who taught me the importance of education during my childhood. Their constant encouragement, unconditional love, and support have been the foundation of my journey.

Table of Contents

Author's Declaration ii

Abstract iii

Acknowledgements iv

Dedication v

List of Figures ix

List of Tables xiv

1 Physiology Background 1

1.1 Kidney Structure and Function 1

1.1.1 Kidney Anatomy 1

1.1.2 Nephron Structure 2

1.1.3 Epithelial Cell 4

1.1.4 Channels and Transporters 7

1.1.5 Diuresis, Natriuresis, and Kaliuresis 10

1.2 Motivation of Thesis 10

1.2.1 Hypertension-induced Renal Adaptations 10

1.2.2 Circadian Rhythm Modulation of Kidney Function 11

2 Mathematical Modeling of Water and Solutes Transport along the Nephron in a Mammalian Kidney **13**

2.1 Computational Cell: Overview . . . 13

2.2 Conservation in Cellular and Paracellular Compartments . . . 15

2.3 Conservation in the Lumen . . . 16

2.4 Flux Calculations . . . 17

2.4.1 Passive Fluxes . . . 17

2.4.2 Transporter-mediated Fluxes . . . 18

3 Sex Differences in Diuretic Response in Hypertension **20**

3.1 Method . . . 21

3.1.1 Model Structure . . . 21

3.1.2 Model Parameters for Hypertension . . . 21

3.1.3 Diuretics Simulations . . . 23

3.2 Baseline Results . . . 23

3.2.1 Hypertensive Effects . . . 23

3.2.2 NHE3 Downregulation in Hypertension . . . 26

3.3 Diuretics Administration Results . . . 29

3.3.1 Loop Diuretics . . . 29

3.3.2 Thiazide . . . 32

3.3.3 K^+-sparing Diuretics . . . 34

4 Circadian Effects on Renal Transporters in Hypertension **37**

4.1 Model Structures . . . 38

4.2 Results . . . 42

4.2.1 Diurnal Oscillations in Clock Gene and Transporter . . . 42

4.2.2 Bmal1-knockout Effects on Na^+ Transport and Excretion . . . 45

4.2.3 Transport and Excretions in Normotension and Hypertension . . . 48

4.2.4 Circadian Regulation of Diuretic Effects in Hypertension . . . 51

5 Conclusion **56**

5.1 Physiological Implications 56

5.1.1 Sex Differences in AngII-induced Hypertension 56

5.1.2 Circadian Regulation in a Hypertensive Rat Kidney 62

5.2 Limitations and Future Work 64

References **66**

A Equations and Parameters of Clock Gene and Transporter Expression **85**

A1 Governing Equations Overview 85

A2 mRNA equations 85

A3 Protein Equations 87

A4 Baseline parameters 89

List of Figures

1.1 Diagram of kidney anatomy. The figure is reproduced from [135]. 2

1.2 Schematic diagram showing a superficial nephron (right) and a juxtamedullary nephron (left). The figure is reproduced from [99]. 5

1.3 The structure of Bowman's capsule and the glomerular capillary tuft. The vascular pole, located on the left, contains the afferent and efferent arterioles, while the urinary pole on the right transitions to the proximal tubule. The figure is reproduced from [115]. 6

1.4 Schematic diagram of the epithelial cell in the proximal tubule (not all transporters are shown). The figure is adapted from [156], with added annotations. 8

2.1 The schematic diagram of the n-th computational cell on a specific segment of the nephron is shown, along with the computational cells before and after it. Compartments include cellular (C), paracellular (P), lumen (L), and blood (B). White arrows represent the fluxes of water or solutes, while the green arrow indicates the direction from the proximal tubule to the collecting duct. 14

3.1 Schematic diagram of a superficial nephron in a rat kidney, with its epithelial cell components. The model accounts for the transport of 15 solutes and water. The cell diagrams show primarily Na^+, K^+, and Cl^- transporters. PCT, proximal convoluted tubule; S3, proximal straight tubule; SDL, short descending limb; mTAL, medullary thick ascending limb; cTAL, cortical thick ascending limb; DCT, distal convoluted tubule; CNT, connecting tubule; CCD, cortical collecting duct; OMCD, outer medullary collecting duct; IMCD, inner medullary collecting duct. Up/down arrow indicates transporter upregulation/downregulation due to hypertension. Transporters not influenced are not shown. Adapted from Ref. [60]. 22

3.2 Segmental transport of Na^+, K^+, and water, obtained for the male and female models, under normotensive (NTN) and hypertensive (HTN) conditions. PT, proximal tubule; mTAL, medullary thick ascending limb; cTAL, cortical thick ascending limb; DCT, distal convoluted tubule; CNT, connecting tubule; CD, collecting duct. U_{Na}, Na^+ excretion; U_K, K^+ excretion; U_V, volume excretion. 27

3.3 Segmental delivery of Na^+, K^+, and water, obtained for the male and female models, under normotensive (NTN) and hypertensive (HTN) conditions. PT, proximal tubule; mTAL, medullary thick ascending limb; cTAL, cortical thick ascending limb; DCT, distal convoluted tubule; CNT, connecting tubule; CD, collecting duct. 28

3.4 Segmental transport of Na^+, K^+, and water, obtained for the male and female models, obtained for normotension (NTN), hypertension (HTN), and hypertension with proximal tubule NHE3 activity set to normotensive value (denoted PT NHE3→ NTN). PT, proximal tubule; mTAL, medullary thick ascending limb; cTAL, cortical thick ascending limb; DCT, distal convoluted tubule; CNT, connecting tubule; CD, collecting duct. U_{Na}, Na^+ excretion; U_K, K^+ excretion; U_V, volume excretion. 30

3.5 Segmental delivery of Na^+, K^+, and water, obtained for the male and female models, obtained for normotension (NTN), hypertension (HTN), and hypertension with proximal tubule NHE3 activity set to normotensive value (denoted PT NHE3→ NTN). PT, proximal tubule; mTAL, medullary thick ascending limb; cTAL, cortical thick ascending limb; DCT, distal convoluted tubule; CNT, connecting tubule; CD, collecting duct. 31

3.6 Segmental transport of Na^+, K^+, and water in male (A1-C1) and in female (A2-C2) for normotension (NTN), normotension with 70% NKCC2 inhibition (NTN+loop), hypertension (HTN), hypertension with 70% NKCC2 inhibition (HTN+loop). PT, proximal tubule; mTAL, medullary thick ascending limb; cTAL, cortical thick ascending limb; DCT, distal convoluted tubule; CNT, connecting tubule; CD, collecting duct. 33

3.7 Segmental transport of Na^+, K^+, and water in male (A1-C1) and in female (A2-C2) for normotension (NTN), normotension with 100% NCC inhibition (NTN+thiazide), hypertension (HTN), hypertension with 100% NCC inhibition (HTN+thiazide). DCT, distal convoluted tubule; CNT, connecting tubule; CD, collecting duct. 35

3.8 Segmental transport of Na^+, K^+, and water in male (A1-C1) and in female (A2-C2) for normotension (NTN), normotension with 100% ENaC inhibition (NTN+K^+-sparing), hypertension (HTN), hypertension with 100% ENaC inhibition (HTN+K^+-sparing). DCT, distal convoluted tubule; CNT, connecting tubule; CD, collecting duct. 36

4.1 Schematic network of our mathematical model, which describes the interactions of core clock components with key renal transporter genes. In the core clock network, mRNAs are denoted by blue boxes, proteins by red boxes, and protein complexes by yellow ovals. Solid lines represent the transactivation and dotted lines represent inhibition. The model nephron includes the proximal convoluted tubule (PCT), S3 segment, medullary thick ascending limb (mTAL), cortical thick ascending limb (cTAL), distal convoluted tubule (DCT), connecting tubule (CNT), cortical collecting duct (CCD), outer medullary collecting duct (OMCD), and inner medullary collecting duct (IMCD). Renal transporters that are regulated by the circadian clock include NHE3, SGLT1, NKCC2, NCC, and ENaC. 40

4.2 Comparison of simulated circadian gene and protein profiles with data from 46-hour experiments starting at ZT18 [167, 114]. **A1-A3, B1-B3**, simulated mRNA expression levels (Simulation) compared with experimental data (Experiment), normalized by mean experimental values; **C1, C2**, simulated concentrations of PER1–CRY1, PER1–CRY2, PER2–CRY1, and PER2–CRY2 protein complexes, normalized by their respective mean simulated values; **C3**, simulated BMAL1 mRNA expression levels (Bmal1, S), experimental BMAL1 mRNA levels (Bmal1, E), and normalized CLOCK–BMAL1 complex concentrations (CB). Gray shading and white regions correspond to dark and light phase, respectively. 43

4.3 Comparison of simulated transporter expression with corresponding experimental data. **A-D**, Transporter expression simulation (Simulation) and experimental profiles (Experiment) of NHE3, SGLT1, NCC, ENaC respectively. **E**, Simulation of NKCC2 expression in wild-type (WT, simulation) and corresponding experimental data at noon and midnight (WT, experiment). **F**, Simulation of NKCC2 expression after Bmal1 knockout (KO, simulation) with corresponding experimental data at noon and midnight (KO, experiment). Values are normalized by mean expression level in wild type. Gray shading and white regions correspond to the dark and light phases, respectively. 44

4.4 Comparison of model GFR and simulated transporter expression between wild type (WT) and conditional Bmal1 knockout (KO) male rat. (A): GFR is normalized by baseline GFR at ZT10 in the wild type; (B-F) simulated transporter expression levels are normalized by mean experimental values the same as in Fig. 4.3. Gray shading and white regions correspond to the dark and light phases, respectively. 46

4.5 Comparison of segmental Na^+ transport and urinary Na^+ in wild type (WT) and Bmal1 knockout (KO) male rats. PT, proximal tubule; TAL, thick ascending limb; DCT, distal convoluted tubule; CNT, connecting tubule; CD, collecting duct. T_{Na}, Na^+ transport; E_{Na}, excretion. 47

4.6 Na^+ inflow and Na^+, K^+, and water excretions. A, Estimated Na^+ inflow into the nephron for our model under both normotension and hypertension. B-D, Na^+, K^+, and water excretions under normotension (NTN) and hypertension (HTN). E_{Na}, Na^+ excretion; E_K, K^+ excretion; E_V, water excretion. 49

4.7 Comparison of segmental Na^+, K^+, and water transport under normotension (NTN) and hypertension (HTN). PT, proximal tubule; TAL, thick ascending limb; DCT, distal convoluted tubule; CNT, connecting tubule; CD, collecting duct. T_{Na}, Na^+ transport; T_K, K^+ transport; T_W, water transport. 50

4.8 Comparison of Na^+ transport and excretion, obtained for ZT4 and ZT16, in normotension (NTN), hypertension (HTN), hypertension with loop diuretic administration (HTN+loop), hypertension with thiazide administration (HTN+thiazide), and hypertension with K^+-spring administration (HTN+K^+-sparing). PT, proximal tubule; TAL, thick ascending limb; DCT, distal convoluted tubule; CNT, connecting tubule; CD, collecting duct. TNa, Na^+ transport; ENa, Na^+ excretion. 52

4.9 Comparison of K^+ transport and excretion, obtained for ZT4 and ZT16, in normotension (NTN), hypertension (HTN), hypertension with loop diuretic administration (HTN+loop), hypertension with thiazide administration (HTN+thiazide), and hypertension with K^+-spring administration (HTN+K^+-sparing). PT, proximal tubule; TAL, thick ascending limb; DCT, distal convoluted tubule; CNT, connecting tubule; CD, collecting duct. TK, K^+ transport; EK, K^+ excretion. 53

4.10 Comparison of water transport and excretion, obtained for ZT4 and ZT16, in normotension (NTN), hypertension (HTN), hypertension with loop diuretic administration (HTN+loop), hypertension with thiazide administration (HTN+thiazide), and hypertension with K^+-spring administration (HTN+K^+-sparing). PT, proximal tubule; TAL, thick ascending limb; DCT, distal convoluted tubule; CNT, connecting tubule; CD, collecting duct. TW, water transport; EW, water excretion. 54

5.1 Segmental delivery of Na^+, K^+, and water for normotension (NTN), normotension with 70% NKCC2 inhibition (NTN+loop), hypertension (HTN), hypertension with 70% NKCC2 inhibition (HTN+loop). PT, proximal tubule; mTAL, medullary thick ascending limb; cTAL, cortical thick ascending limb; DCT, distal convoluted tubule; CNT, connecting tubule; CD, collecting duct. 60

5.2 Segmental delivery of Na^+, K^+, and water for normotension (NTN), normotension with 100% NKCC2 inhibition (NTN+loop), hypertension (HTN), hypertension with 100% NKCC2 inhibition (HTN+loop). PT, proximal tubule; mTAL, medullary thick ascending limb; cTAL, cortical thick ascending limb; DCT, distal convoluted tubule; CNT, connecting tubule; CD, collecting duct. 61

List of Tables

3.1 Hypertensive model parameter adaptations. HTN, hypertension; NTN, normotension; NHE3, Na^+/H^+ exchanger isoform 3; ENaC, epithelial Na^+ channel; NKCC2, Na^+-K^+-$2Cl^-$ cotransporter 2 (A, B, F indicates isoform type); NCC, Na^+-Cl^- cotransporter; SGLT1, sodium-glucose cotransporter 1; SGLT2, sodium-glucose cotransporter 2; P_f , water permeability; P_{urea} , urea permeability. 24

4.1 Peak time and relative amplitude of predicted mRNA oscillations in the kidneys of wild-type normotensive male rats. Relative amplitude is calculated as (peak - trough)/mean. 55

A1 Degradation rates (in $hour^{-1}$) of protein complexes, mRNAs, and proteins . 89

A2 Activation ratios (dimensionless). 89

A3 Hill coefficients (dimensionless). 90

A4 Regulation thresholds (dimensionless). 91

A5 Association and dissociation rates (in $hour^{-1}$) for the protein complexes. . 92

A6 Translation rates (in $hour^{-1}$). 92

A7 Maximal transcription rates (in $hour^{-1}$). 92

Chapter 1

Physiology Background

The kidney is a complex organ that plays a vital role in critical physiological processes, including the regulation of water and solute homeostasis, as well as blood pressure control in mammals. Its ability to maintain electrolyte and fluid balance is significantly altered under hypertension [150]. Additionally, under either normotension [24] or hypertension [173], kidney function is modulated by circadian rhythms, which are governed by molecular-level periodic regulatory mechanisms. However, the interplay between kidney physiology, hypertension, and circadian rhythms has not been extensively studied using modeling approaches. In this chapter, we provide the necessary background on renal physiology to support our modeling studies, along with the motivations for conducting these researches.

1.1 Kidney Structure and Function

1.1.1 Kidney Anatomy

The kidneys are bean-shaped structures, characterized by a concave medial side and a convex lateral side. They are positioned retroperitoneally along the posterior abdominal wall.

As shown in Fig. 1.1, the kidney consists of two regions: the cortex and medulla. The cortex contains renal corpuscles, tubules, collecting ducts, and vasculature, while the medulla features straight tubules, collecting ducts, vasa recta, and pyramids [135]. Medullary rays, made up of straight tubules and collecting ducts, extend from the medulla into the cortex. Pyramids are cone-shaped structures with their base facing the cortex

and apices towards the hilum. The papillae at the pyramid tips drain into minor calyces through the area cribrosa. A lobule consists of a collecting duct and the nephrons it drains [98].

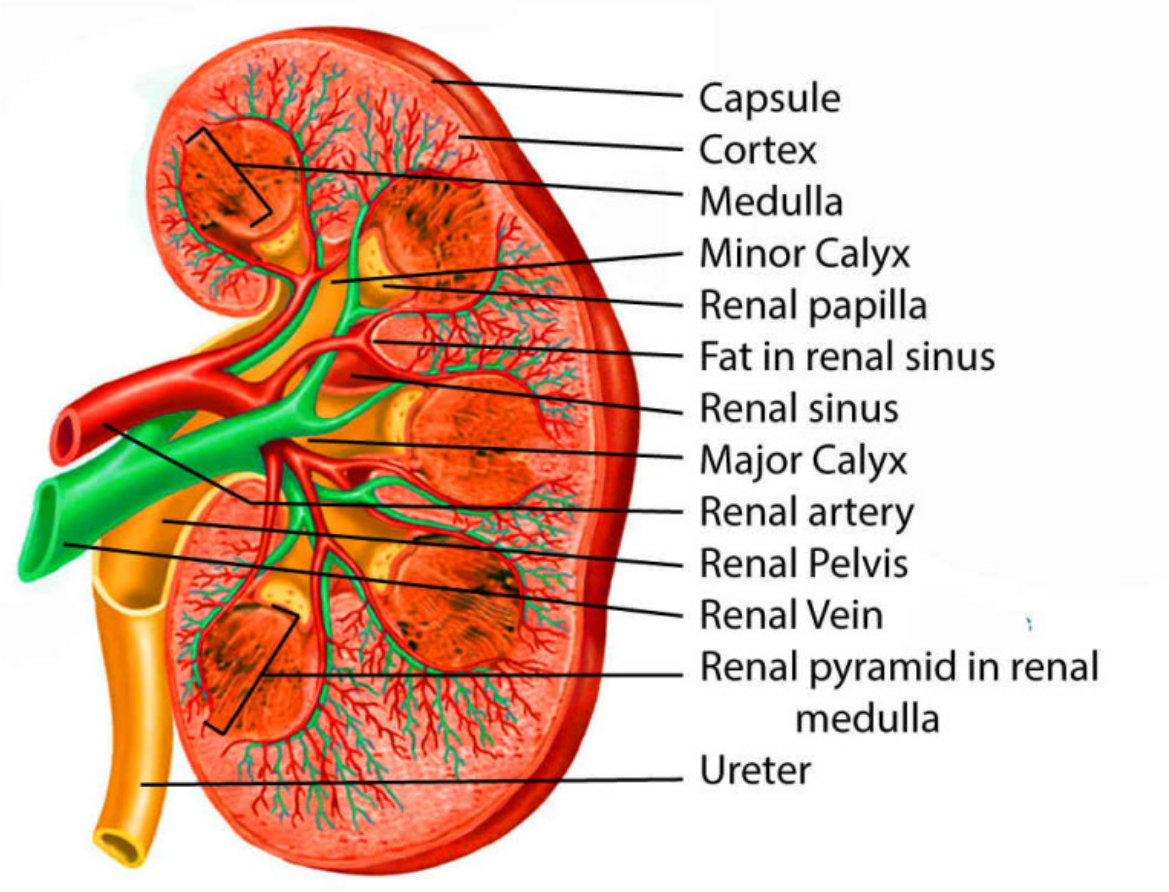


Figure 1.1: Diagram of kidney anatomy. The figure is reproduced from [135].

1.1.2 Nephron Structure

The nephron is the smallest functional unit of the kidney. It consists of a capsule, Bowman's capsule, and a curved tubule with distinct segments responsible for water and solute transport (see Fig. 1.2). Nephrons can be classified based on the length of the Loop of

Henle: superficial nephrons and juxtamedullary nephrons. The superficial nephron is located in the outer cortex and features a short loop of Henle that extends minimally into the medulla. In contrast, the juxtamedullary nephron is positioned near the cortex-medulla boundary and has a long loop of Henle that extends deep into the medulla, enabling efficient urine concentration [40]. Both nephrons include key structures: Bowman's capsule, proximal convoluted tubule, loop of Henle, distal convoluted tubule, and collecting duct.

As shown in Fig. 1.3, blood is filtered into the Bowman's capsule through the glomerular capillaries. The glomerulus, a network of tiny capillaries, receives blood from the afferent arteriole. Due to the high pressure within the glomerulus, small molecules such as water, electrolytes, and waste products are pushed through the filtration barrier. This barrier is formed by the podocytes of Bowman's capsule, whose foot processes create filtration slits, as well as the glomerular basement membrane (GBM) [50]. The filtered fluid then enters the Bowman's capsule, where it becomes the filtrate. The volume of filtrate produced by each nephron is referred to as the single-nephron glomerular filtration rate (SNGFR). The cumulative SNGFR of all nephrons in the kidney is known as the glomerular filtration rate (GFR), which is a key indicator of kidney function [26]. The filtrate then moves on to the proximal convoluted tubule for further processing

The proximal convoluted tubule (PCT) is the first segment of the nephron's tubular portion, located entirely in the cortex and serving as the longest segment of the nephron. Following the PCT, the proximal straight tubule (S3 segment) forms the second segment of the proximal tubule and extends into the medulla. Together, these two segments are referred to as the proximal tubule, which plays a critical role in reabsorbing the majority of sodium filtered by the glomerulus, thereby contributing significantly to the regulation of plasma volume and blood pressure [56].

Following the proximal tubule, the loop of Henle is the next segment of the nephron and plays a crucial role in establishing the kidney's osmotic gradient, essential for water and electrolyte balance. It consists of the descending thin limb, the thin ascending limb, and the thick ascending limb, each with distinct characteristics and functions [91]. The descending thin limb, located in the medulla, is highly permeable to water but not to solutes, facilitating passive water reabsorption and increasing the concentration of the tubular fluid as it descends into the medulla. In contrast, the ascending limb is mostly impermeable to water. The thin ascending limb allows passive solute reabsorption, while the thick ascending limb actively reabsorbs sodium, potassium, and chloride via the N^+-K^+-$2Cl^-$ cotransporter, accounting for approximately 20-25% of filtered sodium [16]. This active transport helps dilute the tubular fluid and contributes significantly to the medullary osmotic gradient [63]. A key distinction exists between superficial and juxtamedullary nephrons: superficial nephrons have shorter loops of Henle that remain in the outer medulla, limiting their

role in creating the osmotic gradient and urine concentration, whereas juxtamedullary nephrons possess long loops extending deep into the medulla. These longer loops amplify the osmotic gradient, making juxtamedullary nephrons essential for producing highly concentrated urine, especially under conditions of water conservation [28].

The subsequent segments are the distal convoluted tubule, the connecting tubule, and the collecting duct. The first two segments are located entirely in the cortex, while the collecting duct spans the cortex, outer medulla, and inner medulla [130]. Multiple connecting tubules converge into a single collecting duct, where the final stages of reabsorption occur, ultimately forming urine as it progresses toward the renal pelvis.

1.1.3 Epithelial Cell

Given the inflow filtration, water and solute transport within the nephron is determined by the cell-level structure of the nephron. The nephron is lined with epithelial cells connected by multiprotein junctional complexes, tight junctions [27]. The space inside the nephron is called the lumen. Luminal water and solute transport occurs through multiple mechanisms, which can be classified based on the pathway and energy usage:

- Classification based on pathway:
    1. **Transcellular Transport:** The water or solute transport occurs through the epithelial cell, crossing both the apical and basolateral membranes.
    2. **Paracellular Transport:** The water or solute transport occurs between epithelial cells, passing through the tight junctions.
- Classification based on energy usage:
    1. **Active Transport:** Active transport refers to the movement of water or solutes across cell membranes, often against their electrochemical or concentration gradients, and requires direct or indirect energy input. Specialized membrane proteins expressed on epithelial cells facilitate this process. For example, the Na^+-K^+-ATPase pump on the basolateral membrane uses adenosine triphosphate (ATP) to transport sodium ions (Na^+) out of the cell into the interstitial fluid and potassium ions (K^+) into the cell against the gradient [22]. However, in some cases, active transport can follow a gradient. For example, in the Na^+-K^+-Cl^- cotransporter, Na^+ is transported along its concentration gradient, which provides the driving force for the cotransport of K^+ and Cl^- against their respective gradients [93].

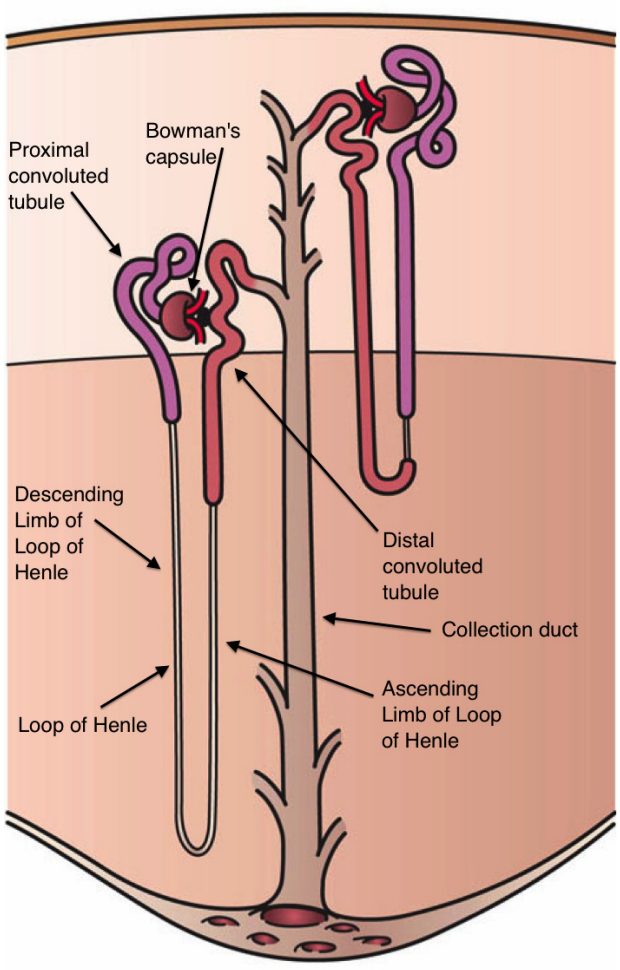


Figure 1.2: Schematic diagram showing a superficial nephron (right) and a juxtamedullary nephron (left). The figure is reproduced from [99].

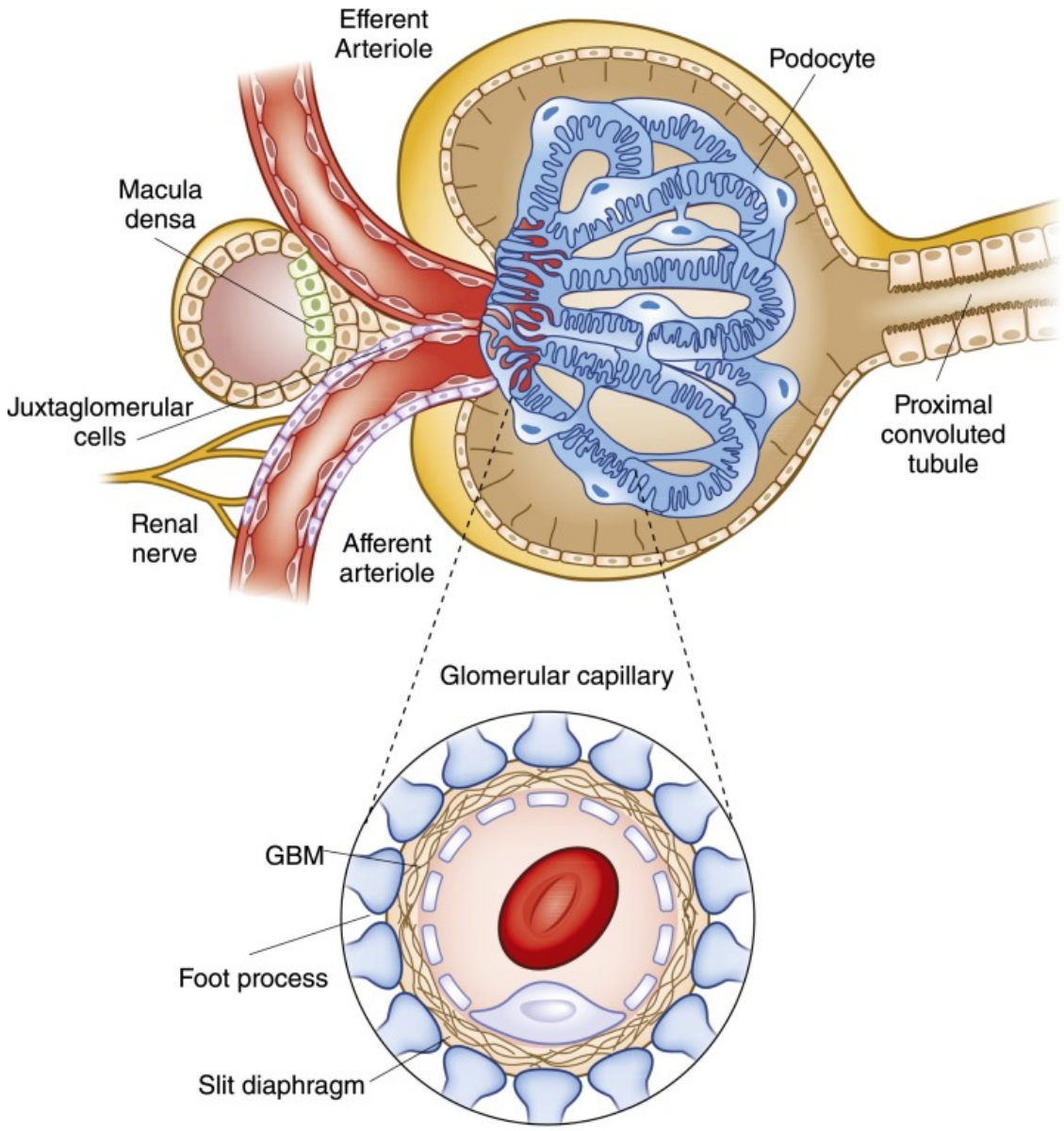


Figure 1.3: The structure of Bowman's capsule and the glomerular capillary tuft. The vascular pole, located on the left, contains the afferent and efferent arterioles, while the urinary pole on the right transitions to the proximal tubule. The figure is reproduced from [115].

2. **Passive Transport:** Transport that does not require direct energy input and occurs due to existing concentration or electrochemical gradients. In addition to paracellular transport due to tight junction permeability and osmotic gradient and concentration gradient, some proteins on epithilieal cell membrane is called channel, can assist passively transport solutes without directly using energy like ATP. For example, ENaC on the distal segments are vital for Na^+ reabsorption.

Take the epithelial cell in the proximal tubule as an example, as shown in Fig. 1.4. NHE3 on the apical membrane facilitates the active transport of Na^+ from the lumen into the cell, driven by the electrochemical gradient of Na^+, which is maintained by the Na^+-K^+-ATPase pump [46]. The Na^+-K^+-ATPase on the basolateral membrane uses ATP to actively transport Na^+ from the cell to the interstitial space, against both its concentration and electrochemical gradients. All paracellular transport through the tight junction is passive, as it occurs due to tight junction permeability and existing gradients [84].

1.1.4 Channels and Transporters

Channels and transporters are integral membrane proteins that facilitate water and solute movement across cell membranes. Channels enable passive transport driven by electrochemical gradients, while transporters mediate both passive and active transport. In the latter case, transporters often require energy input, such as ATP, to move solutes against their concentration gradient.

Adaptations of channels and transporters in the nephron are vital components of the studies presented in this thesis. In this chapter, we will discuss their importance and introduce key examples in detail.

Ion channels in the kidney play a critical role in regulating volume and ionic concentrations by facilitating the absorption or secretion of ions. Each nephron region expresses specific ion channels that ensure proper electrolyte balance. Mutations in these channels can result in renal diseases, including proteinuria, renal hypertension, and progressive loss of renal function [75]. Transporters, such as the Na^+-K^+-ATPase and sodium-glucose cotransporters (SGLTs), are essential for sodium reabsorption and maintaining electrolyte homeostasis, directly influencing blood pressure and volume [41]. Water reabsorption in the nephron depends on aquaporins and sodium-coupled transport mechanisms [69]. Aquaporins, such as AQP1 and AQP2, regulate transcellular water movement, which is vital for urine concentration and hydration.

Below, we introduce some of the important channels and transporters that are the focus of our studies in Chapters 3 and 4.

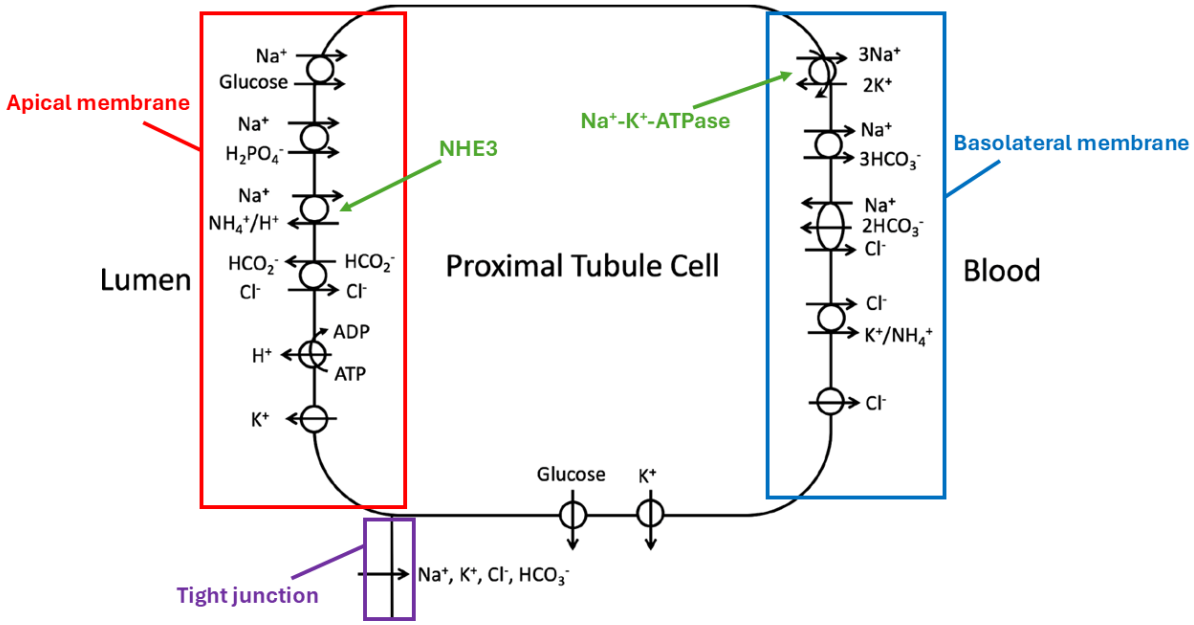


Figure 1.4: Schematic diagram of the epithelial cell in the proximal tubule (not all transporters are shown). The figure is adapted from [156], with added annotations.

1. **NHE3**

   The Na^+/H^+ exchanger 3 (NHE3) is a critical transporter involved in sodium absorption in the gastrointestinal tract and sodium reabsorption in the proximal tubule of the kidney. In the proximal tubule, NHE3 is responsible for reabsorbing more than 50% of the filtered sodium, highlighting its essential role in maintaining sodium and fluid balance, regulating blood pressure homeostasis, and contributing to the pathophysiology of hypertension [106]. Recent evidence identifies NHE3 activity as a key factor in the development of hypertension, particularly in salt-sensitive [49] and angiotensin II (Ang II)-induced [172] hypertension models.

2. **NKCC2**

   The apical Na^+-K^+-$2Cl^-$ cotransporter NKCC2 (SLC12A1) is essential for NaCl reabsorption in the thick ascending limb (TAL) of the loop of Henle. By facilitating the TAL's role in establishing a hyperosmotic renal medulla via the countercurrent multiplier mechanism, NKCC2 is integral to blood pressure regulation [14]. This importance is underscored by loss-of-function mutations in NKCC2, which cause Bartter syndrome in both mice [132] and humans [148]. Loop diuretics target NKCC2 by binding to its ion translocation pathway, effectively inhibiting ion reabsorption [88].

3. **Na^+-K^+-ATPase**

   The Na^+-K^+-ATPase pump is a fundamental transporter in kidney function, with particularly high expression in the distal convoluted tubule, where up to 50 million pumps are present per cell [113]. This pump establishes and maintains a sodium gradient critical for filtering waste products from the blood, reabsorbing essential nutrients such as amino acids and glucose, regulating electrolyte balance, and maintaining blood pH [36]. Its activity is essential for the kidney's critical processes, ensuring effective waste elimination and overall homeostasis.

4. **NCC**

   The sodium-chloride cotransporter (NCC) in the distal convoluted tubule (DCT) plays a critical role in regulating sodium and potassium balance. By controlling sodium delivery to downstream nephron segments, NCC indirectly modulates potassium secretion, ensuring overall potassium homeostasis and facilitating responses to dietary potassium intake [55]. NCC activity is tightly regulated by hormones such as aldosterone and angiotensin II (Ang II) [70]. Aldosterone enhances sodium reabsorption via NCC under conditions of low blood volume, while Ang II promotes NCC phosphorylation and activation, reinforcing its role in blood pressure regulation

[71]. Thiazide diuretics inhibit NCC by binding to an orthosteric site within the ion translocation pathway, locking the transporter in an outward-open conformation and blocking sodium and chloride reabsorption [170].

5. **ENaC**

   The epithelial sodium channel (ENaC) is a key channel for sodium transport in the kidney's collecting duct, playing a central role in maintaining sodium balance and fluid homeostasis. ENaC activity is regulated by multiple mechanisms, including proteolytic activation of its α and γ subunits, as well as ubiquitination and deubiquitination processes [48]. Aldosterone, a critical regulatory hormone, enhances ENaC activity by promoting its membrane insertion and reducing degradation through the action of serum- and glucocorticoid-regulated kinase 1 (SGK1) [90]. Dysregulation of ENaC is associated with conditions such as Liddle's syndrome and nephrotic syndrome [5], highlighting its importance in sodium-related disorders. K^+-sparing diuretics, including amiloride and triamterene, directly bind to the ENaC protein on the apical membrane of collecting duct cells [52]. By blocking the channel's pore, these diuretics prevent sodium ion entry, disrupting the sodium-driven electrochemical gradient that facilitates potassium secretion.

1.1.5 Diuresis, Natriuresis, and Kaliuresis

In this thesis, we will frequently use the terms diuresis, natriuresis, and kaliuresis to refer to the increased excretion of water, Na^+, and K^+, respectively, compared to baseline levels.

1.2 Motivation of Thesis

1.2.1 Hypertension-induced Renal Adaptations

The renin-angiotensin-aldosterone system (RAAS) plays a central role in maintaining blood volume, electrolyte balance, and vascular resistance, but its overactivation is a key driver of hypertension [111]. Chronic infusion of angiotensin II (AngII) is commonly used as a model for hypertension research, as it induces vasoconstriction, anti-natriuresis, and sustained increases in blood pressure [87, 105, 150]. On a molecular level, prolonged AngII infusion alters renal transporter expression, reducing levels of NHE3 and NKCC2 in certain nephron segments while increasing NCC and ENaC abundance in others [105, 150]. These

effects reflect AngII's complex regulatory impact on renal Na^+ transport, which varies significantly between males and females [149].

Research has shown that female rodents exhibit distinct transporter expression patterns compared to males, including increased NHE3 phosphorylation, altered transporter localization, and reduced NaPi2, AQP1, and claudin-2 in the proximal tubule, alongside greater NCC and ENaC abundance in more distal segments [149]. Functionally, males display a larger rise in blood pressure and proteinuria in response to AngII compared to females [165, 146]. However, the mechanisms driving these sex-specific differences in AngII's effects on renal transporters remain poorly understood.

Diuretics, a cornerstone of hypertension treatment, act on various nephron segments to inhibit specific Na^+ transporters, promoting natriuresis and diuresis [10, 76, 39]. The three main classes-loop diuretics, thiazides, and K^+-sparing diuretics—target different transporters, such as NKCC2, NCC, and ENaC, respectively, and are widely used for their effectiveness and safety [39, 117, 118, 13, 95]. However, how these therapies interact with sex-specific transporter expression patterns under AngII-induced hypertension is not well characterized.

To explore these interactions, in our paper [171], we developed a computational model of nephron epithelial transport that incorporate sex-specific differences in transporter patterns under chronic AngII infusion, which will be introduced in detail in Chapter 3. Our model aims to elucidate how sex differences influence renal responses to AngII and the natriuretic and diuretic effects of various diuretics, providing valuable insights for optimizing hypertension management tailored to individual physiological differences.

1.2.2 Circadian Rhythm Modulation of Kidney Function

The kidney plays a central role in regulating extracellular fluid and maintaining whole-body electrolyte homeostasis. It achieves this by adjusting the proportion of sodium (Na^+) reabsorbed from the glomerular filtrate to balance Na^+ intake and excretion in the urine. With the kidneys receiving 20-25% of cardiac output [100], the glomerular filtration rate (GFR) and the filtered Na^+ load are substantial, yet only about 1% of the filtered Na^+ is excreted in the urine under normal conditions [9]. This requires precise regulation of the renal transport system, with nearly all nephron segments contributing to Na^+ reabsorption.

In the proximal tubule, the Na^+/H^+ exchanger 3 (NHE3) mediates the reabsorption of 50%-70% of filtered Na^+ (with a higher proportion in male rodents) [29]. NHE3 is also integral to pressure natriuresis, wherein elevated blood pressure leads to increased Na^+ excretion [97]. Another major site of Na^+ reabsorption is the thick ascending limb,

where the Na^+-K^+-$2Cl^-$ cotransporter 2 (NKCC2) handles 25%-40% of Na^+ transport, with higher activity in females [16, 60]. Further downstream, Na^+-Cl^- cotransporters (NCC) in the distal convoluted tubule and epithelial Na^+ channels (ENaC) in the connecting tubule and collecting duct perform "fine-tuning" of urinary Na^+ excretion. The clinical relevance of these transporters is underscored by the widespread use of thiazide and K^+-sparing diuretics, which target NCC and ENaC, respectively, in hypertension treatment [89].

While the kidney is often described as maintaining homeostasis through feedback and adjustments, this perspective omits the dynamic nature of renal physiology. Like many other systems, the kidney exhibits circadian rhythms with a 24-hour cycle. These rhythms are governed by a central clock in the suprachiasmatic nucleus (SCN) of the hypothalamus and peripheral clocks within renal cells, which can operate independently of the SCN [54]. Both clocks rely on interactions among core clock genes [86, 162, 129]. Briefly, the CLOCK and BMAL1 proteins dimerize to induce the transcription of Period (Per) and Cryptochrome (Cry) genes, whose proteins, in turn, inhibit CLOCK-BMAL1 activity in a feedback loop. This oscillation drives circadian rhythms in kidney function, such as reduced nocturnal urine output in diurnal animals [42, 141]. Similar rhythmic patterns are observed in electrolyte excretion, renal plasma flow, and GFR. Clock proteins regulate key renal transporters, including NHE3, Na^+-glucose cotransporter 1 (SGLT1), NKCC2, NCC, and ENaC [42, 141].

Given the circadian variation in transporter expression, the effects of diuretics targeting NKCC2, NCC, and ENaC—used to manage hypertension—may also vary depending on the time of day [4]. To explore these dynamics, in our submitted paper, we employed the computational model of water and electrolyte transport in the nephrons of a male kidney, incorporating the circadian regulation of transporter activity. This model provides a platform to investigate how the timing of diuretic administration affects natriuretic and diuretic outcomes, which will be introduced in detail in Chapter 4.

Chapter 2

Mathematical Modeling of Water and Solutes Transport along the Nephron in a Mammalian Kidney

This chapter aims to introduce the baseline transport model in our Chapter 3 and Chapter 4 to simulate segmental transport of water and solutes along the nephron. The model is described in details in Refs. [82, 60, 83, 80, 79] and in particular, Ref. [77] has a complete set of equations of the computational model.

2.1 Computational Cell: Overview

The nephron is divided into individual computational cells. As shown in the schematic representations of nephron segments (Fig. 2.1), the four key compartments are illustrated: the lumen ("L") on bottom, blood ("B") on top, and the cellular ("C") denoted with blue boxes, and paracellular ("P") denoted with yellow boxes. The cellular and paracellular compartments represent the interior of the cell and the paracellular space, respectively. Each compartment within a computational cell can exchange water and solutes with other adjacent compartments.

Solute and water transport in the kidney typically operates under homeostasis—where water and solute distributions within the lumen rapidly reach a steady state compared to slower processes, such as AngII-induced transporter adjustments and circadian regulation. Therefore, epithelial transport is modeled as a steady-state problem. This modeling

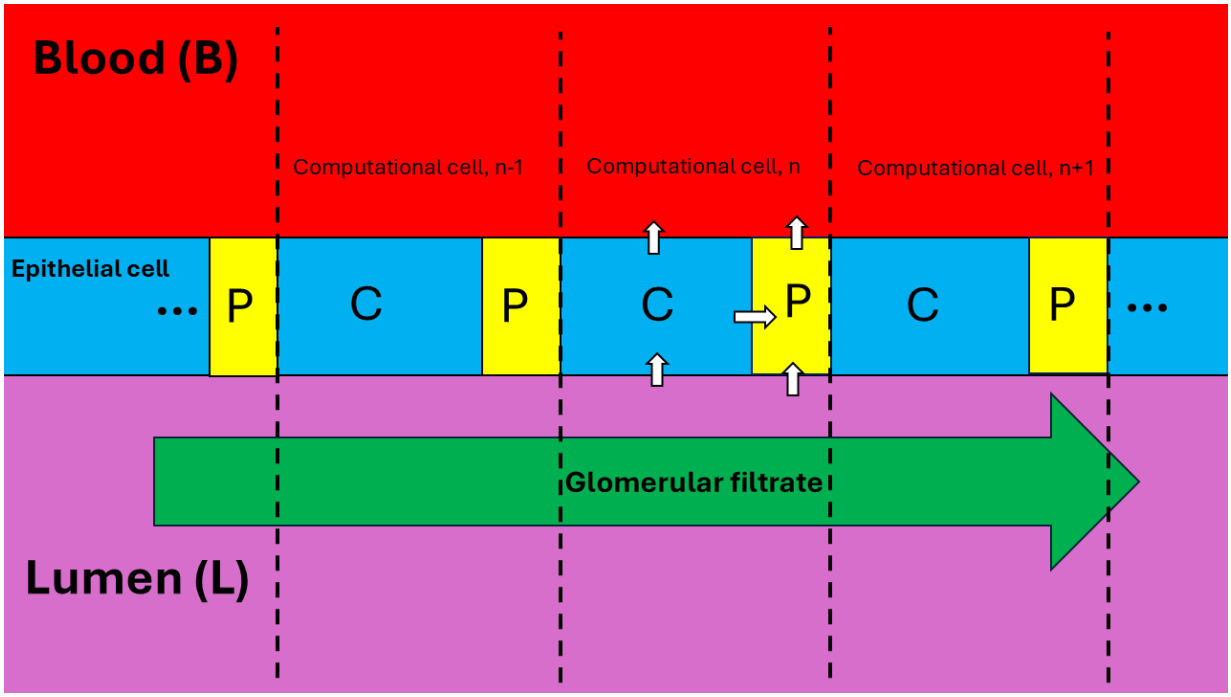


Figure 2.1: The schematic diagram of the n-th computational cell on a specific segment of the nephron is shown, along with the computational cells before and after it. Compartments include cellular (C), paracellular (P), lumen (L), and blood (B). White arrows represent the fluxes of water or solutes, while the green arrow indicates the direction from the proximal tubule to the collecting duct.

employs multiple conservation laws and specific transporter flux functions, complemented by equations accounting for physical factors like pressure and tubular dimensions. The problem is formulated as an optimization task to efficiently compute the steady-state distribution of water and solutes along the nephron, using an in-house optimization solver.

The remainder of this chapter introduces the key equations used for steady-state simulation. The notations, structure, and much of the detailed content in this section are based on the well-known and widely regarded model described in Ref. [77], which is a cornerstone in renal physiology modeling.

2.2 Conservation in Cellular and Paracellular Compartments

These cellular and paracellular compartments are assumed to be rigid, simplifying the conservation of water within them for each tubular segment i. Water flux between compartments is represented by $J^i_{v,ab}$, where positive values indicate transport from compartment a to compartment b.

The conservation of water within the cellular and paracellular compartments, respectively, is represented as

$$J^i_{v,LC} + J^i_{v,BC} + J^i_{v,PC} = 0 \tag{2.1}$$
$$J^i_{v,LP} + J^i_{v,BP} + J^i_{v,CP} = 0 \tag{2.2}$$

Analogously, for a non-reacting solute, k

$$J^i_{k,LC} + J^i_{k,BC} + J^i_{k,PC} = 0 \tag{2.3}$$
$$J^i_{k,LP} + J^i_{k,BP} + J^i_{k,CP} = 0 \tag{2.4}$$

For the reacting solutes, conservation is maintained for the total buffer

$$\hat{J}^i_{CO_2,m} + \hat{J}^i_{HCO_3^-,m} + \hat{J}^i_{H_2CO_3,m} = 0 \tag{2.5}$$
$$\hat{J}^i_{HCO_2^-,m} + \hat{J}^i_{H_2CO_2,m} = 0 \tag{2.6}$$
$$\hat{J}^i_{HPO_4^{2-},m} + \hat{J}^i_{H_2PO_4^-,m} = 0 \tag{2.7}$$
$$\hat{J}^i_{NH_3,m} + \hat{J}^i_{NH_4^+,m} = 0 \tag{2.8}$$

where $\hat{J}^i_{s,m}$ represents on the segment i, the gross fluxes of solute s into the compartment $m = P$ or C, i.e.

$$\hat{J}^i_{s,C} = J^i_{s,LC} + J^i_{s,BC} + J^i_{s,PC} \tag{2.9}$$

$$\hat{J}^i_{s,P} = J^i_{s,LP} + J^i_{s,BP} + J^i_{s,CP} \tag{2.10}$$

Each compartment m has conservation of H^+:

$$\sum_{k \in S_H} \hat{J}^i_{k,m} = 0 \tag{2.11}$$

where $S_H = \{H^+, NH_4^+, H_2PO_4^-, H_2CO_3, H_2CO_2\}$.

The buffer pairs are assumed to remain at equilibrium:

$$pH^i_m = pK_A - \log \frac{C^i_{A,m}}{C^i_{B,m}} \tag{2.12}$$

where buffer pair (A,B) are one of $(HCO_3^-, H_2CO_3), (HCO_2^-, H_2CO_2), (HPO_4^{2-}, H_2PO_4^-)$, and (NH_3, NH_4^+). pK_A is the negative logarithm of the acid dissociation constant, KA, of solute A. pH^i_m is pH of the compartment m.

2.3 Conservation in the Lumen

To reflect the physical reality that, as filtrate in the lumen moves forward, there are continuous water and solute fluxes between the lumen and cellular or transcellular compartments due to the mechanisms mentioned in Subsection 1.1.3—even at steady state—the conservation of luminal volume and solutes is reflected by equations follows:

$$\frac{dQ^i}{dx} = \hat{J}^i_{v,L} \tag{2.13}$$

$$\frac{d}{dx}(Q^i C^i_{k,L}) = \hat{J}^i_{k,L} \tag{2.14}$$

where $\hat{J}^i_{v,L} = J^i_{v,CL} + J^i_{v,PL}$ represents the gross volume flux into the lumen (primarily water reabsorption, which is negative along most parts of the nephron). $\hat{J}^i_{k,L}$ is the gross solute k flux into the lumen. Q^i denotes the volume flow, and $C^i_{k,L}$ is the concentration of solute k in the lumen of segment i.

Similar to Section 2.2, for reacting solutes in the lumen, we consider conservation of buffer pairs in equilibrium:

$$\frac{d}{dx}(Q^i(C^i_{CO_2,L} + C^i_{HCO_3^-,L} + C^i_{H_2CO_3,L})) = \hat{J}^i_{CO_2,L} + \hat{J}^i_{HCO_3^-,L} + \hat{J}^i_{H_2CO_3,L} \tag{2.15}$$

$$\frac{d}{dx}(Q^i(C^i_{HCO_2^-,L} + C^i_{H_2CO_2,L})) = \hat{J}^i_{HCO_2^-,L} + \hat{J}^i_{H_2CO_2,L} \tag{2.16}$$

$$\frac{d}{dx}(Q^i(C^i_{HPO_4^{2-},L} + C^i_{H_2PO_4^-,L})) = \hat{J}^i_{HPO_4^{2-},L} + \hat{J}^i_{H_2PO_4^-,L} \tag{2.17}$$

$$\frac{d}{dx}(Q^i(C^i_{NH_3,L} + C^i_{NH_4^+,L})) = \hat{J}^i_{NH_3,L} + \hat{J}^i_{NH_4^+,L} \tag{2.18}$$

2.4 Flux Calculations

2.4.1 Passive Fluxes

Though multiple mechanisms of water and solute exchange among lumen, epithelial cell, and interstitial space as discussed in Subsection 1.1.3 and in [81, 158, 92], we introduce three types of passive fluxes that occur without the involvement of any transporters:

1. **Volume fluxes calculated by Kedem-Katchalsky equation** [68]:

$$J^{i,ab}_v = \hat{A}^i_{ab} L^i_{p,ab} \left(\sigma^i_{ab} \Delta\pi^i_{ab} + \Delta P^i_{ab}\right) \tag{2.19}$$

   where $\hat{A}ab^i$ represents a scaling factor that defines the area available for transport between compartments a and b, Lp, ab^i denotes the hydraulic permeability, $\Delta\pi^i_{ab} = RT \sum \Delta C^i_{ab}$ represents the osmotic pressure gradient, RT is the product of the gas constant and the thermodynamic temperature, σ^i_{ab} is the reflection coefficient, and ΔP^i_{ab} signifies the hydrostatic pressure gradient.

2. **Transmembrane fluxes of uncharged solute, driven across a membrane passively by a chemical gradient**:

$$J^{i,ab}_k = \hat{A}^i_{ab} \rho^i_{k,ab} \left(C^i_{k,a} - C^i_{k,b}\right) \tag{2.20}$$

   where $\rho^i_{k,ab}$ denotes membrane permeability to solute k.

3. **Fluxes of charged particles, calculated using the Goldman-Hodgkin-Katz current equation**:

$$J_k^{i,ab} = \hat{A}_{ab}^i \rho_{k,ab}^i \frac{z_k F \Delta V_{ab}^i}{RT} \frac{C_{k,a}^i - C_{k,b}^i \exp\left(-z_k F \Delta V_{ab}^i / RT\right)}{1 - \exp\left(-z_k F \Delta V_{ab}^i / RT\right)} \tag{2.21}$$

where ΔV_{ab}^i represents the electrical potential gradient, z_k is the ion valence, and F denotes Faraday's constant. For ion channels that display circadian variations in expression (e.g., ENaC or ROMK), the channel permeability ($\rho_{k,ab}^i$) is modeled as time-dependent.

2.4.2 Transporter-mediated Fluxes

In this subsection, we present the flux of some key active Na^+ transporters in our baseline nephron model, providing the audience with an understanding of their typical forms and behavior.

1. **NHE3**

   NHE3 is located on the apical membrane of the proximal tubule (PT) and thick ascending limb (TAL). It moves Na^+ into the cell and transports H^+ and $NH_4{}^+$ out. The flux functions are derived in [157] and are represented below:

$$J_a = \frac{x_T T_a}{\Sigma}(T_b(\alpha^i\beta^e - \alpha^e\beta^i) + T_c(\alpha^i\gamma^e - \alpha^e\gamma i)) \tag{2.22}$$

$$J_b = \frac{x_T T_b}{\Sigma}(T_a(\beta^i\alpha^e - \beta^e\alpha^i) + T_c(\beta^i\gamma^e - \beta^e\gamma i)) \tag{2.23}$$

$$J_c = \frac{x_T T_c}{\Sigma}(T_a(\gamma^i\alpha^e - \gamma^e\alpha^i) + T_b(\gamma^i\beta^e - \gamma^e\beta i)) \tag{2.24}$$

$$\Sigma = (1 + \alpha^i + \beta^i + \gamma^i)(T_a\alpha^e + T_b\beta^e + T_c\gamma^e) + (T_a\alpha^i + T_b\beta^i + T_c\gamma^i)(1 + \alpha^e + \beta^e + \gamma^e) \tag{2.25}$$

   where x_T, T_a, T_b, and T_c are parameters. α^i, β^i, and β^i represents $[Na^+]$, $[H^+]$, and $[NH_4{}^+]$ in the cell, while α^e, β^e, and β^e represents $[Na^+]$, $[H^+]$, and $[NH_4{}^+]$ in the lumen.

2. **Na^+-K^+-ATPase**

   Na^+-K^+-ATPase is an active transporter located on the basolateral membrane of epithelial cells. Utilizing ATP, it drives Na^+ out of the cell and K^+ into the cell,

thereby maintaining essential ionic gradients. The pump operates with a precise stoichiometric ratio of 3 Na^+ efflux to 2 K^+ influx [112]. In our model, the functions of fluxes through the pump are based on the derivation in subsection 8.2.2 of [78], represented as:

$$J_{Na}^{NaK} = J_{Na}^{NaK,max}(\frac{C_{Na}^i}{C_{Na}^i + K_{Na}^i})^3(\frac{C_K^e}{C_K^e + K_K^e})^2 \tag{2.26}$$

$$J_K^{NaK} = -\frac{2}{3}J_{Na}^{NaK} \tag{2.27}$$

where J_{Na}^{NaK} and J_K^{NaK} are fluxes of Na^+ and K^+, respectively (out of cell is positive). C_s^i and C_s^e represent the concentration of solute s inside the cell and in the blood, respectively. $J_{Na}^{NaK,max}$, K_{Na}^i and K_K^e are parameters.

For transporters not mentioned, some, like the Na^+-K^+-$2Cl^-$ (NKCC2) and K^+-Cl^- (KCC) cotransporters of the thick ascending limb, are modeled similarly to NHE3 [78]. The remaining transporters, such as ENaC, are modeled as described in other references, including [18].

Chapter 3

Sex Differences in Diuretic Response in Hypertension

We conducted an investigation into the effects of chronic angiotensin II (AngII) infusion, a commonly used experimental model for hypertension in rodents. Male and female kidneys exhibit notable differences in their physiological responses to AngII-induced hypertension, stemming from inherent sex differences in renal structure and function. These differences influence key processes such as natriuresis, diuresis, and blood pressure regulation. To explore these dynamics, we developed sex-specific computational models of renal epithelial transport. In this chapter, we will describe the development of these models and their application in analyzing the impact of AngII-induced hypertension on segmental electrolyte transport. Additionally, we will examine predictions of the natriuretic and diuretic effects of loop, thiazide, and K^+-sparing diuretics under hypertensive conditions. This analysis provides insights into the mechanisms underlying sex differences in renal function and diuretic efficacy.

The contents of this chapter are adapted from the paper: Kaixin Zheng and Anita T. Layton, "Predicting Sex Differences in the Effects of Diuretics in Renal Epithelial Transport during Angiotensin II-Induced Hypertension," published in American Journal of Physiology-Renal Physiology [171]. The material has been reformatted and adjusted to meet the structural and stylistic requirements of this thesis.

3.1 Method

3.1.1 Model Structure

In this study, we simulate the effects of hypertension, induced by a 14-day infusion of AngII, on kidney function in male and female rats. This is achieved by adapting previously published sex-specific computational models of solute and water transport in the epithelial cells of the superficial nephron of the rat kidney [60, 83]. The details of the computational model are described extensively in Chapter 2. The model nephron is divided into several functionally distinct segments: proximal convoluted tubule (PCT), proximal straight tubule (S3), short descending limb (SDL), medullary thick ascending limb (mTAL), cortical thick ascending limb (cTAL), distal convoluted tubule (DCT), connecting tubule (CNT), cortical collecting duct (CCD), outer medullary collecting duct (OMCD), and inner medullary collecting duct (IMCD). Each segment is modelled with different physical dimensions, transporter profile, permeability, and features like coalescence. In each computational cell of individual segment, steady state luminal, cellular, and paracellular concentrations and fluxes are calculated based on water conservation, non-reacting solute conservation, and pH conservation. Model parameters are specified to simulate nephron function in a male or female rat kidney, under normotensive or hypertensive conditions; see Table 3.1 in Subsection 3.1.2. The model includes transporters shown in schematic diagram Fig. 3.1.

3.1.2 Model Parameters for Hypertension

After a 21-day AngII infusion at 200 µg/min/kg, male and female Wistar rats do not exhibit a significant change in GFR [146]. After a 14-day AngII infusion at 3.5 ng/min [58], or 10 ng/kg/min [120], 60 ng/min [154], GFR in male Sprague–Dawley rats is not significantly influenced. Consequently, we assume in both hypertensive male and female models that both single-nephron glomerular filtration rate (SNGFR) and nephron number remain unchanged. Transporter activities in a hypertensive male rat are primarily based on measurements of transporter protein abundance [105]. Though the measured increases in abundance of ENaC subunits vary over a wide range, a 21% increase in ENaC activity of hypertensive male rats is assumed to yield Na^+ excretion consistent with observation [34]. Chronic AngII infusion lowers urine osmolality [105], which can be attributed in part to AngII-stimulated thirst and water intake. As such, we lower interstitial urea concentration by a factor of 2.5 in the inner medulla. Interstitial concentrations of other solutes are assumed to remain at baseline values. Further, the increased water intake suppressed

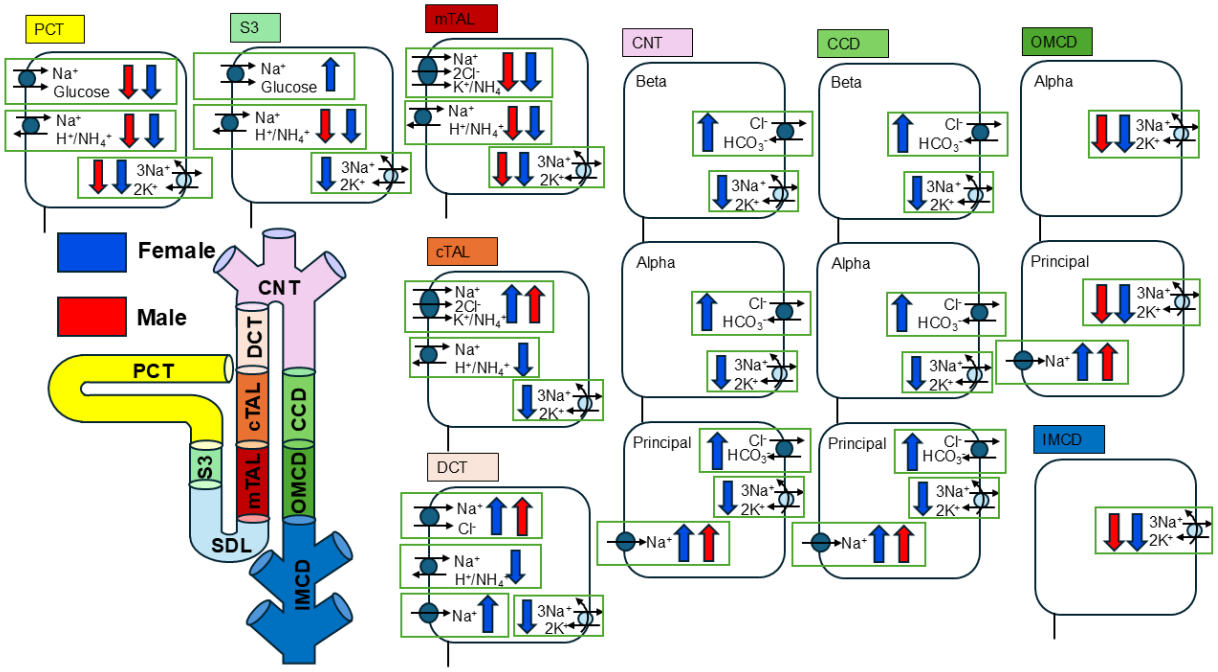


Figure 3.1: Schematic diagram of a superficial nephron in a rat kidney, with its epithelial cell components. The model accounts for the transport of 15 solutes and water. The cell diagrams show primarily Na^+, K^+, and Cl^- transporters. PCT, proximal convoluted tubule; S3, proximal straight tubule; SDL, short descending limb; mTAL, medullary thick ascending limb; cTAL, cortical thick ascending limb; DCT, distal convoluted tubule; CNT, connecting tubule; CCD, cortical collecting duct; OMCD, outer medullary collecting duct; IMCD, inner medullary collecting duct. Up/down arrow indicates transporter upregulation/downregulation due to hypertension. Transporters not influenced are not shown. Adapted from Ref. [60].

arginine vasopressin (AVP) secretion. AVP increases water and urea permeabilities along the inner-medullary collecting duct [128]. To account for these changes, we follow the approach in [34] and assume that the tight junction accounts for 30% of total permeabilities in the absence of AVP stimulation. With this assumption, AVP-induced increases in water and urea permeabilities are estimated to be 3.4- and 5.4-fold, respectively. Thus, in the hypertension simulations, inner-medullary collecting duct water and urea permeabilities are reduced by factors of 3.4 and 5.4, respectively.

Transporter activities in a hypertensive female rat are also primarily based on measurements of transporter protein abundance [150, 35]. Using the reported mean values did not yield sufficiently large increases in urinary volume, Na^+ excretion, and K^+ excretion. As such, most Na^+ transporter activities were lowered to within one standard deviation of mean values (see Table 3.1). It is noteworthy that inhibition of SGLT2 in the proximal convoluted tubule is experimentally observed to be coordinated with inhibition of NHE3 [108], so NHE3 activity is assumed to be further decreased. We assume in hypertensive female, fold increase of ENaC is significantly higher than in hypertensive male [150]. Changes in inner-medullary collecting duct permeabilities to water and urea, as well as interstitial urea concentration profile, are also adjusted the same way as in the hypertensive male rat model (see above). Lower Na^+-K^+-ATPase activity is assumed to reflect the inhibition of Na^+-K^+-ATPase in hypertension [160].

3.1.3 Diuretics Simulations

The effect of loop diuretics on NKCC2 activity is dose dependent. We simulated the administration of loop diuretics by inhibiting NKCC2 by 70%. And to simulate the effect on the urine concentrating ability of the kidney, we lowered the interstitial concentrations of Na^+, K^+, Cl^-, and urea, as was done in [80]) for a normotensive kidney. The effects of thiazide diuretics and K^+-sparing diuretics were simulated by 100% inhibition of NCC and ENaC, respectively. Other model parameters were assumed unaffected.

3.2 Baseline Results

3.2.1 Hypertensive Effects

We conducted simulations to predict luminal fluid flow, solute concentrations, transcellular and paracellular fluxes, urine output, and solute excretions at steady state, under

Table 3.1: Hypertensive model parameter adaptations. HTN, hypertension; NTN, normotension; NHE3, Na^+/H^+ exchanger isoform 3; ENaC, epithelial Na^+ channel; NKCC2, Na^+-K^+-$2Cl^-$ cotransporter 2 (A, B, F indicates isoform type); NCC, Na^+-Cl^- cotransporter; SGLT1, sodium-glucose cotransporter 1; SGLT2, sodium-glucose cotransporter 2; P_f , water permeability; P_{urea} , urea permeability.

	HTN-to-NTN ratios	
Parameter	**Male**	**Female**
Proximal Convoluted Tubule		
NHE3	0.78 [105]	0.79 [150]
Na^+-K^+-ATPase	1	0.8 [160]
SGLT2	1	0.65 [35]
S3		
NHE3	0.55 [105]	0.67 [150]
Na^+-K^+-ATPase	1	0.8 [160]
SGLT1	1	2.05 [35]
Medullary Thick Ascending Limb		
NHE3	0.55 [105]	0.67 [150]
NKCC2A	0.83 [105]	0.70 [150]
NKCC2F	0.83 [105]	0.70 [150]
Na^+-K^+-ATPase	0.7 [105]	0.62 [150, 160]
Cortical Thick Ascending Limb		
NKCC2A	1.74 [105]	1.50 [150]
NKCC2B	1.74 [105]	1.50 [150]
NHE3	1	0.88 [150]
Na^+-K^+-ATPase	1	0.80 [160]
Distal Convoluted Tubule		
NCC	1.93 [105]	2 [150]
Na^+-K^+-ATPase	1	0.80 [160]
NHE3	1	0.88 [150]
ENaC	1	2.42 [150]
Connecting Tubule		
ENaC	1.21 [105, 34]	2.42 [150]
Na^+-K^+-ATPase	1	0.8 [160]
Apical Pf, principal cell	1	0.5 [35]
Pendrin	1	1.47 [35]
Cortical Collecting Duct		
ENaC	1.21 [105, 34]	2.42 [150]
Na^+-K^+-ATPase	1	0.8 [160]
Pendrin	1	1.47 [35]
Apical Pf, principal cell	1	0.5 [35]
Outer-Medullary Collecting Duct		
ENaC	1.21 [105, 34]	1.57 [150, 35]
Na^+-K^+-ATPase	0.7 [105]	0.77 [150]
Apical Pf, principal cell	1	0.6 [35]
Inner-Medullary Collecting Duct		
Na^+-K^+-ATPase	0.7 [105]	0.616 [150]
P_f	1/5.4 [34, 128]	1/5.4 [34, 128]
P_{urea}	1/3.4 [34, 128]	1/3.4 [34, 128]
Papillary Tip		
Interstitial [urea]	1/2.5 [34]	1/2.5 [34]

normotensive and hypertensive conditions. Figures 3.2, 3.3 summarize the predicted segmental fluid, Na^+, and K^+ flows, and corresponding segmental transport and delivery. In hypertension, Na^+ transport is reduced along the proximal nephron segments, i.e., the proximal tubule, via the downregulation of NHE3, and the medullary thick ascending limb, via the downregulation of NKCC2 and Na^+-K^+-ATPase (Table 3.1). Consequently, the reabsorption of Na^+ along these segments decreases, by 7% in male and 9% in female (see Figs. 3.2A1, 3.2A2). In contrast, along nephron segments downstream of the medullary thick ascending limb, which include the cortical thick ascending limb, distal convoluted tubule, connecting tubule, and collecting duct, segmental Na^+ transport capacity is generally enhanced; activities of NKCC2, NCC, and ENaC are increased, although in female the activities of NHE3 and Na^+-K^+-ATPase are assumed lowered (Table 3.1). With these changes, Na^+ reabsorption along these segments is predicted to be higher in the hypertensive models compared to normotension, by 38% in male and 35% in female (see Figs. 3.2A1, 3.2A2), indicating a significant downstream shift in Na^+ transport in hypertension.

Particularly noteworthy is the differential regulation of Na^+ transport capacity along the thick ascending limb: in hypertension and in both male and female models, NKCC2 activity is reduced along the medullary thick ascending limb but increased along the cortical thick ascending limb (Table 3.1). As a result, Na^+ transport is predicted to change in opposing directions along the medullary versus cortical segments (see Figs. 3.2A1, 3.2A2). Those changes mostly cancel out, resulting in a 5% increase in male and a 1% decrease in female from the corresponding normotensive model in overall thick ascending limb Na^+ reabsorption. These small changes suggest that the differential regulation of Na^+ transport capacity along the thick ascending limb is not to adjust the segmental Na^+ reabsorption, but perhaps to adapt to any changes in medullary oxygenation in hypertension (see Conclusion). The models predict an 110% increase in urinary Na^+ excretion in hypertensive male, compared to normotensive male, and an 80% increase in urinary Na^+ excretion in hypertensive female above normotensive female. The AngII-induced natriuresis is less strong in females can be explained by their lower baseline NHE3 activity and lower fractional reabsorption of Na^+ by the proximal tubules. As such, the downregulation of NHE3 activity in hypertension, by similar percentages in both sexes, yielded larger downstream shift of Na^+ load in males, and eventually a larger increase in urinary Na^+ excretion.

Water transport is driven primarily by Na^+ reabsorption; thus, hypertension induces a shift in water transport like that of Na^+, with water reabsorption significantly decreases along the proximal tubule and distal convoluted tubule; in contrast, water reabsorption generally increases along the downstream segments. Taken together, in hypertension urine output is predicted to more than double in both sexes (Figs. 3.2C1, 3.2C2).

The reduced water reabsorption in hypertension lowers luminal $[K^+]$ and thus K^+ trans-

port along the proximal tubule. AngII-induced proximal tubule NHE3 downregulation results in a significantly lower luminal [$NH4^+$] into the downstream segment. While the combined reabsorption of K^+ and $NH4^+$ is lower than in normotension, net K^+ reabsorption increases in the medullary thick ascending limb. Along the cortical ascending limb, the upregulated NKCC2 drives higher K^+ reabsorption. Along the distal convoluted tubule, the lower luminal [K^+] elevates K^+ secretion by 16% and 19% above normotension in male and female, respectively. This trend is magnified along the connecting tubule, where K^+ secretion is higher in hypertension by 115% in male (Fig. 3.2B1) and 142% in female (Fig. 3.2B2).

Along the collecting duct, K^+ reabsorption increases by 52% in hypertensive male (Fig. 3.2B1) and 67% in hypertensive female (Fig. 3.2B2). Collectively, the models predict 78% and 110% increases in urinary K^+ excretion in hypertensive male and female, respectively, above normotension.

3.2.2 NHE3 Downregulation in Hypertension

Our simulations suggest that NHE3 downregulation in the proximal tubule may be the primary factor contributing to natriuresis and diuresis in hypertension.

We assessed the effect of the downregulation of NHE3 in hypertension (Table 3.1) by conducting simulations in which proximal tubule NHE3 activity is set to normotensive levels. Other hypertension-induced adaptations in the proximal tubule (specifically, the downregulation of Na^+-K^+-ATPase and SGLT2 in female) and in other segments are represented. As might be expected, given the essential role of NHE3 in reclaiming filtered Na^+, returning NHE3 activity to the higher normotensive level substantially reduces Na^+ excretion to close to normotensive levels in both sexes (see Figs. 3.4A1, 3.4A2). The effect on urine output is similar. These results support the downregulation of NHE3 in the proximal tubule as the primary factor contributing to natriuresis and diuresis in hypertension.

Eliminating NHE3 downregulation increases proximal reabsorption of Na^+ and decreases its delivery to distal segment. Consequently, ENaC-mediated Na^+ is reduced, which in turn attenuates K^+ secretion. It is noteworthy that the extent to which K^+ excretion is reduced differs significantly between male and female. In the hypertensive male model without NHE3 downregulation, Na^+ delivery to the connecting tubule is 43% lower than the baseline hypertensive model (Fig. 3.5A1), resulting in a substantial 56% decrease in K^+ secretion along that segment (Fig. 3.4A1). In the hypertensive female model, Na^+-K^+-ATPase and SGLT2 remain downregulated along the proximal tubule. Also, the thick ascending limb accounts for a larger fraction of total Na^+ transport. Consequently, even

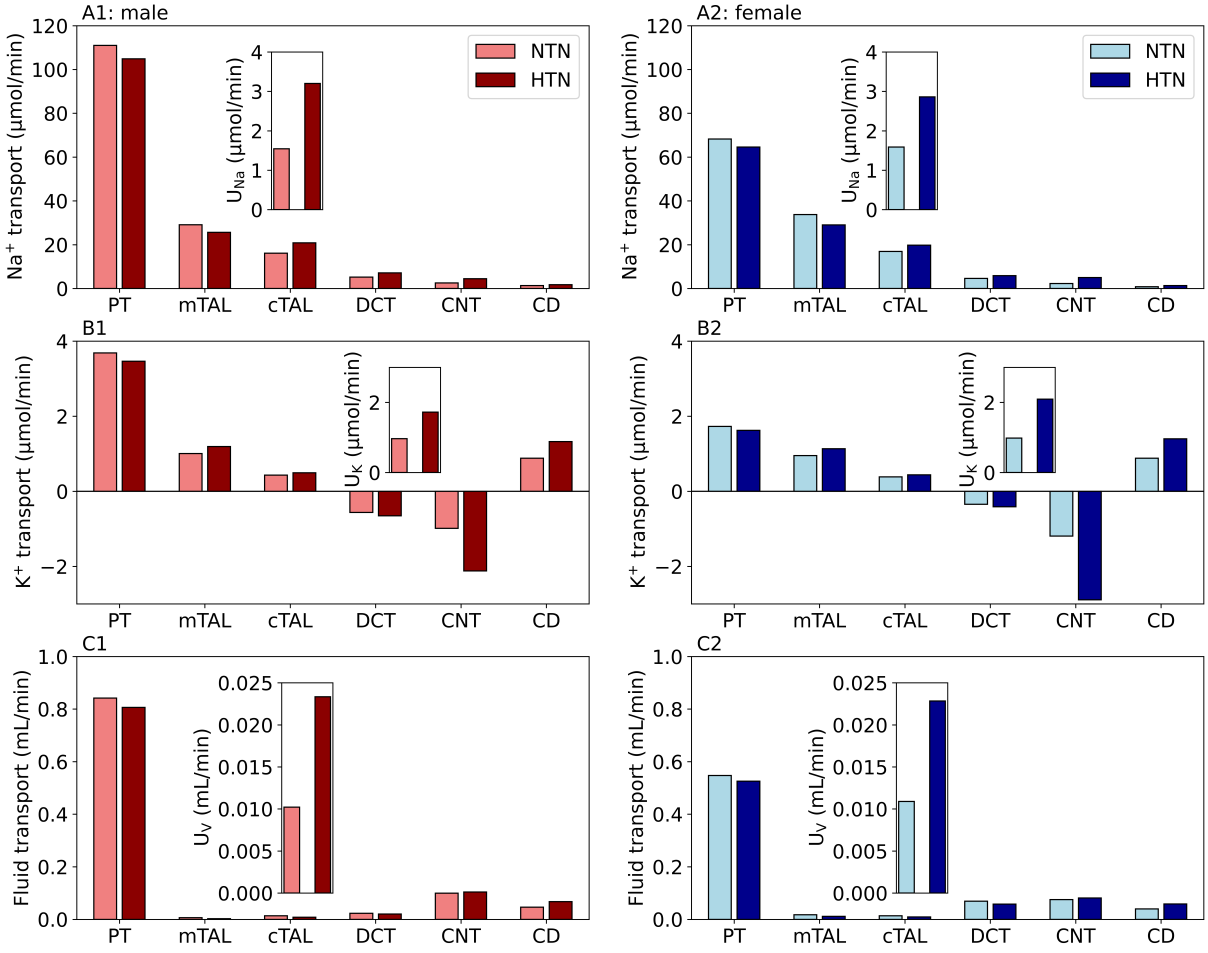


Figure 3.2: Segmental transport of Na^+, K^+, and water, obtained for the male and female models, under normotensive (NTN) and hypertensive (HTN) conditions. PT, proximal tubule; mTAL, medullary thick ascending limb; cTAL, cortical thick ascending limb; DCT, distal convoluted tubule; CNT, connecting tubule; CD, collecting duct. U_{Na}, Na^+ excretion; U_K, K^+ excretion; U_V, volume excretion.

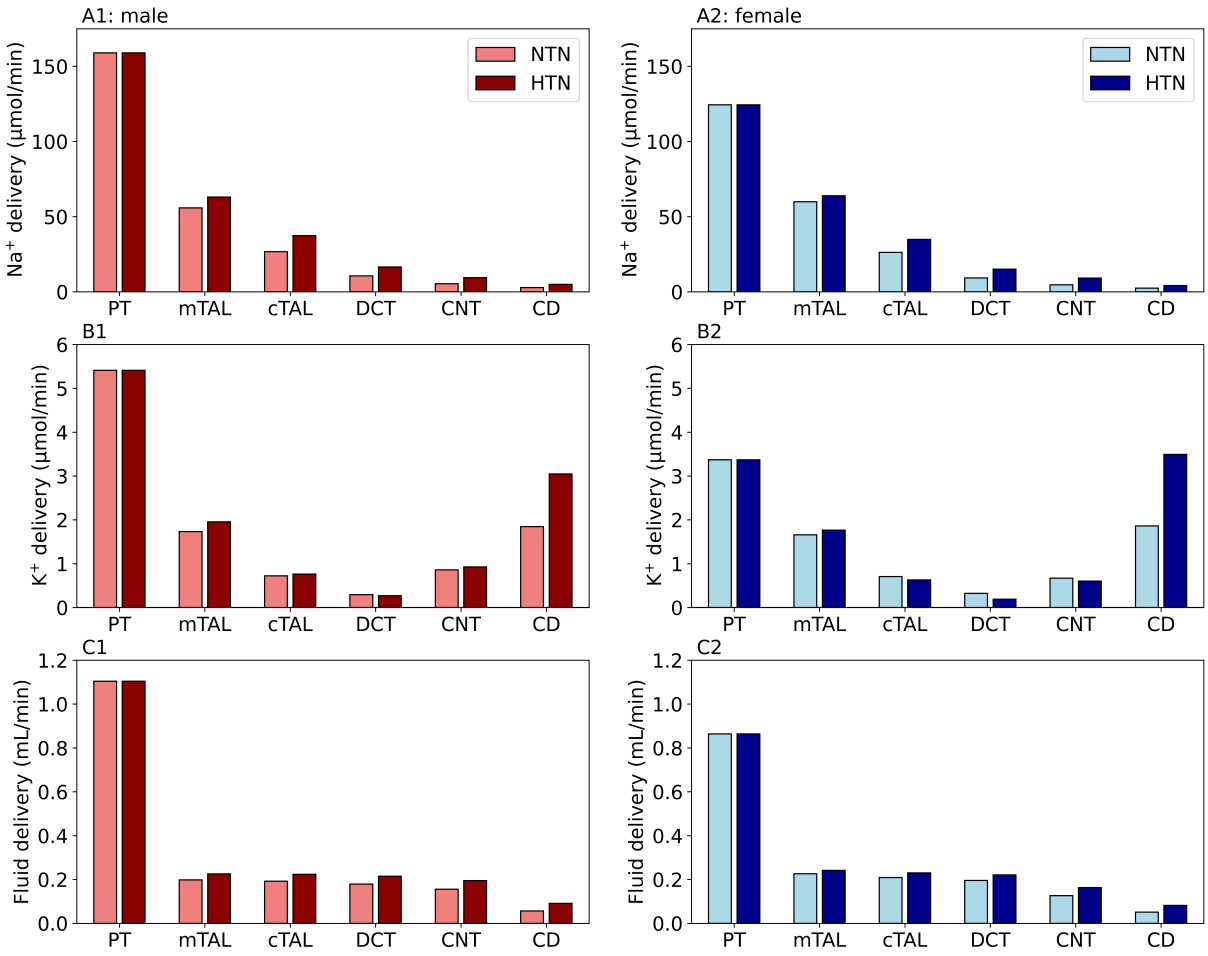


Figure 3.3: Segmental delivery of Na^+, K^+, and water, obtained for the male and female models, under normotensive (NTN) and hypertensive (HTN) conditions. PT, proximal tubule; mTAL, medullary thick ascending limb; cTAL, cortical thick ascending limb; DCT, distal convoluted tubule; CNT, connecting tubule; CD, collecting duct.

with NHE3 activity at the normotensive level, Na^+ delivery to the connecting tubule is only 24% lower than baseline hypertension (compare to 43% in male) as shown in Fig. 3.5A2, and the resulting reduction in connecting tubule K^+ secretion is only 10% (compared to 56% in male) as shown in Fig. 3.4A2. These results explain why the downregulation of NHE3 in hypertension plays a more important role in hypertension-induced kaliuresis in male than in female.

3.3 Diuretics Administration Results

3.3.1 Loop Diuretics

Loop diuretics is predicted to enhance hypertension-induced natriuresis, kaliuresis, and diuresis.

We simulate the administration of loop diuretics by inhibiting NKCC2 by 70%. Simulations were conducted using the normotensive and hypertensive models. Results for the male and female models are shown in Fig. 3.6.

With a 70% inhibition of NKCC2, Na^+ reabsorption along thick ascending limb decreases by 16% in both normotensive and hypertensive male, and by 12% and 11% in normotensive and hypertensive female, from their respective baseline (i.e., without loop diuretics) models. Downstream segments compensate. In particular, Na^+ reabsorption increases significantly along the connecting tubule (see Figs. 3.6A1, 3.6A2). Together, these changes result in substantial increases in Na^+ excretion (67% and 66% in normotensive and hypertensive male; 140% and 98% in normotensive and hypertensive female), above the respective baseline cases. It is noteworthy that these are relative changes. Recall that hypertension induces natriuresis. Thus, while these percentages are smaller in the hypertensive models, especially in female, the administration of loop diuretics is predicted to yield net Na^+ excretion that is substantially higher in hypertension (with loop diuretics) for both male (Fig. 3.6A1) and female (Fig. 3.6A2), compared to normotension (with loop diuretics). The stronger natriuretic response in hypertension can be explained by the downstream shift in Na^+ transport in hypertension, such that the distal segments cannot reabsorb much more Na^+ even when some transporter activities are enhanced in hypertension.

Partial NKCC2 inhibition is predicted to attenuate K^+ reabsorption in thick ascending limb, although that reduction is less than that in Na^+ reabsorption. The higher Na^+ delivery to the connecting tubule stimulates K^+ secretion, by 160%, 58%, 26%, and 17%

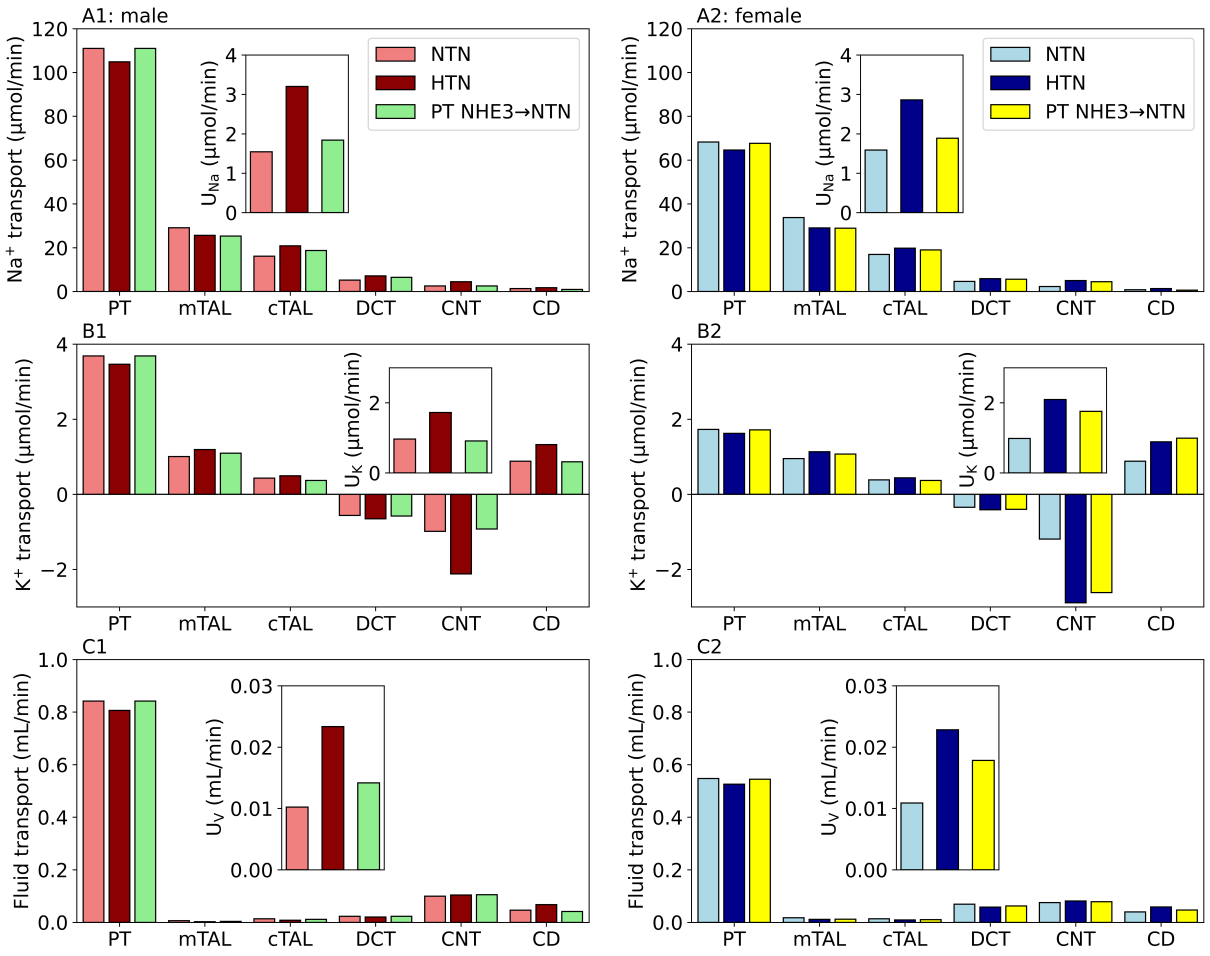


Figure 3.4: Segmental transport of Na^+, K^+, and water, obtained for the male and female models, obtained for normotension (NTN), hypertension (HTN), and hypertension with proximal tubule NHE3 activity set to normotensive value (denoted PT NHE3→ NTN). PT, proximal tubule; mTAL, medullary thick ascending limb; cTAL, cortical thick ascending limb; DCT, distal convoluted tubule; CNT, connecting tubule; CD, collecting duct. U_{Na}, Na^+ excretion; U_K, K^+ excretion; U_V, volume excretion.

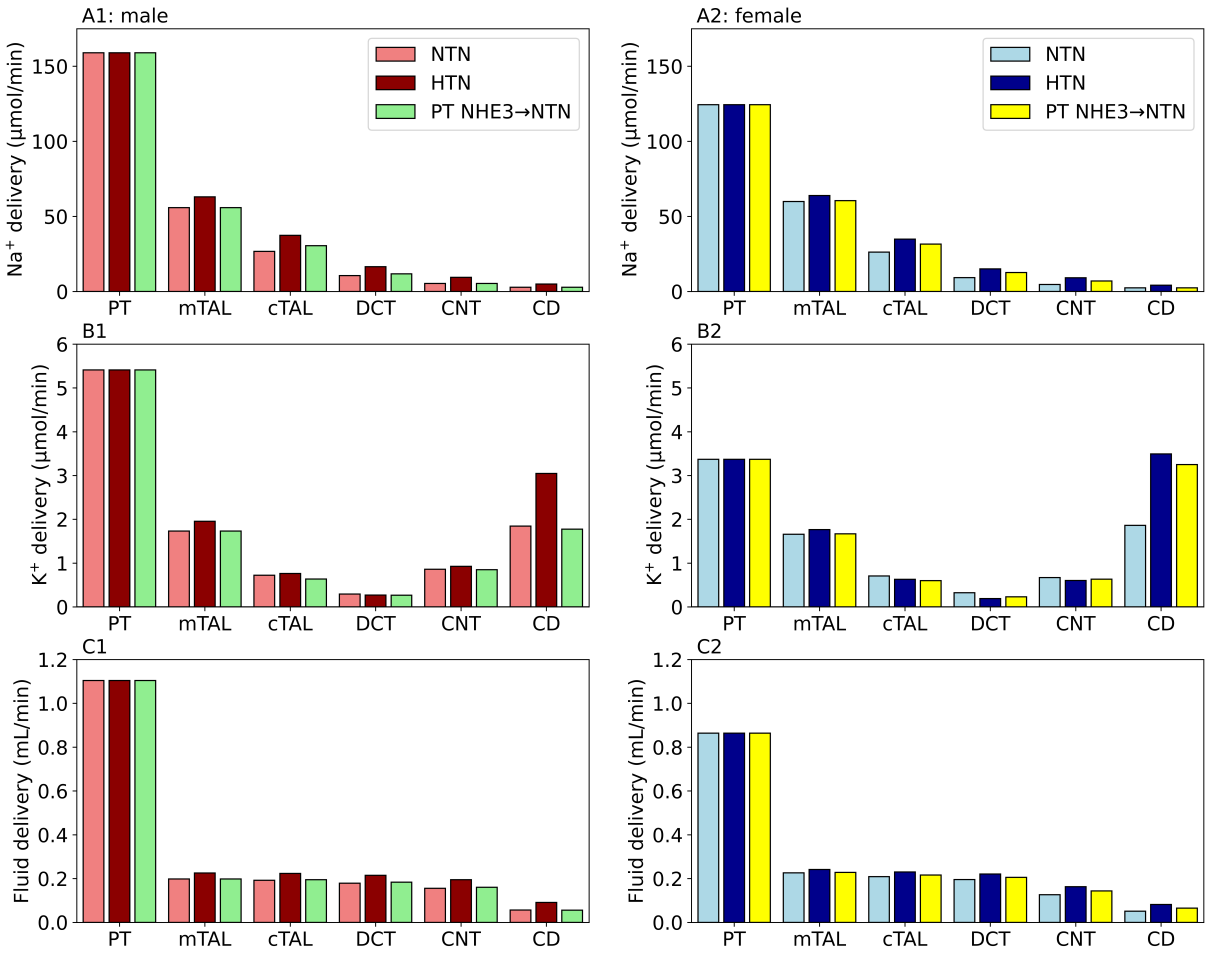


Figure 3.5: Segmental delivery of Na^+, K^+, and water, obtained for the male and female models, obtained for normotension (NTN), hypertension (HTN), and hypertension with proximal tubule NHE3 activity set to normotensive value (denoted PT NHE3→ NTN). PT, proximal tubule; mTAL, medullary thick ascending limb; cTAL, cortical thick ascending limb; DCT, distal convoluted tubule; CNT, connecting tubule; CD, collecting duct.

in normotensive male, hypertensive male, normotensive female, and hypertensive female, respectively. Consequently, K^+ excretion increases by 120% in normotensive male, 65% in hypertensive male, 47% in normotensive female, and 38% in hypertensive female. In both sexes, urinary K^+ excretion is higher in hypertension than normotension (both with loop diuretics), even though the relative increases are smaller in the former (Figs.3.6B1, 3.6B2).

Fluid excretions are enhanced in all cases, by 160% and 98% in normotensive and hypertensive male (Fig. 3.6C1) and by 190% and 100% in normotensive and hypertensive female (Fig. 3.6C2). Because thick ascending limb is essentially water impermeable, the diuretic effect is attributable to the solute concentration increase due to NKCC2 downregulation, which then attenuates water reabsorption downstream.

3.3.2 Thiazide

Thiazide diuretics is predicted to induce a stronger natriuretic response in hypertension, especially in females.

We simulate the effects of the administration of a thiazide diuretic to the normotensive and hypertensive models, for both males and females (Fig. 3.7). With NCC fully inhibited, Na^+ reabsorption along the distal convoluted tubule drops precipitously (Figs. 3.7A1, 3.7A2). The reduction in Na^+ is partially compensated for along the connecting tubule and collecting duct. Nonetheless, the models predict that the inhibition of NCC causes a substantial natriuretic effect, with urinary Na^+ excretion increases by 52% (40%) and 74% (49%) in the normotensive and hypertensive female (male) models, respectively. As previously noted, the stronger natriuretic effect predicted in the hypertensive models can be attributed, in large part, to the substantially higher Na^+ flow into the distal segments (without a diuretic). Indeed, to handle that larger Na^+ flow, NCC activity is assumed to essentially double in hypertension in both sexes. When NCC is inhibited by a thiazide diuretic, it is more challenging for the segments downstream of the distal convoluted tubule to compensate in the hypertensive models. Between the two sexes, the stronger natriuretic response is predicted for the female models. That sex difference may be explained by the relatively limited capacity of the female models' other Na^+ transport pathways in the distal convoluted tubule and downstream segments to elevate their Na^+ transport.

The enhanced ENaC-mediated Na^+ transport increases K^+ secretion along the connecting tubule, resulting in kaliuresis (Figs. 3.7B1, 3.7B2). The elimination of NCC-mediated Na^+ reabsorption along the distal convoluted tubule is followed by a reduction in water reabsorption, although the effect is much smaller (Figs. 3.7B1, 3.7B2). Unlike Na^+, where the connecting tubule partially makes up for the upstream transport impairment, water

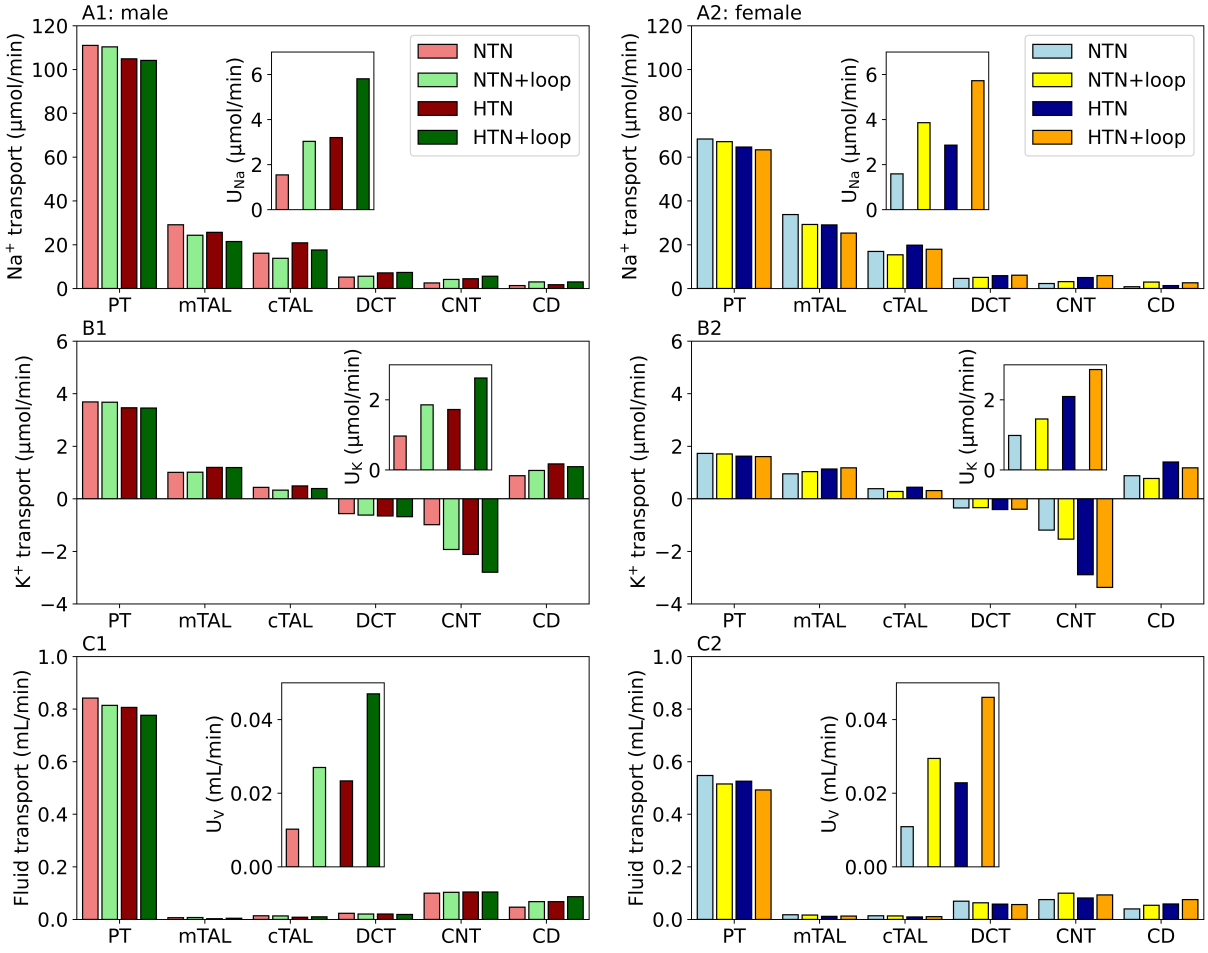


Figure 3.6: Segmental transport of Na^+, K^+, and water in male (A1-C1) and in female (A2-C2) for normotension (NTN), normotension with 70% NKCC2 inhibition (NTN+loop), hypertension (HTN), hypertension with 70% NKCC2 inhibition (HTN+loop). PT, proximal tubule; mTAL, medullary thick ascending limb; cTAL, cortical thick ascending limb; DCT, distal convoluted tubule; CNT, connecting tubule; CD, collecting duct.

reabsorption along the connecting tubule also decreases. Despite some partial compensation along the collecting duct, the models predict substantial diuretic effects (Figs. 3.7C1, 3.7C2).

3.3.3 K^+-sparing Diuretics

K^+-sparing diuretics is predicted to induce a stronger natriuretic response in hypertension.

We then consider the effect of K^+-sparing diuretics. All models predict that, when ENaC is fully inhibited, Na^+ transport along the connecting tubule reverses direction, switching from reabsorption in baseline normotension or hypertension to (a small amount of) secretion (see Figs. 3.8A1, 3.8A2). Despite some compensation along the collecting duct, the inhibition of ENaC induces a substantial natriuretic effect, with urinary Na^+ excretion increases by 200% (190%) and 210% (150%) in the normotensive and hypertensive female (male) models, respectively. The stronger natriuretic effect predicted in the hypertensive models is due to the enhanced Na^+ transport by connecting tubule in hypertension: in both hypertensive male and female models, the connecting tubule reabsorbs about twice as much Na^+ as the corresponding normotensive models (see Figs. 3.8A1, 3.8A2). As such, when that Na^+ transport capacity is blocked, it results in a larger natriuretic effect in the hypertensive models.

The removal of ENaC-mediated Na^+ reabsorption also abolishes K^+ secretion along the connecting tubule. This results in a substantial reduction of urinary K^+ excretion. The elimination of Na^+ reabsorption and K^+ secretion has opposing effects on water transport. These competing effects result in some reduction in water reabsorption along the connecting tubule (Figs. 3.8C1, 3.8C2); eventually, urine output increases by 59% (68%) and 50% (44%) in the normotensive and hypertensive female (male) models, respectively.

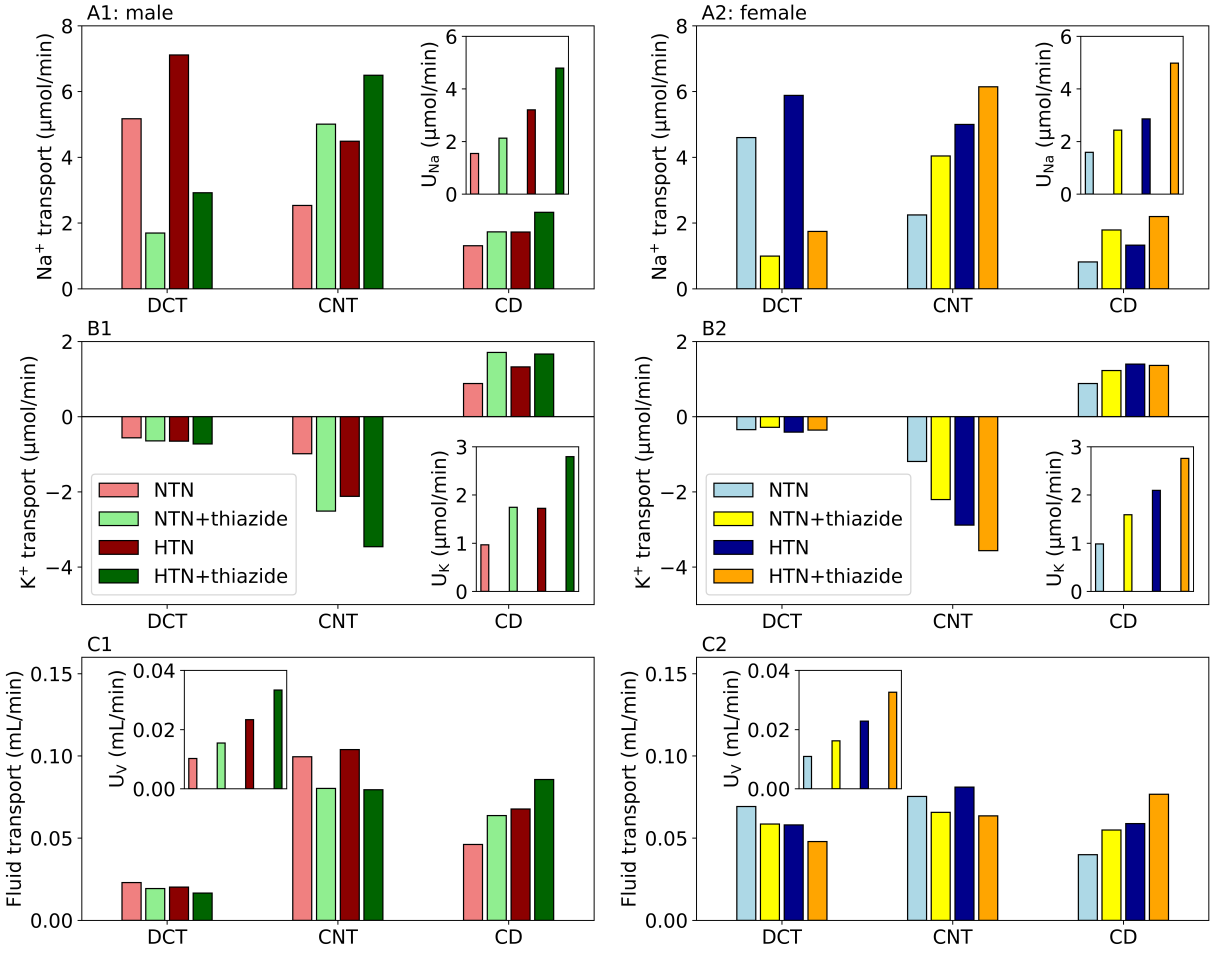


Figure 3.7: Segmental transport of Na^+, K^+, and water in male (A1-C1) and in female (A2-C2) for normotension (NTN), normotension with 100% NCC inhibition (NTN+thiazide), hypertension (HTN), hypertension with 100% NCC inhibition (HTN+thiazide). DCT, distal convoluted tubule; CNT, connecting tubule; CD, collecting duct.

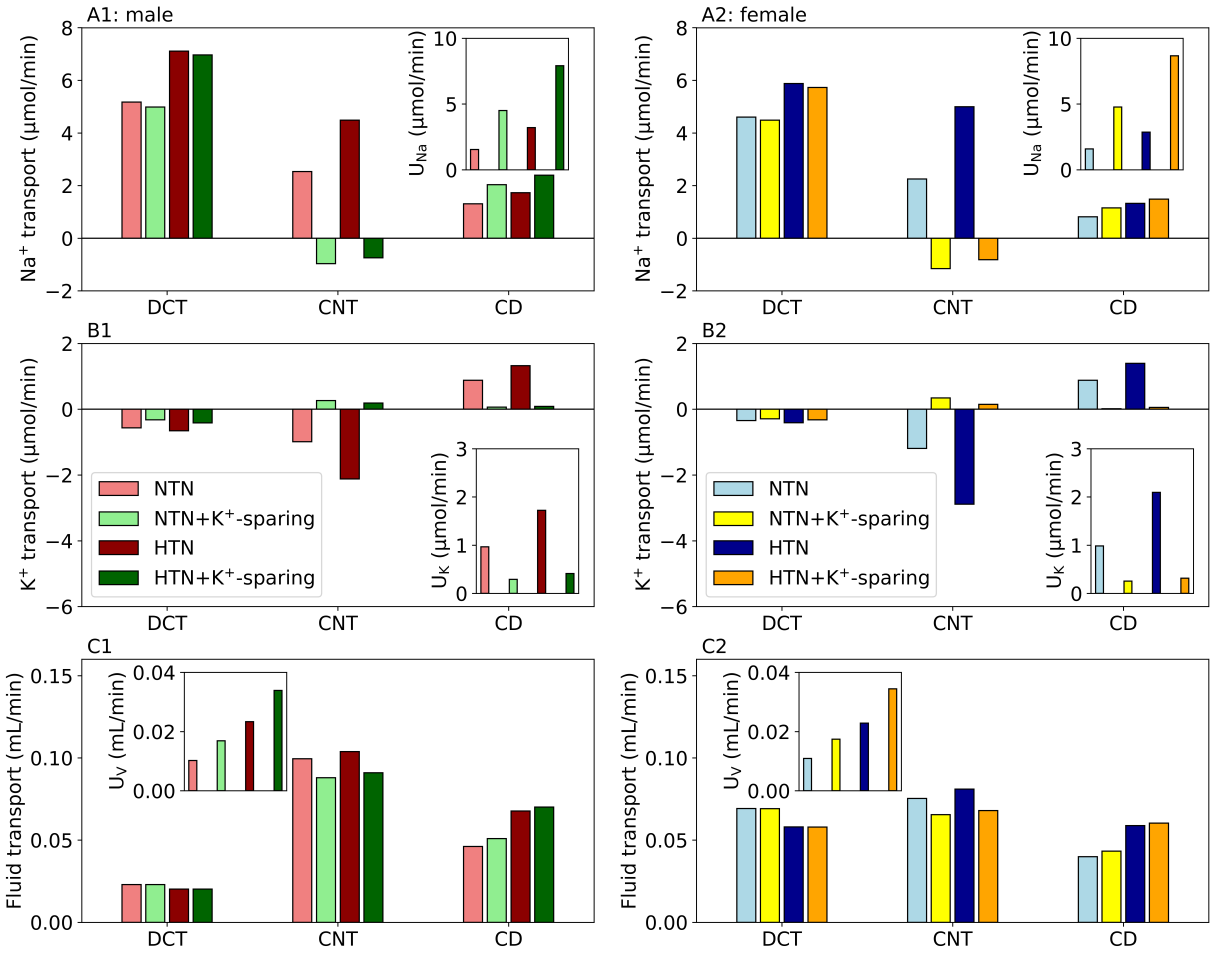


Figure 3.8: Segmental transport of Na^+, K^+, and water in male (A1-C1) and in female (A2-C2) for normotension (NTN), normotension with 100% ENaC inhibition (NTN+K^+-sparing), hypertension (HTN), hypertension with 100% ENaC inhibition (HTN+K^+-sparing). DCT, distal convoluted tubule; CNT, connecting tubule; CD, collecting duct.

Chapter 4

Circadian Effects on Renal Transporters in Hypertension

In this chapter, we investigate the impact of circadian rhythms on the efficacy of diuretic therapies for hypertension. As previously discussed in Subsection 1.2.2, the kidney plays a critical role in maintaining fluid and electrolyte balance, and its function is significantly influenced by the renin-angiotensin-aldosterone system (RAAS) and circadian clocks. Overactivation of the RAAS, as observed in chronic Ang II infusion, leads to vasoconstriction, sodium retention, and hypertension.

Key renal transporters, including NHE3, SGLT1, NKCC2, NCC, and ENaC, are regulated by circadian clock genes and are targeted by diuretics used to treat hypertension. To assess the potential impact of circadian rhythms on diuretic efficacy, we employed computational models of kidney function. Our simulations predicted significant time-of-day differences in the natriuretic, diuretic, and kaliuretic responses to loop, thiazide, and K^+-sparing diuretics, both in normotensive and hypertensive conditions. These findings highlight the importance of considering circadian rhythms in optimizing diuretic therapy for hypertension.

The contents of this chapter are adapted from a paper by Dr. Anita T. Layton and me (under review). The material has been reformatted and adjusted to meet the structural and stylistic requirements of this thesis.

4.1 Model Structures

Modeling the circadian clock network

We aim to simulate the modulation of key renal transporter activities in a male rat by the circadian clock. We first develop a mathematical model of the core clock in the male rat kidney. The clock model comprises a number of transcription factors that regulate gene expression: the period homologs Per1 and Per2, the cryptochromes homologs Cry1 and Cry2, Rev-Erb and RAR-related orphan receptor (Ror), brain and muscle ARNT-Like 1 (Bmal1), and circadian locomotor output cycles kaput (CLOCK). A schematic diagram of the clock network is shown in Fig. 4.1. Equations for the clock model are given in Appendix A. Model parameters were obtained by fitting predicted profiles for mRNA expression levels of core clock genes (Per1, Per2, Cry1, Cry2, Rev-Erb, Ror, Bmal1) with their corresponding measured data reported in Ref. [167] and database [114], obtained for the dark-dark cycles. The error of each parameter set is evaluated by first running a simulation with the parameter set for a sufficiently long time. The least squares error is then calculated by comparing the experimental data to the periodic solution with varying phase shifts. Numerically determining the phase difference that yields the minimum error defines the objective function to be minimized.

Modeling the circadian clock network

The model represents a superficial nephron of a male rat kidney. As depicted in Fig. 1, the model nephron is divided into 10 functionally distinct segments: proximal convoluted tubule (PCT), proximal straight tubule (S3), short descending limb (SDL), medullary thick ascending limb (mTAL), cortical thick ascending limb (cTAL), distal convoluted tubule (DCT), connecting tubule (CNT), cortical collecting duct (CCD), outer medullary collecting duct (OMCD), and inner medullary collecting duct (IMCD). Each segment is modeled with a series of computational cells assigned with specific physical dimensions, transporter profile, and membrane permeability. The model accounts for the following 15 solutes: Na^+, K^+, Cl^-, HCO_3^-, H_2CO_3, CO_2, NH_3, NH_4^+, HPO_4^{2-}, $H_2PO_4^-$, H^+, HCO_2^-, H2CO2, urea, and glucose. In each computational cell, steady-state luminal, cellular, and paracellular concentrations and fluxes are calculated based on water conservation, nonreacting solute conservation, and pH conservation. Model equations can be found in Ref. [77].

We represent the circadian regulation of key Na^+ transporters. Specifically, NHE3 expressed on the PCT, S3, mTAL, and cTAL, sodium-glucose cotransporter 1 (SGLT1) on the S3, NKCC2 on the mTAL and cTAL, NCC on the DCT, and ENaC along the DCT, CNT, and CD.

Rohman et al. [126] experimentally verified that that NHE3 in the rat kidney is transactivated by CLOCK-BMAL1, and that Cry1 and Per2 inhibit the CLOCK-BMAL1-mediated transactivation of the NHE3 promoter, with the inhibition much stronger for Cry1. Solocinski et al. [134] demonstrated that Per1 enhances NHE3 expression. Therefore, we assume that NHE3 is activated by CLOCK-BMAL1 and PER1-CRY2, but inhibited by PER1-CRY1, PER2-CRY1 and PER2-CRY2.

Crislip et al. [24] reported a significant increase in NKCC2 mRNA expression in Bmal1 knockout male mice compared to wild-type. Thus, we assume that NKCC2 is inhibited by CLOCK-BMAL1. Given that NKCC2 mRNA exhibits sustained oscillations in Bmal1 knockout mice [24], we assume additionally that NKCC2 is also inhibited by PER1-CRY1, PER1-CRY2, PER2-CRY1, and PER2-CRY2. Supporting experimental evidence is limited and indirect: estrogen-related receptor beta (ERR), which displays a circadian rhythm in the kidney with peak expression at ZT4, is known to positively regulate NKCC2 expression in male mice [74], and estrogen receptor beta (ERβ) is downregulated by the PER-CRY complexes [15].

SGLT1 is assumed to be activated by PER1-CRY1 and PER1-CRY2 but inhibited by CLOCK-BMAL1. This assumption is supported by evidence that Per1 knockout decreases SGLT1 expression in male mice [134], and that BMAL1 inhibits SGLT1 in Caco-2 cells via activation of paired-homeodomain transcription factor 4 (PAX4) [142]. Additionally, Stevenson et al. [140] demonstrated that activation of Bmal1 decreases renal SGLT1 levels in an SHP-dependent manner, whereas Clock-mutant and Bmal1-knockout mice show elevated SGLT1 expression, supporting the idea that CLOCK-BMAL1 inhibits SGLT1.

In both male and female mouse kidneys ,NCC expression is positively regulated by WNK4 [144], the expression of which increases significantly in male Bmal1-knockout mice compared to wild-type [24]. Also, Per1 blockade inhibits NCC activity in male mice [122]. Thus, in the model NCC expression is suppressed by CLOCK-BMAL1 and activated by PER1-CRY1 and PER1-CRY2. Based on findings in mice [45], ENaC is assumed to be activated by CLOCK-BMAL1 and also by PER1-CRY1 and PER1-CRY2, which colocalizes with CLOCK-BMAL1.

Transporter activities are assumed proportional to the corresponding mRNA expression levels, and thus fluctuates with core clock protein levels. The links are described in Eqs. A8-A12 in the Appendix and summarized in Fig. 4.1. Model parameters were obtained by fitting predicted profiles for the transporters (NHE3, SGLT1, NKCC2, NCC, ENaC) with data reported in Refs. [24, 168, 79].

Modeling the circulation regulation of renal hemodynamics

As was done in Ref. (36), the model represents the single-nephron GFR (SNGFR) of

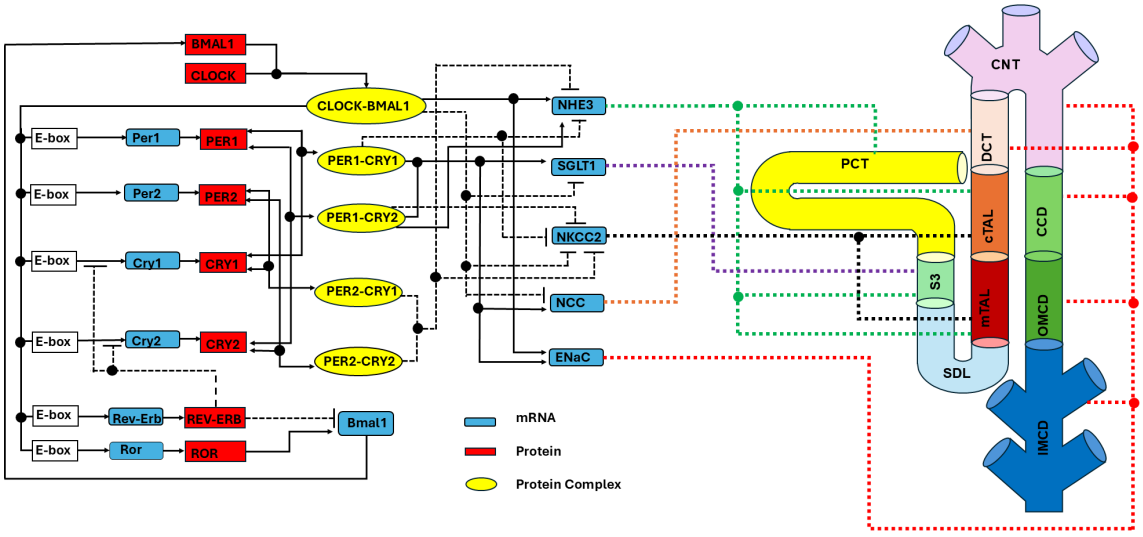


Figure 4.1: Schematic network of our mathematical model, which describes the interactions of core clock components with key renal transporter genes. In the core clock network, mRNAs are denoted by blue boxes, proteins by red boxes, and protein complexes by yellow ovals. Solid lines represent the transactivation and dotted lines represent inhibition. The model nephron includes the proximal convoluted tubule (PCT), S3 segment, medullary thick ascending limb (mTAL), cortical thick ascending limb (cTAL), distal convoluted tubule (DCT), connecting tubule (CNT), cortical collecting duct (CCD), outer medullary collecting duct (OMCD), and inner medullary collecting duct (IMCD). Renal transporters that are regulated by the circadian clock include NHE3, SGLT1, NKCC2, NCC, and ENaC.

a wild-type male rat in a light-dark cycle, denoted $\mathrm{SNGFR_{WT}}$, as a sinusoidal function of the Zeitgeber Time (ZT), denoted t, with a peak at ZT16:

$$\mathrm{SNGFR_{WT}} = \mathrm{SNGFR_0} \cdot (1 + 0.12 \cdot \sin(\frac{2\pi(\mathrm{t} - 16 + 6)}{24})) \tag{4.1}$$

ZT=0 (lights on) marks the start of the rest phase for nocturnal animals, whereas ZT12 (lights off) denotes the start of the active phase. The baseline $\mathrm{SNGFR_0}$ is taken to be 32 nl/min for the superficial nephron of a male rat.

GFR in Bmal1 knockout mice exhibits an ultradian rhythm different from wild-type, with two peaks at ZT4 and ZT16; the 24-hour cumulative GFR are similar in the two genotypes (37). Based on these findings, we model SNGFR in Bmal1-knockout rat, denoted $\mathrm{SNGFR_{KO}}$, as:

$$\mathrm{SNGFR_{WT}} = \mathrm{SNGFR_0} \cdot (1 + 0.12 \cdot \sin(\frac{2\pi(\mathrm{t} - 4 + 3)}{12})) \tag{4.2}$$

Modeling the effects of hypertension on renal epithelial transport

We investigate the effect on kidney function in a male rat with hypertension induced by 14-day infusion of ANG II. Following the approach in Ref. [171], we incorporate hypertension-induced changes into the renal epithelial transport model described above. These changes include changes in transport activities, membrane permeabilities, and interstitial fluid composition. Among the transporters of which the circadian regulation is represented in the present model, NHE3 and NKCC2 along the mTAL are downregulated in hypertension; NKCC2 along the cTAL, NCC, and ENaC are upregulated, whereas SGLT1 remains unchanged. The links between clock proteins and transporter activities are assumed the same in normotension and hypertension, as is the SNGFR profile.

Modeling the effects of diuretics on renal epithelial transport

We consider the effects of loop diuretics, thiazide diuretics, and K^+-sparing diuretics on renal transport and excretions. Loop diuretics inhibit NKCC2, and its administration is assumed to significantly impair the model kidney's ability to generate an axial osmolality gradient. Thus, we lower the interstitial fluid concentrations of selected solutes [80], but keep the interstitial urea concentration at the papillary at the baseline hypertension value (which is assumed to be lower than in normotension) [171]. SNGFR is assumed to retain its baseline profile. Thiazide diuretics inhibit NCC. We simulate a dosage of thiazide diuretics that induces 100% inhibition of NCC. All other model parameters remain at baseline values. Interstitial concentration profiles are assumed unchanged. K^+-sparing diuretics inhibit ENaC. We simulate a dosage of K^+-sparing diuretics that induces 100% inhibition of ENaC. Interstitial concentration profiles are again assumed unchanged.

4.2 Results

4.2.1 Diurnal Oscillations in Clock Gene and Transporter

Using the baseline model parameters (see A), the circadian clock network model predicts that the expression levels of all core clock components exhibit limit-cycle oscillations with a 24-h period. Time-profiles of core clock components, together with the experimental data [167], are shown in Fig. 4.2. Model parameters were chosen to ensure good agreement between the predicted profiles and data.

Oscillations in the core clock components drive oscillations in the expression levels of NHE3, SGLT1, NKCC2, NCC, and ENaC. We identify parameters that describe the regulation of NHE3 expression by CLOCK-BMAL1 and the PER-CRY complexes that the predicted NHE3 time profiles agree with the normotensive male mouse data in the database [114] from the mice experiment [167] in constant dark environment. As shown in Fig. 4.3A, the predicted NHE3 expression profile exhibits good agreement with experimental data. Similarly, model parameters that link the expression levels of SGLT1, NCC, and ENaC to core clock proteins were fitted, so that the predicted transporter expression levels approximate rat data obtained in light-dark cycles [168]. Results are shown in Fig. 4.3B, 4.3C, and 4.3D.

Like NHE3, NKCC2 expression is also regulated by CLOCK-BMAL1 and the PER-CRY complexes. We fit those parameters against data measured in wild-type and Bmal1-knockout rats [24]. To simulate the renal peripheral clock in Bmal1-knockout rats, we reduce the maximal transcription rate for Bmal1 by 40%. We then compare the predicted NKCC2 expression levels in these two groups at noon and midnight with values reported in Ref. [24]. Results are shown in Fig. 4.3E and 4.3F. Using these parameters, the predicted NKCC2 levels for both wild-type and Bmal1-knockout align with experimental data obtained at noon and midnight. The suppression of Bmal1 transcription is predicted to cause a significant phase shift in NKCC2 oscillations: the peak time occurs at ZT15 in wild-type, but shifts to ZT0 in Bmal1-knockout. Additionally, Bmal1 knockout substantially increases average NKCC2 expression (46%), whereas the oscillation amplitude decreases (85%).

The amplitudes and peaks (normalized by means) of the predicted core clock gene and transporter mRNA time profiles for the wild-type model are summarized in Table 4.1.

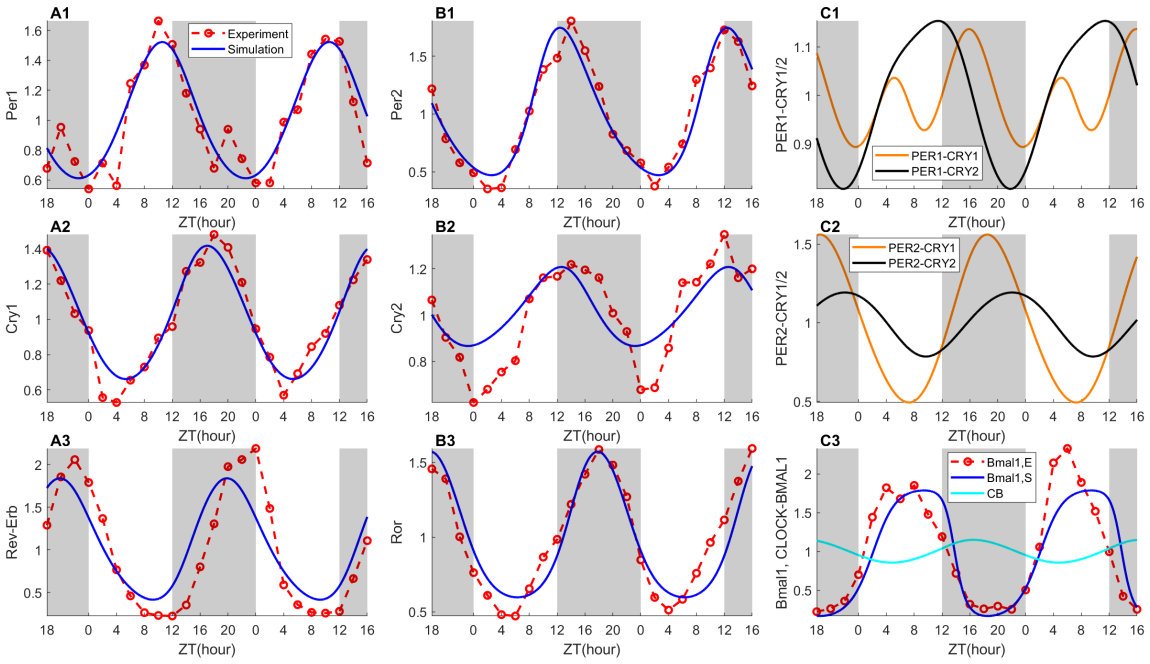


Figure 4.2: Comparison of simulated circadian gene and protein profiles with data from 46-hour experiments starting at ZT18 [167, 114]. **A1-A3, B1-B3**, simulated mRNA expression levels (Simulation) compared with experimental data (Experiment), normalized by mean experimental values; **C1, C2**, simulated concentrations of PER1–CRY1, PER1–CRY2, PER2–CRY1, and PER2–CRY2 protein complexes, normalized by their respective mean simulated values; **C3**, simulated BMAL1 mRNA expression levels (Bmal1, S), experimental BMAL1 mRNA levels (Bmal1, E), and normalized CLOCK–BMAL1 complex concentrations (CB). Gray shading and white regions correspond to dark and light phase, respectively.

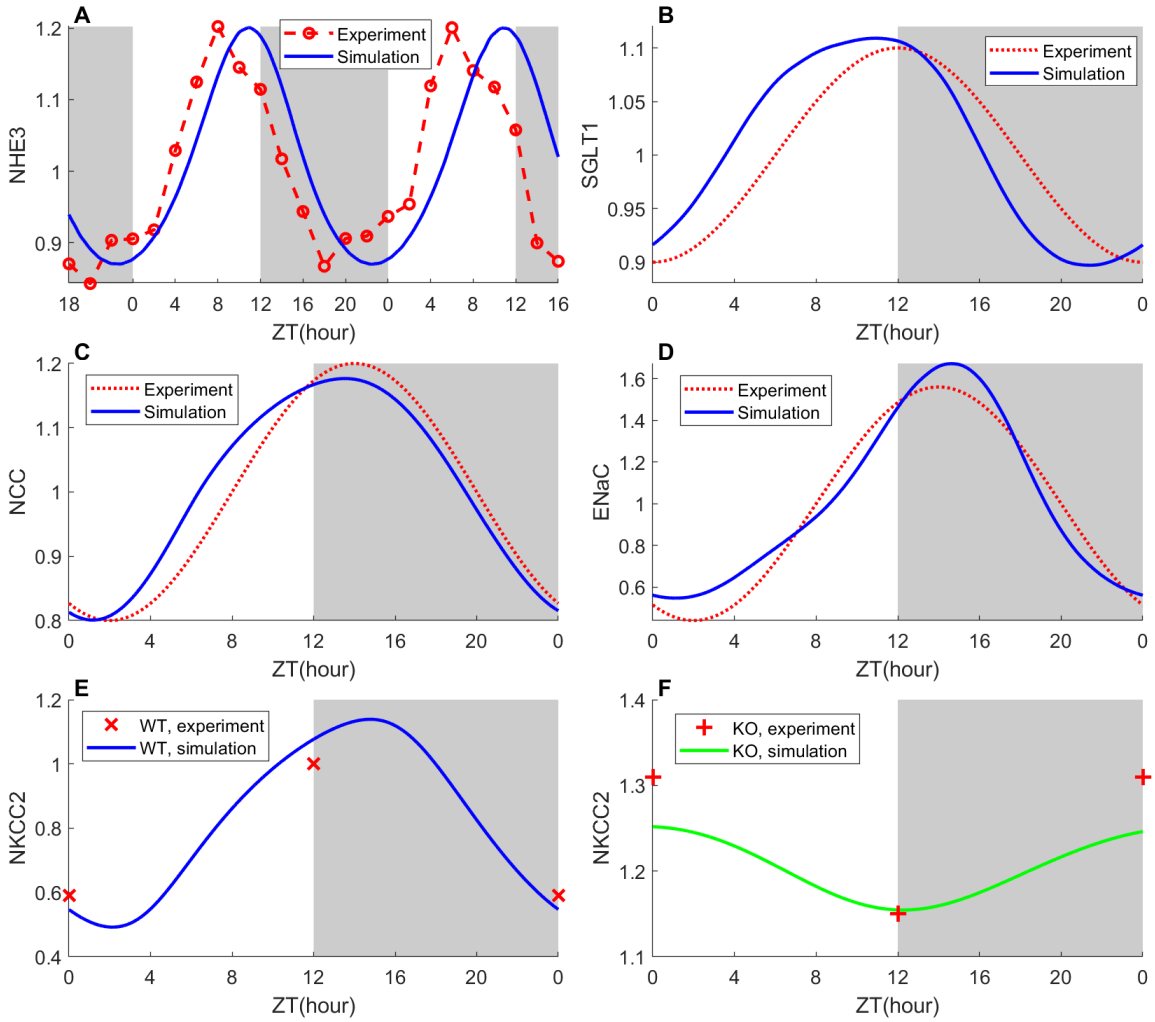


Figure 4.3: Comparison of simulated transporter expression with corresponding experimental data. **A-D**, Transporter expression simulation (Simulation) and experimental profiles (Experiment) of NHE3, SGLT1, NCC, ENaC respectively. **E**, Simulation of NKCC2 expression in wild-type (WT, simulation) and corresponding experimental data at noon and midnight (WT, experiment). **F**, Simulation of NKCC2 expression after Bmal1 knockout (KO, simulation) with corresponding experimental data at noon and midnight (KO, experiment). Values are normalized by mean expression level in wild type. Gray shading and white regions correspond to the dark and light phases, respectively.

4.2.2 Bmal1-knockout Effects on Na^+ Transport and Excretion

We then investigate how Bmal1 knockout affects nephron function at different times of day. To that end, we incorporate the predicted time profiles of NHE3, SGLT1, NKCC2, NCC, and ENaC (Fig. 4.3), together with the time-varying SNGFR (Eqs. 4.1 and 4.2), into the nephron transport model, and we conduct simulations to predict water and solute transport along individual nephron segments and urine excretions, at different ZT. As noted above, we simulate conditional Bmal1 knockout by reducing the maximal transcription rate of Bmal1 by 40%. SNGFR and the predicted transporter profiles are shown in Fig. 4.4. Segmental Na^+ reabsorption and Na^+ excretion are summarized in Fig. 4.5.

Bmal1 knockout leads to a significant reduction in circadian oscillation amplitudes in CLOCK-BMAL1 (results not shown), in NKCC2 as previously noted, and in all other transporters (Fig. 4.4). The mean transporter expression levels over 24 hours significantly increase, except for NHE3 and ENaC, consistent with the assumption that CLOCK-BMAL1 inhibits these transporters (Fig. 4.4). Mean NHE3 and ENaC expression levels remain close to wild type. This result may be attributed to the non-linearity of the model, where the mean expressions of NHE3 and ENaC are initially less sensitive to Bmal1 knockout due to the high CLOCK-BMAL1 regulation threshold (Appendix, Table A4). When the maximal Bmal1 transcription rate is reduced to zero, oscillations for all transporters disappear, with the mean expressions of NHE3 and ENaC reduced by 24% and 65%, respectively, relative to wild type.

A comparison between SNGFR in the model wild-type and Bmal1-knockout rats (Fig. 4.4A) and the predicted urinary Na^+ excretion (Fig. 4.5F) suggests that Na^+ excretion is primarily driven by SNGFR. In Bmal1-knockout rats, cumulative Na^+ excretion during the inactive (light) phase is 110% higher than wild-type. This difference is primarily due to the higher cumulative SNGFR and thus filtered Na^+ load in Bmal1-knockout rats in the inactive phase (by 7%). In contrast, during the active (dark) phase, the cumulative SNGFR is 6% lower in Bmal1-knockout rats, and perhaps more importantly, their cumulative activity of NHE3 is 10% higher. As a result, cumulative Na^+ excretion in Bmal1-knockout rats is predicted to be 55% lower than wild-type. This pattern aligns with experimental findings [66], in which cumulative Na^+ excretion in Bmal1-knocout male mice was found to be 46% higher than wild type during inactive phase but 24% lower than in active phase.

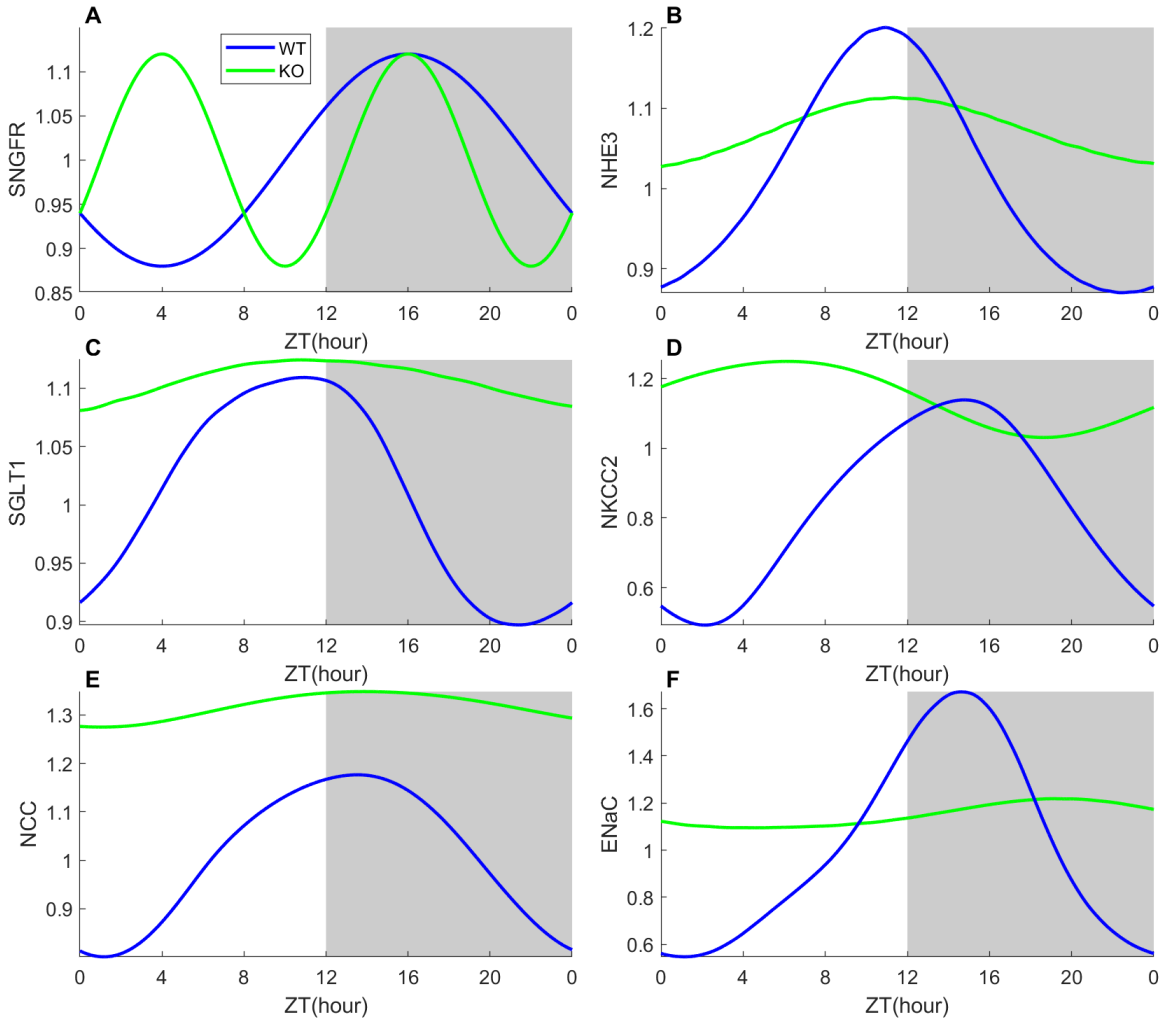


Figure 4.4: Comparison of model GFR and simulated transporter expression between wild type (WT) and conditional Bmal1 knockout (KO) male rat. (A): GFR is normalized by baseline GFR at ZT10 in the wild type; (B-F) simulated transporter expression levels are normalized by mean experimental values the same as in Fig. 4.3. Gray shading and white regions correspond to the dark and light phases, respectively.

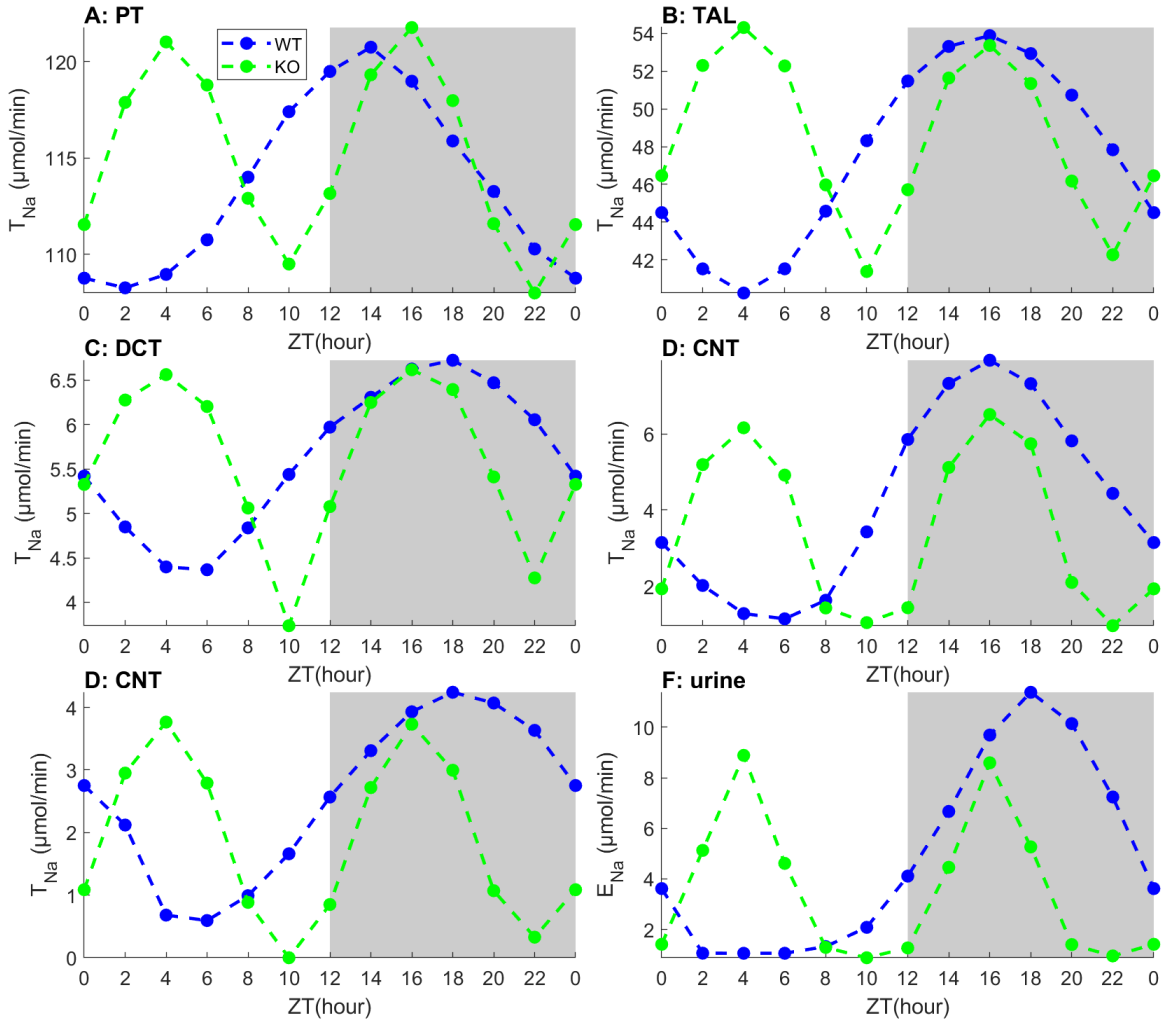


Figure 4.5: Comparison of segmental Na^+ transport and urinary Na^+ in wild type (WT) and Bmal1 knockout (KO) male rats. PT, proximal tubule; TAL, thick ascending limb; DCT, distal convoluted tubule; CNT, connecting tubule; CD, collecting duct. T_{Na}, Na^+ transport; E_{Na}, excretion.

4.2.3 Transport and Excretions in Normotension and Hypertension

In the next set of simulations, we assess the differences in nephron function in a normotensive and hypertensive rat throughout the day. Simulations were conducted for a normotensive and a hypertensive rat kidney, using the same SNGFR and clock gene profiles. The predicted filtered Na^+ load, urinary output, Na^+ and K^+ excretions are shown in Fig. 4.6. Selected predicted segmental transport profiles are shown in Fig. 4.7.

As expected, the hypertensive-induced downregulation of NHE3 results in reduced Na^+ reabsorption along the proximal tubule (Fig. 4.7A). In both normotension and hypertension, proximal tubule Na^+ reabsorption peaks around ZT14, a result of the competing effects of the diurnal rhythms in SNGFR and NHE3, which peak at ZT16 and ZT11, respectively. Proximal tubule outflow and thus Na^+ delivery to the loop of Henle downstream peak at ZT16; as a result, Na^+ reabsorption along the thick ascending limb also peaks at ZT16 (Fig. 4.7B). Na^+ transport along the thick ascending limb is similar in normotension and hypertension throughout the day, because the hypertension-induced downregulation of NHE3, NKCC2, and Na^+-K^+-ATPase along the medullary thick ascending limb, and the resulting decrease in Na^+ reabsorption, is compensated by the upregulation of NKCC2 along the cortical thick ascending limb.

Along the downstream segments, Na^+ reabsorption and K^+ transport (secretion or reabsorption, depending on the segment) are enhanced by the upregulation of NCC and ENaC in hypertension (Figs. 4.7C-4.7I), with the exception of the collecting duct, a result that is consistent with published modeling results [171]. That increase persists throughout the day. It is noteworthy that model simulations did not predict a significant phase shift in the segmental transport profiles in hypertension. This result is attributable, in large part, to the assumption of the same diurnal oscillations in SNGFR in normotension and hypertension, which yield similarly shaped oscillations in Na^+ transport in all segments and in urinary Na^+ excretion.

Changes in SNGFR and transporter activities together yield oscillations in urine output and excretion rates that are essentially in phase with SNGFR rhythms; see Fig. 4.6. Urine output and excretions are elevated in hypertension, with larger increases during the dark (active) phase. At ZT4, urine output, Na^+, K^+, and water excretions are 90%, 72%, and 140%, respectively, higher in hypertension; at ZT16, the increases are 61%, 20%, and 58%, respectively. It is noteworthy that urinary Na^+ and volume peak at ZT18, a consequence of high SNGFR and low Na^+ transporter activities. The predicted patterns of Na^+ and water excretions align with experimental reports for normotensive and hypertensive mice [30].

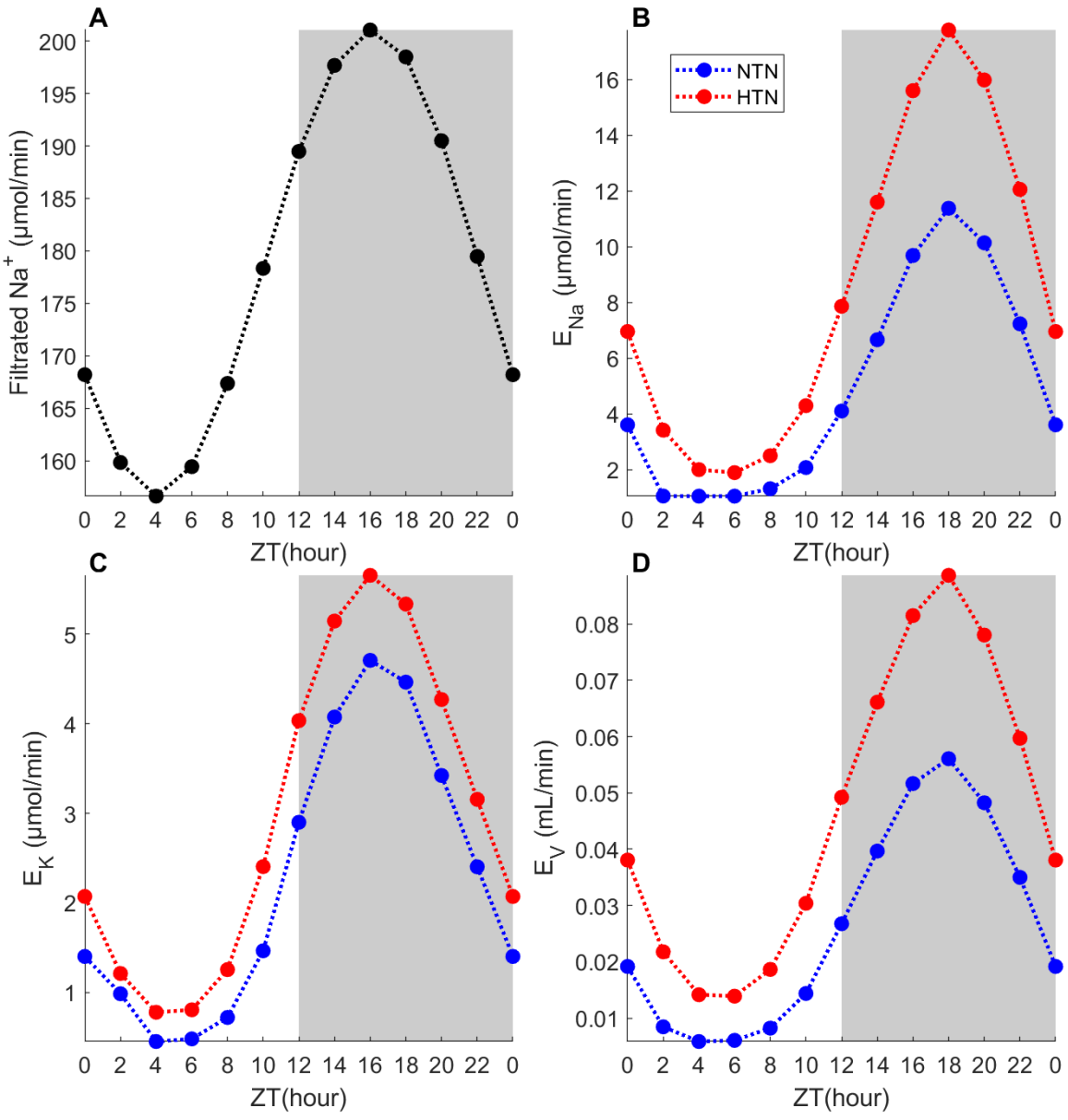


Figure 4.6: Na^+ inflow and Na^+, K^+, and water excretions. A, Estimated Na^+ inflow into the nephron for our model under both normotension and hypertension. B-D, Na^+, K^+, and water excretions under normotension (NTN) and hypertension (HTN). E_{Na}, Na^+ excretion; E_K, K^+ excretion; E_V, water excretion.

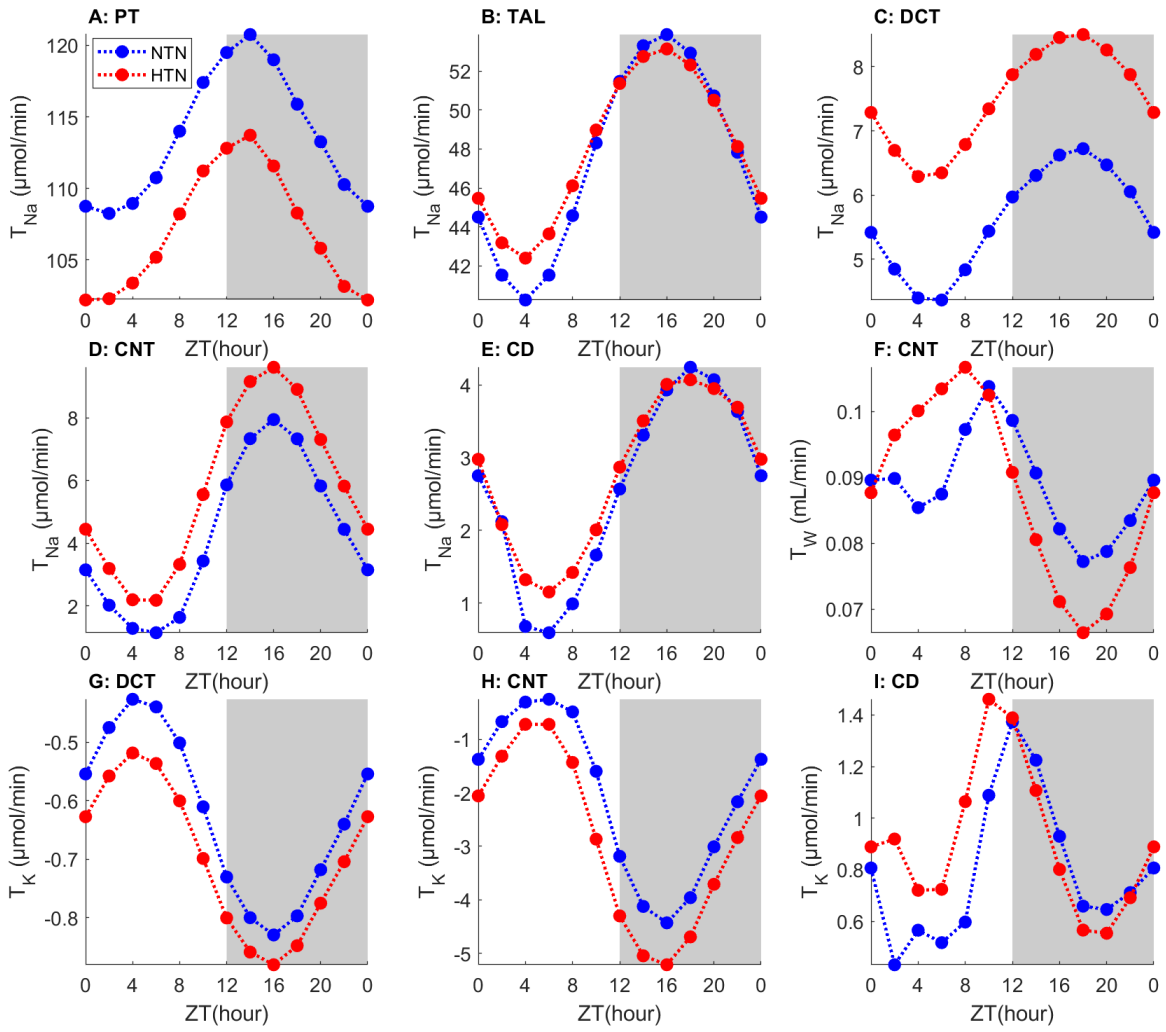


Figure 4.7: Comparison of segmental Na^+, K^+, and water transport under normotension (NTN) and hypertension (HTN). PT, proximal tubule; TAL, thick ascending limb; DCT, distal convoluted tubule; CNT, connecting tubule; CD, collecting duct. T_{Na}, Na^+ transport; T_K, K^+ transport; T_W, water transport.

4.2.4 Circadian Regulation of Diuretic Effects in Hypertension

Model simulations are then conducted to investigate the effects of administration time of loop, thiazide, and K^+-sparing diuretics on the function of a hypertensive rat kidney. Predicted segmental Na^+ transport and urinary excretion are shown in Fig. 4.8 for ZT4 and ZT16, which correspond to the trough and peak times in the simulated SNGFR. Analogous results for K^+ and water are shown in Figs. 4.9 and 4.10, respectively. As expected, each class of diuretics exerts the largest effect on Na^+ reabsorption along the primary segment that expresses the target transport: thick ascending limb for loop diuretics, distal convoluted tubule for thiazide diuretics, and connecting tubule and collecting duct for K^+-sparing diuretics. The lowered Na^+ reabsorption enhances natriuresis throughout the day, with the effect being larger during the active (dark) phase for all three diuretics. The dark phase is also when Na^+ reabsorption is higher in each of these segments; see Figs. 8B-8E. The ratio between urinary Na^+ excretion at ZT16 and ZT4 is approximately 6 for three diuretics (Fig. 4.8). The natriuretic effect is the largest for the K^+-sparing diuretics, for both ZT4 and ZT16 (Fig. 4.8F) because there are fewer segments downstream of its target site (connecting tubule and collecting duct) to compensate for the suppressed ENaC-mediated Na^+ reabsorption.

Consistent with Na^+ excretion, predicted urinary K^+ excretion is higher during the dark (active) phase, in both normotension and hypertension, with and without diuretics. Loop and thiazide diuretics both enhance K^+ excretion, with the increases (but not the actual excretions) somewhat larger during the light (inactive) phase. K^+-sparing diuretics essentially eliminate K^+ secretion along the CNT, in fact switching it to a small amount of net reabsorption during the light phase. As intended, K^+-sparing diuretics lowers K^+ excretion throughout the day, with the effect larger at ZT16 (-83%) than at ZT4 (-65%); see Fig. 4.9F.

Water transport essentially follows Na^+ transport along water-permeable segments. Thus, the predicted segmental water transport and urine output results are qualitatively similar to Na^+, with the diuretic effect predicted to be larger during the active (dark) phase; see Fig. 4.10. The diuretic effect is largest for loop diuretics, because it impairs the concentrating mechanism and lowers interstitial fluid osmolality, resulting in attenuated water reabsorption and elevated urine volume (Fig. 4.10F). This is true for both normotension and hypertension.

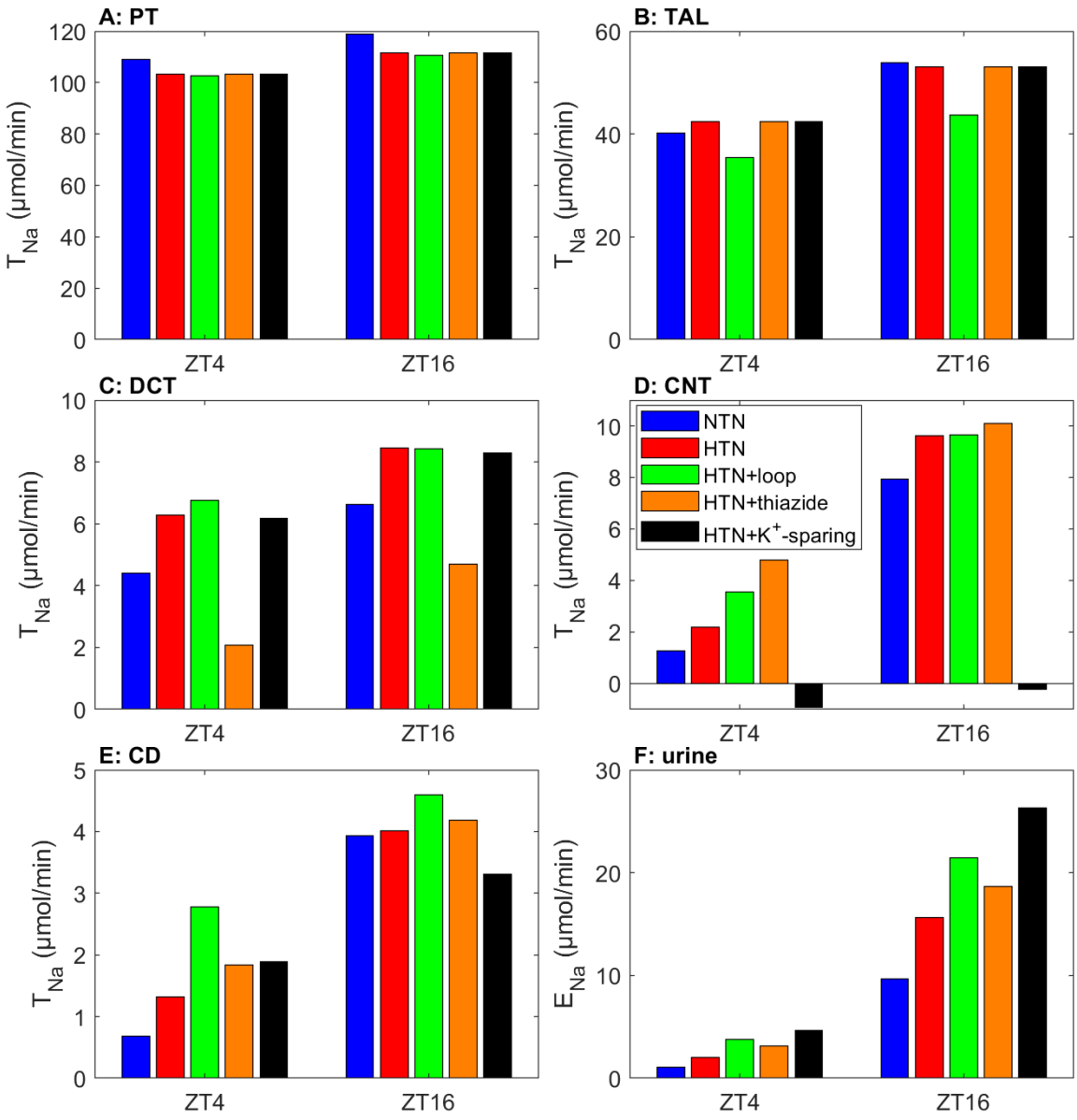


Figure 4.8: Comparison of Na^+ transport and excretion, obtained for ZT4 and ZT16, in normotension (NTN), hypertension (HTN), hypertension with loop diuretic administration (HTN+loop), hypertension with thiazide administration (HTN+thiazide), and hypertension with K^+-spring administration (HTN+K^+-sparing). PT, proximal tubule; TAL, thick ascending limb; DCT, distal convoluted tubule; CNT, connecting tubule; CD, collecting duct. TNa, Na^+ transport; ENa, Na^+ excretion.

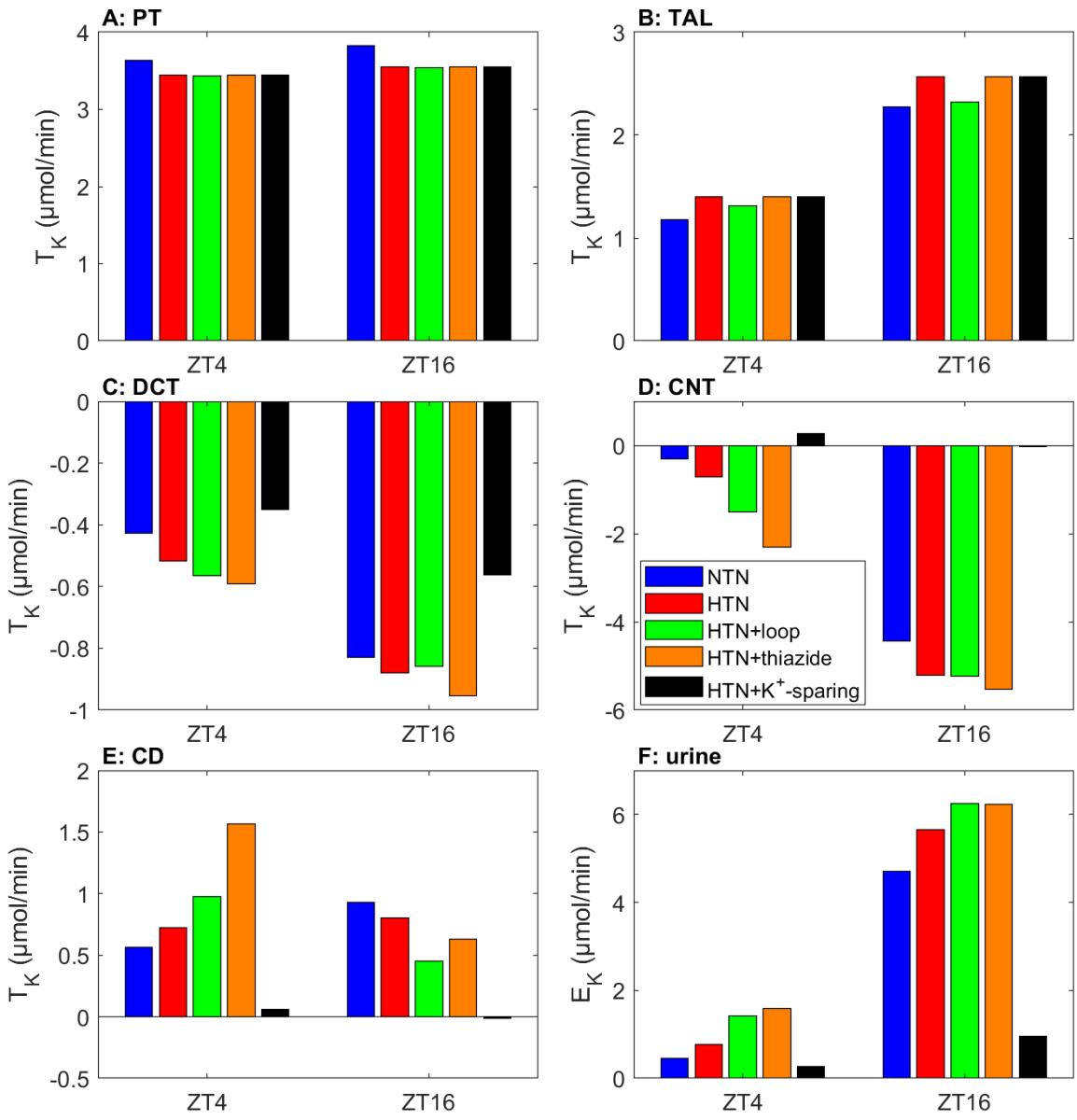


Figure 4.9: Comparison of K^+ transport and excretion, obtained for ZT4 and ZT16, in normotension (NTN), hypertension (HTN), hypertension with loop diuretic administration (HTN+loop), hypertension with thiazide administration (HTN+thiazide), and hypertension with K^+-spring administration (HTN+K^+-sparing). PT, proximal tubule; TAL, thick ascending limb; DCT, distal convoluted tubule; CNT, connecting tubule; CD, collecting duct. TK, K^+ transport; EK, K^+ excretion.

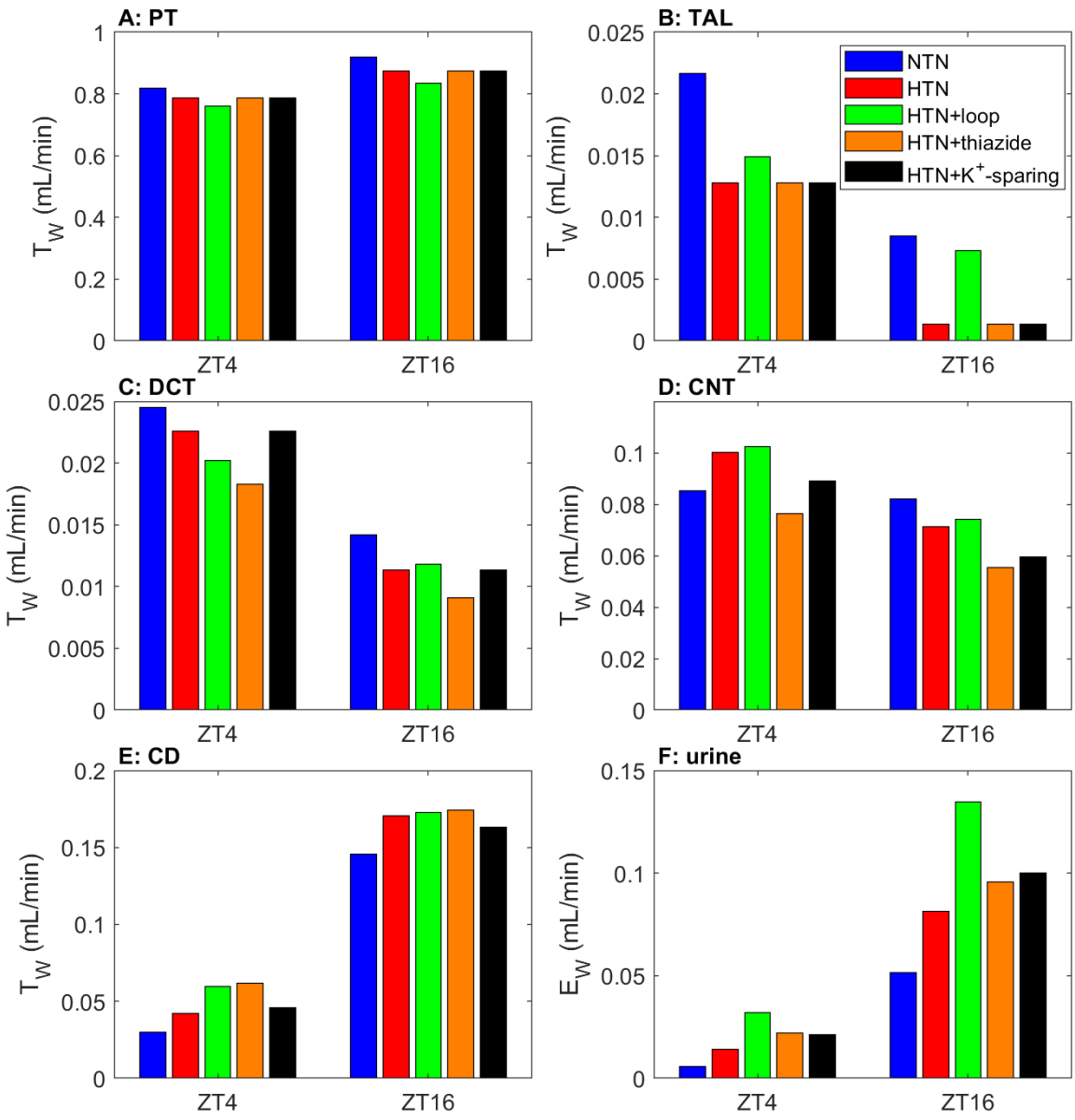


Figure 4.10: Comparison of water transport and excretion, obtained for ZT4 and ZT16, in normotension (NTN), hypertension (HTN), hypertension with loop diuretic administration (HTN+loop), hypertension with thiazide administration (HTN+thiazide), and hypertension with K^+-spring administration (HTN+K^+-sparing). PT, proximal tubule; TAL, thick ascending limb; DCT, distal convoluted tubule; CNT, connecting tubule; CD, collecting duct. TW, water transport; EW, water excretion.

Table 4.1: Peak time and relative amplitude of predicted mRNA oscillations in the kidneys of wild-type normotensive male rats. Relative amplitude is calculated as (peak - trough)/mean.

mRNA	**Peak time (ZT)**	**Relative amplitude**
Per1	10	91%
Per2	12	127%
Cry1	17	76%
Cry2	12	34%
Rev-Erb	20	140%
Ror	18	98%
Bmal1	10	160%
NHE3	11	32%
NKCC2	15	64%
SGLT1	11	21%
NCC	14	31%
ENaC	15	110%

Chapter 5

Conclusion

5.1 Physiological Implications

5.1.1 Sex Differences in AngII-induced Hypertension

In many mammalian and avian species, pre-menopausal females have a lower blood pressure and a lower prevalence of hypertension compared to age-matched males [127, 161]. This phenomenon is observed not only in humans but also in genetic models of hypertension, including spontaneously hypertensive rats and Dahl salt-sensitive rats, where males tend to experience hypertension at an earlier stage and with more severity than their female counterparts [109]. Despite these observations, the precise mechanisms responsible for these differences in blood pressure regulation between males and females remain inadequately elucidated. One of the suggested mechanisms underlying this sexual dimorphism is differences in the function of the RAAS. The RAAS is important in the regulation of body fluid and blood pressure homeostasis, and overactivation of the RAAS contributes to the development of numerous pathophysiological processes, notably, the development and progression of hypertension. There is an expanding literature regarding sex differences in the expression of RAAS components [94, 103, 53, 73], as well as in functional responses to RAAS activation to both acute and chronic AngII infusion [110].

A widely utilized experimental model of hypertension is the infusion of AngII via osmotic minipump at 400 ng/kg/min [87, 43, 166, 17]. The kidney's response to the chronic infusion of AngII, a Na^+-retaining hormone, is biphasic. In male rodents, 3-day low-dose infusion of AngII stimulates the activation of sodium transporters all along the nephron [104]. With continued AngII infusion, pressure natriuresis takes effect to reinstate fluid and

electrolyte homeostasis, whereby proximal and medullary NHE3 and medullary NKCC2 pool sizes decrease, while cortical NKCC2, NKCC2p, NCC, NCC-p, and cleaved ENaC subunits remain activated [105, 150]. Notably, the shift of Na^+ transport capacity to distal segments in AngII-induced hypertensive male rodents renders their transporter more similar to that of normotensive females, allowing for better fine-tuning of Na^+ transport. AngII infusion in female C57BL/6J mice amplified the baseline profile by decreasing the pool size of NHE3 and increasing the pool sizes of NCC and ENaC [150].

Model simulations indicate that this beneficial pattern, with the lower proximal and medullary thick ascending limb Na^+ transporter abundance along with enhanced distal and collecting duct transport capacity, facilitates pressure natriuresis by significantly suppressing proximal and medullary thick ascending limb Na^+ transport. Model simulations predict that fractional Na^+ transport along proximal tubule and medullary thick ascending limb in male and female rat nephrons decreases by approximately 10%. Most of that reduction can be attributed to the inhibition of NHE3 along the proximal tubule. Without that adaptation, the natriuretic effect would be much attenuated, with urinary Na^+ excretion decreased by more than 1/3 from the baseline hypertensive models (Figs. 3.4A1, 3.4A2).

Oxygen tension is lower in the renal medulla than in renal cortex [169]. AngII-induced vasoconstriction can lead to pathogenesis of pulmonary hypertension [47], which may result in hypoxemia [152]. Because tubular Na^+ reabsorption is a major contributor of oxygen consumption in kidney [82, 83], a partial redistribution of the workload required for Na^+ reabsorption from the renal medulla to the cortex may serve to avoid severe medullary hypoxia. Model simulations suggest that upregulation of ENaC and NCC shifts Na^+ reabsorption load from medullary segments (collecting duct) to cortical segments (distal convoluted tubule and connecting tubule); see Fig. 3.2.

Increased urinary Na^+ excretions are observed in both humans with essential hypertension [101, 64] and rodents with spontaneous [155] or AngII-induced hypertension [104, 150]. Model simulations predict that female rats with AngII-induced hypertension have smaller increase in urinary Na^+ excretions than that in male (Figs. 3.2A1, 3.2A2), consistent with findings in AngII infusion experiments [105, 150]. Model simulations suggest that difference may be attributed to the lower baseline NHE3 activity in females. When AngII infusion leads to a reduction of proximal tubule Na^+ transport, distal Na^+ flow is increased more in males, resulting in a stronger natriuretic effect. Indeed, females appear to be more resistant to AngII-induced hypertension, a sex difference that may be attributed to higher bioavailability of nitric oxide in females [163, 164] and a less reactive RAAS [65].

In separate studies, Edwards et al. applied computational models of epithelial transport in nephrons to study the impact of 14-day AngII infusion on the handling of Na^+ and K^+ in

male [34] and female [35] rats. Their simulations predict that in both sexes AngII infusion stimulates distal Na^+ reabsorption and K^+ secretion, and that a substantial downregulation of proximal tubule NHE3 is needed to reestablish Na^+ balance at 2 weeks. As discussed above, a similar downstream shift in Na^+ reabsorptive and K^+ secretive loads is seen in our simulation results. A comparison between the predicted urinary excretion (Fig. 3.4) indicates that the contribution of hypertension-induced downregulation of PT NHE3 activity to downstream shift of Na^+ transport is stronger in the hypertensive male model than female. When PT NHE3 activity was returned to the (higher) normotensive value, the male model predicted substantially lower urine output and Na^+ and K^+ excretion rates that are close to normotensive excretions (Fig. 3.4). In contrast, K^+ excretion in particular is notably higher than the normotensive excretion and closer to the hypertensive value in the female model (Figs. 3.4B1, 3.4B2). That sex difference can be attributed to the hypertension-induced transporter alterations in the PCT. In males, that is limited to a reduction in NHE3 activity, whereas in females, Na^+-K^+-ATPase and SGLT2 activities are also downregulated. Our simulations of the administration of diuretics on nephron transport in a hypertensive kidney indicate that the natriuretic and diuretic effects are generally stronger in females, consistent with experimental findings [21, 11, 12]; more below.

Loop diuretics.

Expressed on the apical membrane of the thick ascending limb and macula densa cells, NKCC2 can be inhibited by loop diuretics such as furosemide. Micropuncture studies by Hropot et al. [57] on male Sprague-Dawley rats reported an approximately four-fold increase in early distal Na^+ delivery after the administration of furosemide. Reyes reported that administration of furosemide to healthy adults yielded dose-dependent natriuresis [121]. In humans, dysfunction of NKCC2 in humans is linked to type 1 Bartter syndrome [132], a nephropathy that involves severe salt-wasting and the inability to generate concentrated urine. A mouse model of Bartter's syndrome exhibit polyuria [145]. Consistent with these observations, model simulations suggest that a partial (70%) inhibition of NKCC2 in normotension leads a substantial increase in early distal delivery of Na^+ (see Figs. 5.1A1, 5.1A2), resulting in approximately 0.67- to 1.4-fold increase in urinary Na^+ excretion. A completely inhibition of NKCC2 in normotension yields 8.6- to 18-fold increase in Na^+ excretion, coupled with a rise of approximately 2.0- to 4.3-fold in early distal Na^+ flow (see Figs. 5.2A1, 5.2A2). Alterations of segmental Na^+, K^+, and water transport are predicted to be similar in hypertension, with segmental transport shifted downstream, and a magnification of the natriuresis, diuresis, and kaliuresis induced in hypertension. Model simulations predict that the loop diuretics induced natriuretic response is stronger in hypertension than normotension, in both sexes. That is because of the downstream shift in Na^+

transport that is already present in hypertension; as a result, the distal segments are less able to reabsorb an elevated Na^+ load even with some transporter activities upregulated in hypertension.

Thiazide diuretics.

NCC plays a crucial role in kidney function, specifically electrolyte and fluid homeostasis by mediating Na^+ and Cl^- reabsorption in the initial segment of the distal convoluted tubule. Mutations in the NCC result in Gitelman syndrome, a salt-wasting disorder [147]. Given its major role in the regulation of salt, fluid, blood pressure, NCC is a target for a class of antihypertensive medications, thiazide diuretics [116]. Thiazide diuretics, an FDA-approved drug class, target NCC and impede the reabsorption of 3% to 5% of luminal Na^+ in the distal convoluted tubule of the nephron [3]. This action facilitates natriuresis and diuresis. Commonly utilized thiazide diuretics include hydrochlorothiazide (HCTZ), chlorthalidone, and indapamide [38].

Model simulations identify a notable sex difference: thiazide diuretics induce a stronger natriuretic response in normotensive and hypertensive females, compared to males. That prediction is consistent with the observed higher prevalence of hyponatremia in women taking thiazide diuretics compared to men [124, 131, 51]. That sex difference may be explained by the higher Na^+ transport already handled by the distal tubular segments in females (without thiazides). When NCC is inhibited, the other Na^+ transport pathways in the distal convoluted tubule and downstream segments are less able to further elevate their Na^+ transport to compensate.

Inhibition of NCC results in substantially increased delivery of Na^+ to the distal segment of the distal convoluted tubule and collecting tubule (Figs. 3.7A1, 3.8A1). The higher Na^+ flow enhances Na^+ reabsorption in the principal cells via ENaC on the apical membrane and the aldosterone-sensitive Na^+-K^+-ATPase pump on the basolateral membrane. The enhanced Na^+ flux generates an electrical potential favorable for K^+ secretion into the lumen. Model simulations predicted considerable increases in urinary K^+ excretion (Figs. 3.7B1, 3.7B2). Indeed, a drop in serum K^+ is a well-known effect of thiazide diuretics [102].

K^+-sparing diuretics.

The final adjustment of Na^+ reabsorption occurs along the distal segments, which include terminal segment of the distal convoluted tubule, the connecting tubule, and the collecting duct. Along these segments, Na^+ reabsorption is mediated by the amiloride-sensitive ENaC [44], located on the apical membrane. Loss-of-function mutations in ENaC occurs in pseudohypoaldosteronism type 1, the dominant form of which is very severe [19]. Gain-of-function mutations in ENaC leads to Liddle syndrome, which is characterized by

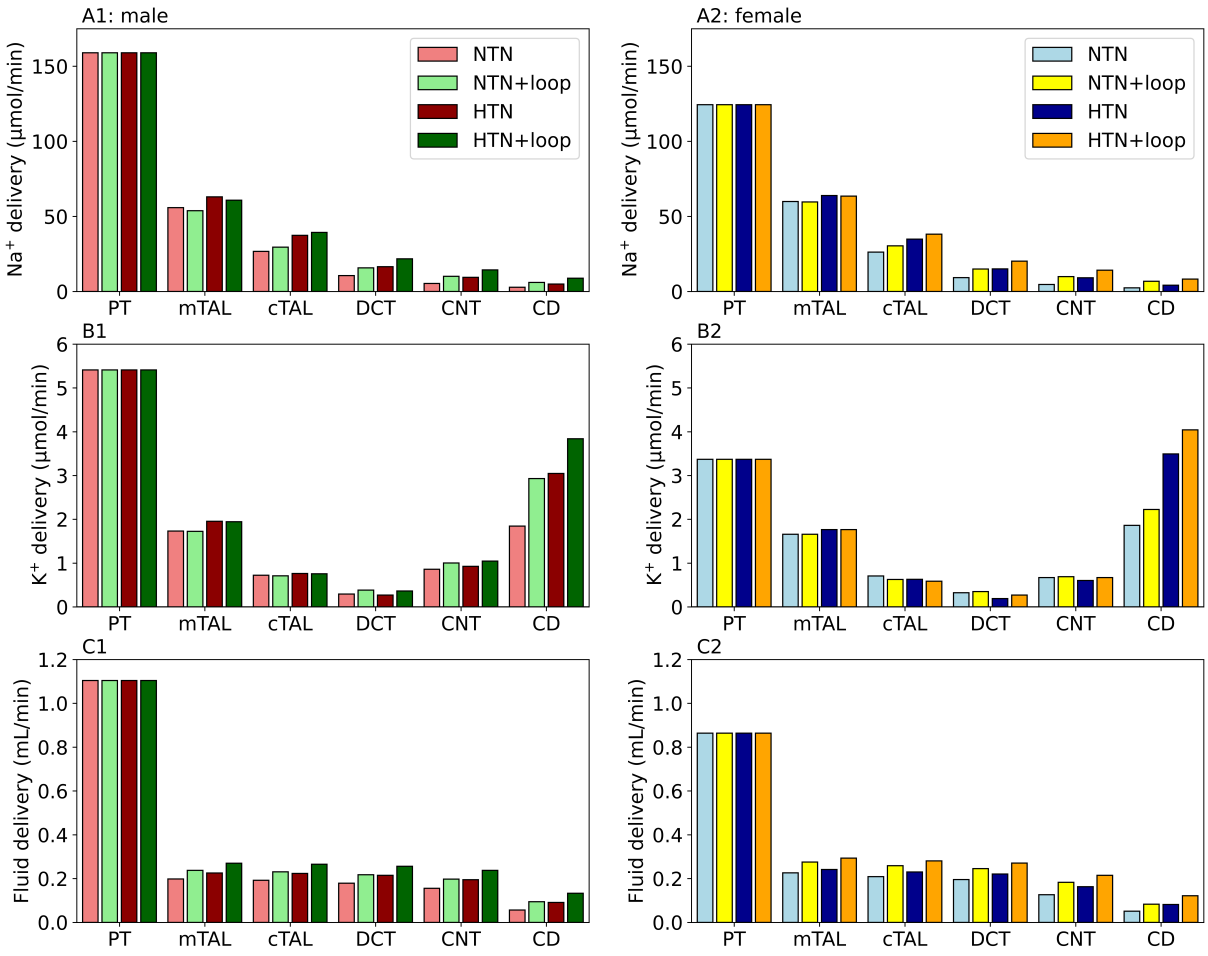


Figure 5.1: Segmental delivery of Na^+, K^+, and water for normotension (NTN), normotension with 70% NKCC2 inhibition (NTN+loop), hypertension (HTN), hypertension with 70% NKCC2 inhibition (HTN+loop). PT, proximal tubule; mTAL, medullary thick ascending limb; cTAL, cortical thick ascending limb; DCT, distal convoluted tubule; CNT, connecting tubule; CD, collecting duct.

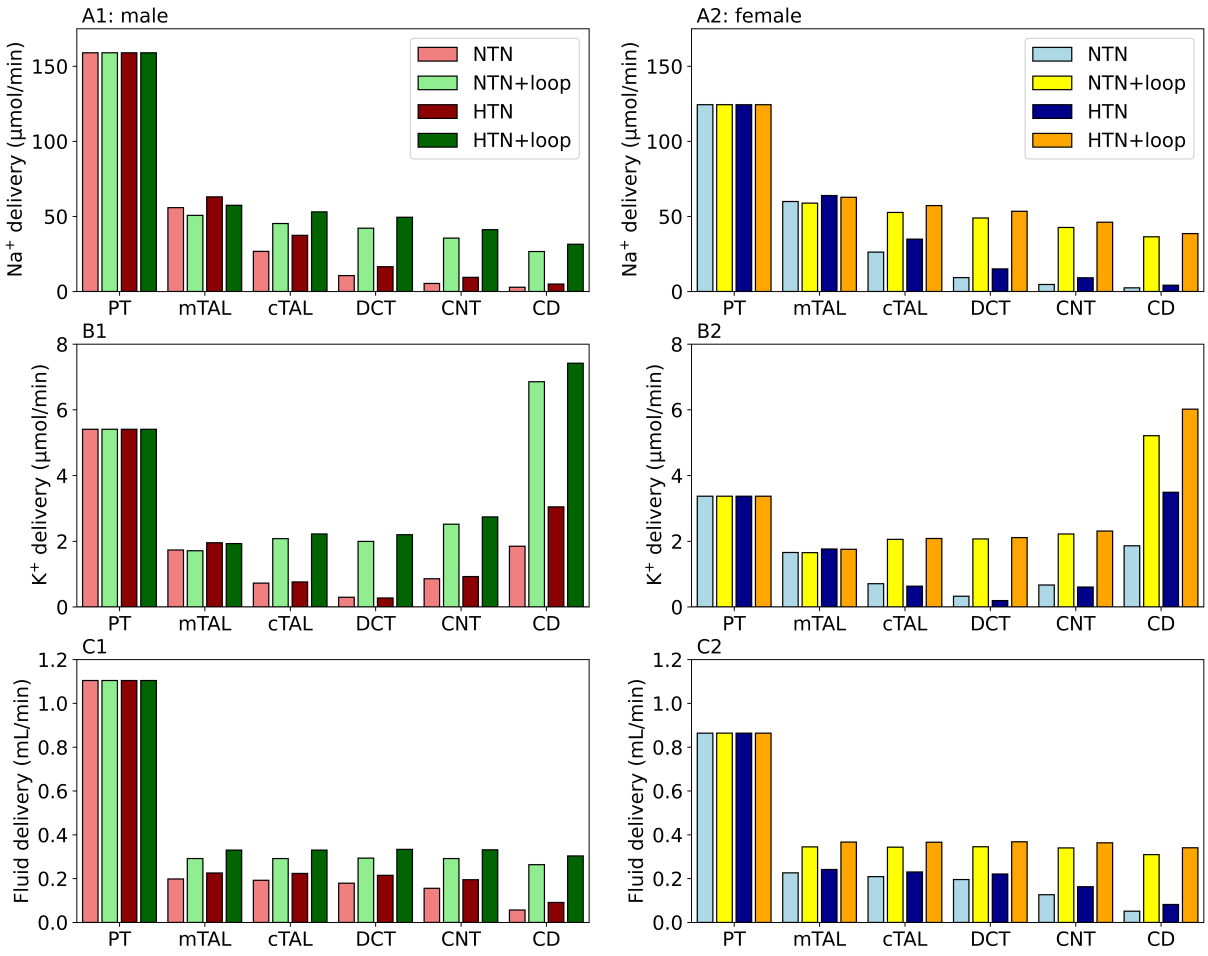


Figure 5.2: Segmental delivery of Na^+, K^+, and water for normotension (NTN), normotension with 100% NKCC2 inhibition (NTN+loop), hypertension (HTN), hypertension with 100% NKCC2 inhibition (HTN+loop). PT, proximal tubule; mTAL, medullary thick ascending limb; cTAL, cortical thick ascending limb; DCT, distal convoluted tubule; CNT, connecting tubule; CD, collecting duct.

hypertension and hypokalemic alkalosis associated with hypoaldosteronemia [1]. Both the hypertensive male and female models predict that the connecting tubule reabsorbs twice as Na^+ as much Na^+ as the corresponding normotensive models (Figs. 3.2A1, 3.2A2). Consequently, when the major Na^+ transport pathway is blocked, the natriuretic effect is predicted to be stronger in hypertension (Figs. 3.8A1, 3.8A2). Under most conditions, loop diuretics are K^+-wasting, and patients may require K^+ supplementation. Remarkably, Wang et al. [153] demonstrate that in mice fed a low-Na^+, high-K^+ diet, loop diuretics are K^+-sparing. Normally, K^+ is absorbed along the thick ascending limb. However, when the mice are fed a low-Na^+, high-K^+ diet, their thick ascending limb of these mice mediate significant K^+ secretion. That switch is driven by the elevated activities of NKCC2 and Renal Outer-Medullary K^+ channels (ROMK), which provide an electrochemical gradient that favors K^+ secretion, transforming loop diuretics into K^+-sparing agents.

5.1.2 Circadian Regulation in a Hypertensive Rat Kidney

Even though the occurrence of circadian rhythms is well known in several renal functions [67, 23], their clinical importance has yet to be completely understood. In both humans and rodents, disruption of the circadian rhythms, including changes in time zone, is associated with an increased risk of cardiovascular disease [119, 31]. Given the marked diurnal variations in urinary excretion, the plasma concentration or bioavailability of drugs that are eliminated by the kidneys might depend on the circadian expression of renal transporters, even if these drugs do not target renal transporters. The circadian rhythm is also known to affect the pathogenesis or progression of some renal diseases, such as renal tissue fibrosis [20] and kidney stones [133, 123]. The morbidity of patients with chronic kidney disease, as well as patients on hemodialysis or peritoneal dialysis, may be partially attributed to the disruption of the circadian rhythm of key renal functions [72, 125]. The circadian rhythm is followed by blood pressure in humans as well, with values 10–15% lower during nighttime than during daytime, in a phenomenon known as dipping [7]. The absence of a nocturnal blood pressure decrease (i.e., non-dipping) is associated with target organ damage [151]. The interactions among the central and peripheral clocks, and the organ and tissue systems, are intriguing and complex. What are the underlying mechanisms that lead to the emergence of circadian rhythms in these processes? For example, the determinants of blood pressure dipping and its disappearance has yet to be understood. What are the clinical implications of the disappearance of these circadian rhythms? And how should pharmacological treatments be timed to maximize their effectiveness?

As a step towards answering these questions, we developed a detailed computational model of the circadian regulation of epithelial transport in a rat kidney. Most published

modeling studies of nephron epithelial transport focus on steady-state results [60, 171, 80, 59, 139], with a few exceptions such as Refs. [79, 33, 32, 137], where the circadian regulation of key renal transporters is represented. A key difference between those published studies [79, 33] and the present model is that the former represent mouse kidneys, whereas the present model simulates a rat kidney. Also, the published studies [79, 33, 32, 137] prescribe the circadian oscillations of the transporter activities, whereas in the present study, transporter activities are computed based on circadian protein levels, which are predicted by a detailed computational model of the renal circadian clock that simulates the interactions among Per, Cry, Bmal1, Clock, Ror, and Rev-Erb. By modeling the clock explicitly, we are able to predict the effect of clock gene knockout on kidney function (see Fig. 4.1).

By modeling the renal circadian clock and its regulation of transporter activities, our model can predict the extent to which Na^+, K^+ and water transport by a nephron is modulated by the renal circadian clock. A similar renal circadian clock was developed in Ref. [107] to predict the circadian regulation of Na^+ and water transport by a proximal convoluted tubule cell. That model [107] does not differentiate between homologs of Per and Cry. However, Per1 and Per2 have been shown to exert opposite effects on NHE3 expression [126, 134]. Even though direct evidence is not currently available, it does not seem unreasonable to imagine that distinct roles of Per and Cry homologs on the circadian regulation of key renal transporters may be revealed in the future. Thus, the present model represents the Per and Cry homologs separately and allows the four protein complexes (PER1-CRY1, PER1-CRY2, PER2-CRY1, PER2-CRY2) to have different effects on transporter expression levels.

Emans et al. [37] reported that wild-type rats exhibit a circadian rhythm in kidney tissue oxygenation, with lower levels during the light phase and higher levels during the dark phase, peaking at ZT16.9. Kidney oxygenation is a result of the balance of oxygen delivery and consumption, which in turn are determined by renal hemodynamics and metabolism, respectively. In contrast to the 24-hour circadian rhythm in wild-types, SNGFR and thus Na^+ transport in Bmal1-knockout exhibit a double-peak, 12-hour rhythm (Fig. 4.4A). Given that renal metabolism is driven primarily by tubular active Na^+ transport, we hypothesize that renal tissue oxygenation in Bmal1-knockout exhibits a different rhythm, with a 12-hour period instead of 24.

In Ref. [171], we published the first computational model of epithelial transport in the kidney of a rat with hypertension. That model was formulated for steady state. With circadian rhythms incorporated, the present model predicts that due to pressure natriuresis, Na^+, K^+, and water transport is suppressed along the proximal tubule in the hypertensive rat, but is generally elevated along the distal segments (Fig. 4.7). These competing effects result in hypertension-enhanced natriuresis, diuresis, and kaliuresis throughout the day

(Fig. 4.6). The hypertensive kidney model allows us to investigate how administration time may impact the natriuretic and diuretic effects of diuretics in a rat with hypertension. In fact, while Dutta et al. simulated the administration of the same three classes of diuretics [33], they used a normotensive kidney. Our simulations indicate that effects of the diuretics are qualitatively similar in the normotensive and hypertensive kidneys (Fig. 4.8, 4.9, 4.10). All three diuretics yield stronger natriuretic and diuretic effects during the active phase, with K^+-sparing and loop diuretics producing the strongest natriuretic and diuretic effects, respectively (Figs. 4.8, 4.9).

5.2 Limitations and Future Work

The goal of this study is to develop computational tools for conducting in silico experiments to advance our understanding of the kidney's role in pathogenesis and treatments of hypertension. As we apply the models to conduct simulations and analyze data, it is important to understand and acknowledge their limitations. These limitations include the scarcity of direct measurements of transport activities, and the limited availability of experimental data at the cellular level, including details of intracellular signaling pathways, especially in female species [96]. Additionally, the current models represent a superficial nephron, which account for two-thirds of the total nephron population of a rat kidney [6]. Focus on the superficial nephron allows us to better understand the impact of hypertension-induced alternations in individual transporters. The rest of the nephrons are juxtamedullary one, which can be incorporated in a more comprehensive computational model of kidney function to provide more accurate predictions of whole-kidney function (e.g., Refs. [136, 61].

The present models are formulated for AngII-induced hypertension, which accounts for a disproportionally large fraction (nearly half) of published hypertension animal research studies [43]. Other forms of hypertension, e.g., genetic animal models of hypertension, mineralocortical-salt hypertension, L-NAME-induced hypertension, etc. likely have different effects on kidney function. However, sex-specific renal transporter measurements are mostly unavailable in these animal models. Furthermore, people with hypertension often suffer from other diseases such as diabetes, which induces renal hypertrophy, hyperfiltration, and alterations in transporter expression [59, 143]. Normal pregnancy is characterized by massive increases in plasma volume and electrolyte retention. In humans, GFR increases by 40–50% during pregnancy [8]; in rats, about 30% [159]. That marked increase in filtration matched by major adaptations in nephron transport, to avoid excessive water and electrolyte loss. How gestational hypertension modifies renal transporter pattern is now known. Understanding kidney function in pregnancy [138, 139] and hypertension may lead

to better treatment options for gestational hypertension and preeclampsia.

The effectiveness of an antihypertensive medication is typically measured by how much it lowers blood pressure. The kidney model used in the present study predicts urine output and excretions, but not extracellular fluid volume or blood pressure. Indeed, the present model does not include other key regulatory mechanisms in blood pressure regulation, such as the renin-angiotensin system, renal sympathetic nervous system, oxidative stress/nitric oxide pathway, and endothelin system. Some of these systems regulate blood pressure by acting on the kidneys. Furthermore, circadian oscillations in GFR and urinary excretion may impact the drug's excretion and pharmacokinetics. Thus, while diuresis and natriuresis, taken in isolation, would lower blood pressure, the picture is complicated by the contributions of the other systems noted above. To assess the time-of-day variations of the effectiveness of antihypertensive drugs, the present nephron models can be combined with whole-body blood pressure regulation models [85, 2]. The resulting integrative model would take into account the multiple feedback controls and correctly link natriuresis and diuresis to extracellular fluid volume and blood pressure.

Besides the circadian clock, sex is another key modulator of blood pressure regulation. Sex-based differences in blood pressure and its dysregulation have been observed across various mammalian and avian species [127]. Studies in animal models of hypertension, such as spontaneously hypertensive rats [62] and Dahl salt-sensitive rats [25], reveal that males tend to develop hypertension earlier and more severely than females. Similarly, premenopausal women typically exhibit lower blood pressure and a lower incidence of hypertension compared to men of the same age [161], although that female advantage vanishes in postmenopausal women over the age of 60. Sex differences are evident across organ and tissue systems that are involved in blood pressure regulation, collectively contributing to differences in blood pressure and hypertension between the sexes. The present model simulates kidney function in a male rat. Future studies should extend the circadian regulation model to a female rat kidney, followed by whole-body models of circadian regulation of blood pressure control in both sexes. Model simulations may yield insights into the mechanisms via which each transcription factor contributes to blood pressure phenotype, and explain any sex differences.

References

[1] Aamer Abbass, Jason D'Souza, Sameen Khalid, Fnu Asad-Ur-Rahman, Joseph Limback, Jeremy Burt, and Rajesh Shah. Liddle syndrome in association with aortic dissection. *Cureus*, 2017.

[2] Sameed Ahmed, Rui Hu, Jessica Leete, and Anita T. Layton. Understanding sex differences in long-term blood pressure regulation: insights from experimental studies and computational modeling. *American Journal of Physiology-Heart and Circulatory Physiology*, 316(5):H1113–H1123, 2019.

[3] Pegah Akbari and Arshia Khorasani-Zadeh. Thiazide diuretics. In *StatPearls*. StatPearls Publishing, 2023.

[4] Vijay B. Arumugham and Mohamed H. Shahin. Therapeutic uses of diuretic agents. In *StatPearls*. StatPearls Publishing, 2024.

[5] Mohammed Aufy, Ahmed M Hussein, Tamara Stojanovic, Christian R Studenik, and Mohamed H Kotob. Proteolytic activation of the epithelial sodium channel (enac): Its mechanisms and implications. *International Journal of Molecular Sciences*, 24(24):17563, 2023.

[6] L. Bankir and C. De Rouffignac. Urinary concentrating ability: insights from comparative anatomy. *American Journal of Physiology-Regulatory, Integrative and Comparative Physiology*, 249(6):R643–R666, 1985.

[7] Lise Bankir, Murielle Bochud, Marc Maillard, Pascal Bovet, Anne Gabriel, and Michel Burnier. Nighttime blood pressure and nocturnal dipping are associated with daytime urinary sodium excretion in african subjects. *Hypertension*, 51(4):891–898, 2008.

[8] Kelly Beers and Niralee Patel. Kidney physiology in pregnancy. *Advances in chronic kidney disease*, 27(6):449–454, 2020.

[9] Peter Bie. Mechanisms of sodium balance: total body sodium, surrogate variables, and renal sodium excretion. *American Journal of Physiology-Regulatory, Integrative and Comparative Physiology*, 315(5):R945–R962, 2018.

[10] Douglas L. Blowey. Diuretics in the treatment of hypertension. *Pediatric Nephrology*, 31(12):2223–2233, 2016.

[11] Anabel Brandoni, Silvina R. Villar, and Adriana M. Torres. Gender-related differences in the pharmacodynamics of furosemide in rats. *Pharmacology*, 70(2):107–112, 2004.

[12] Vadym Buncha, Alena Cherezova, Sati Alexander, Irina Baranovskaya, Kathleen A. Coleman, Mary Cherian-Shaw, Michael W. Brands, Jennifer C. Sullivan, Paul M. O'Connor, and Mykola Mamenko. Aldosterone antagonism is more effective at reducing blood pressure and excessive renal ENaC activity in AngII-infused female rats than in males. *Hypertension*, 80(10):2196–2208, 2023.

[13] Michel Burnier, George Bakris, and Bryan Williams. Redefining diuretics use in hypertension: why select a thiazide-like diuretic? *Journal of Hypertension*, 37(8):1574–1586, 2019.

[14] Paulo S Caceres and Pablo A Ortiz. Molecular regulation of NKCC2 in blood pressure control and hypertension. *Current opinion in nephrology and hypertension*, 28(5):474–480, 2019.

[15] Wen Cai, Juliette Rambaud, Michèle Teboul, Ingrid Masse, Gerard Benoit, Jan-Åke Gustafsson, Franck Delaunay, Vincent Laudet, and Ingemar Pongratz. Expression levels of estrogen receptor are modulated by components of the molecular clock. *Molecular and Cellular Biology*, 28(2):784–793, 2008.

[16] Hayo Castrop and Ina Maria Schießl. Physiology and pathophysiology of the renal Na-K-2Cl cotransporter (NKCC2). *American Journal of Physiology-Renal Physiology*, 307(9):F991–F1002, 2014.

[17] Graziela S. Ceravolo, Augusto C. Montezano, Maria T. Jordão, Eliana H. Akamine, Tiago J. Costa, Ana P. Takano, Denise C. Fernandes, Maria L. Barreto-Chaves, Francisco R. Laurindo, Rita C. Tostes, Zuleica B. Fortes, Renato P. Chopard, Rhian M. Touyz, and Maria Helena C. Carvalho. An interaction of renin-angiotensin and kallikrein-kinin systems contributes to vascular hypertrophy in angiotensin II-induced hypertension: In vivo and in vitro studies. *PLoS ONE*, 9(11):e111117, 2014.

[18] Hangil Chang and Toshiro Fujita. A numerical model of the renal distal tubule. *American Journal of Physiology-Renal Physiology*, 276(6):F931–F951, 1999.

[19] Sue S. Chang, Stefan Grunder, Aaron Hanukoglu, Ariel Rösler, P.M. Mathew, Israel Hanukoglu, Laurent Schild, Yin Lu, Richard A. Shimkets, Carol Nelson-Williams, Bernard C. Rossier, and Richard P. Lifton. Mutations in subunits of the epithelial sodium channel cause salt wasting with hyperkalaemic acidosis, pseudohypoaldosteronism type 1. *Nature Genetics*, 12(3):248–253, 1996.

[20] Wei-Dar Chen, Jih-Kai Yeh, Meng-Ting Peng, Shian-Sen Shie, Shuei-Liong Lin, Chia-Hung Yang, Tien-Hsing Chen, Kuo-Chun Hung, Chun-Chieh Wang, I-Chang Hsieh, Ming-Shien Wen, and Chao-Yung Wang. Circadian CLOCK mediates activation of transforming growth factor- signaling and renal fibrosis through cyclooxygenase 2. *The American Journal of Pathology*, 185(12):3152–3163, 2015.

[21] Z Chen, D A Vaughn, and D D Fanestil. Influence of gender on renal thiazide diuretic receptor density and response. *Journal of the American Society of Nephrology*, 5(4):1112–1119, 1994.

[22] R.G. Contreras, A. Torres-Carrillo, C. Flores-Maldonado, L. Shoshani, and A. Ponce. Na^+/K^+-atpase: More than an electrogenic pump. *International Journal of Molecular Sciences*, 25(11):6122, June 2024.

[23] Hannah M. Costello, Jermaine G. Johnston, Alexandria Juffre, G. Ryan Crislip, and Michelle L. Gumz. Circadian clocks of the kidney: function, mechanism, and regulation. *Physiological Reviews*, 102(4):1669–1701, 2022.

[24] G Ryan Crislip, Lauren G Douma, Sarah H Masten, Kit-Yan Cheng, I Jeanette Lynch, Jermaine G Johnston, Dominique Barral, Krystal B Glasford, Meaghan R Holzworth, Jill W Verlander, et al. Differences in renal bmal1 contribution to na+ homeostasis and blood pressure control in male and female mice. *American Journal of Physiology-Renal Physiology*, 318(6):F1463–F1477, 2020.

[25] L K Dahl, K D Knudsen, E V Ohanian, M Muirhead, and R Tuthill. Role of the gonads in hypertension-prone rats. *The Journal of experimental medicine*, 142(3):748–759, 1975.

[26] Rajeev Dalal, Zachary S Bruss, and Jasjit S Sehdev. Physiology, renal blood flow and filtration. 2018.

[27] Bradley M. Denker and Eduardo Sabath. The biology of epithelial cell tight junctions in the kidney. *Journal of the American Society of Nephrology*, 22(4):622–625, April 2011.

[28] Stephen P DiBartola. *Fluid, electrolyte, and acid-base disorders in small animal practice*. Elsevier Health Sciences, 2011.

[29] Jessica A. Dominguez Rieg and Timo Rieg. New functions and roles of the Na+-H+-exchanger NHE3. *Pflügers Archiv - European Journal of Physiology*, 476(4):505–516, 2024.

[30] Lauren G. Douma, Hannah M. Costello, G. Ryan Crislip, Kit-Yan Cheng, I. Jeanette Lynch, Alexandria Juffre, Dominique Barral, Sarah Masten, Emilio Roig, Kevin Beguiristain, Wendy Li, Phillip Bratanatawira, Charles S. Wingo, and Michelle L. Gumz. Kidney-specific KO of the circadian clock protein PER1 alters renal Na^+ handling, aldosterone levels, and kidney/adrenal gene expression. *American Journal of Physiology-Renal Physiology*, 322(4):F449–F459, 2022.

[31] Lauren G. Douma and Michelle L. Gumz. Circadian clock-mediated regulation of blood pressure. *Free Radical Biology & Medicine*, 119:108–114, 2018.

[32] Pritha Dutta and Anita T. Layton. Sex and circadian regulation of metabolic demands in the rat kidney: A modeling analysis. *PLOS ONE*, 19(7):e0293419, 2024.

[33] Pritha Dutta, Mehrshad Sadria, and Anita T. Layton. Influence of administration time and sex on natriuretic, diuretic, and kaliuretic effects of diuretics. *American Journal of Physiology-Renal Physiology*, 324(3):F274–F286, 2023.

[34] Aurélie Edwards and Alicia A. McDonough. Impact of angiotensin II-mediated stimulation of sodium transporters in the nephron assessed by computational modeling. *American Journal of Physiology-Renal Physiology*, 317(6):F1656–F1668, 2019.

[35] Aurélie Edwards, Donna L. Ralph, Adriana Mercado, and Alicia A. McDonough. Angiotensin II hypertension along the female rat tubule: predicted impact on coupled transport of Na^+ and k $^+$. *American Journal of Physiology-Renal Physiology*, page ajprenal.00232.2023, 2023.

[36] Ghazi El Mernissi, Catherine Barlet-Bas, Chakir Khadouri, Sophie Marsy, Lydie Cheval, and Alain Doucet. Characterization and localization of ouabain-insensitive Na-dependent atpase activities along the rat nephron. *Biochimica et Biophysica Acta (BBA)-Biomembranes*, 1064(2):205–211, 1991.

[37] Tonja W. Emans, Ben J. Janssen, Jaap A. Joles, and C. T. Paul Krediet. Circadian rhythm in kidney tissue oxygenation in the rat. *Frontiers in Physiology*, 8, 2017.

[38] Michael E Ernst and Michelle A Fravel. Thiazide and the thiazide-like diuretics: Review of hydrochlorothiazide, chlorthalidone, and indapamide. *American Journal of Hypertension*, 35(7):573–586, 2022.

[39] Michael E. Ernst and Samuel J. Mann. Diuretics in the treatment of hypertension. *Seminars in Nephrology*, 31(6):495–502, 2011.

[40] Joseph Feher. 7.2-functional anatomy of the kidneys and overview of kidney function. *Quantitative Human Physiology. Boston, MA: Academic*, pages 626–632, 2012.

[41] Eric Feraille and Alain Doucet. Sodium-potassium-adenosinetriphosphatase-dependent sodium transport in the kidney: hormonal control. *Physiological reviews*, 81(1):345–418, 2001.

[42] Dmitri Firsov and Olivier Bonny. Circadian rhythms and the kidney. *Nature Reviews Nephrology*, 14(10):626–635, 2018.

[43] Zorina S. Galis, Terry Thrasher, Diane M. Reid, Dennis V. Stanley, and Young S. Oh. Investing in high blood pressure research: A national institutes of health perspective. *Hypertension*, 61(4):757–761, 2013.

[44] Luciano Galizia, Alejandro Ojea, and Basilio A. Kotsias. [amiloride sensitive sodium channels (ENaC) and their regulation by proteases]. *Medicina*, 71(2):179–182, 2011.

[45] Michelle L. Gumz, Kit-Yan Cheng, I. Jeanette Lynch, Lisa R. Stow, Megan M. Greenlee, Brian D. Cain, and Charles S. Wingo. Regulation of ENaC expression by the circadian clock protein period 1 in mpkCCDc14 cells. *Biochimica et Biophysica Acta (BBA) - Gene Regulatory Mechanisms*, 1799(9):622–629, 2010.

[46] M. A. Gurney, D. Laubitz, F. K. Ghishan, and P. R. Kiela. Pathophysiology of intestinal Na^+/h^+ exchange. *Cellular and Molecular Gastroenterology and Hepatology*, 3(1):27–40, January 2017.

[47] Charaka M. Hadinnapola, Mark Southwood, Jules Hernández – Sánchez, Katherine Bunclark, Michael Newnham, Emilia M. Swietlik, John Cannon, Stephen D. Preston, Karen Sheares, Dolores Taboada, Nicholas Screaton, David P. Jenkins, Nicholas W. Morrell, Mark Toshner, and Joanna Pepke-Zaba. Angiopoietin 2 and hsCRP are associated with pulmonary hemodynamics and long-term mortality respectively in

CTEPH—results from a prospective discovery and validation biomarker study. *The Journal of Heart and Lung Transplantation*, 42(3):398–405, 2023.

[48] L Lee Hamm, Zhuang Feng, and Kathleen S Hering-Smith. Regulation of sodium transport by enac in the kidney. *Current opinion in nephrology and hypertension*, 19(1):98–105, 2010.

[49] David G Harrison, Thomas M Coffman, and Christopher S Wilcox. Pathophysiology of hypertension: the mosaic theory and beyond. *Circulation research*, 128(7):847–863, 2021.

[50] Hiddo JL Heerspink, Ton Rabelink, and Dick de Zeeuw. Pathophysiology of proteinuria: Albuminuria as a target for treatment. *Chronic Renal Disease*, pages 211–224, 2020.

[51] Linda C Hendriksen, Paul D van der Linden, Ron MC Herings, Bruno H Stricker, and Loes E Visser. Women on diuretics have a higher risk of hospital admission because of hyponatremia than men. *Pharmacoepidemiology and drug safety*, 32(6):635–642, 2023.

[52] Balraj S Heran, Jenny MH Chen, Josh J Wang, and James M Wright. Blood pressure lowering efficacy of potassium-sparing diuretics (that block the epithelial sodium channel) for primary hypertension. *Cochrane Database of Systematic Reviews*, (1), 2010.

[53] Lucinda M. Hilliard, Amanda K. Sampson, Russell D. Brown, and Kate M. Denton. The "his and hers" of the renin-angiotensin system. *Current Hypertension Reports*, 15(1):71–79, 2013.

[54] Sato Honma. The mammalian circadian system: a hierarchical multi-oscillator structure for generating circadian rhythm. *The Journal of Physiological Sciences*, 68(3):207–219, 2018.

[55] Ewout J Hoorn, Martin Gritter, Catherina A Cuevas, and Robert A Fenton. Regulation of the renal nacl cotransporter and its role in potassium homeostasis. *Physiological reviews*, 100(1):321–356, 2020.

[56] Shoichiro Horita, Masayuki Nakamura, Masaki Suzuki, Naoya Satoh, Ayako Suzuki, Yoshio Homma, and Masaomi Nangaku. The role of renal proximal tubule transport in the regulation of blood pressure. *Kidney Research and Clinical Practice*, 36(1):12–21, March 2017.

[57] Max Hropot, Nicole Fowler, Bertil Karlmark, and Gerhard Giebisch. Tubular action of diuretics: Distal effects on electrolyte transport and acidification. *Kidney International*, 28(3):477–489, 1985.

[58] Lufei Hu, Daniel F. Catanzaro, Tina-Marie Pitarresi, John H. Laragh, and Jean E. Sealey. Identical hemodynamic and hormonal responses to 14-day infusions of renin or angiotensin II in conscious rats:. *Journal of Hypertension*, 16(9):1285–1298, 1998.

[59] Rui Hu and Anita Layton. A computational model of kidney function in a patient with diabetes. *International Journal of Molecular Sciences*, 22(11):5819, 2021.

[60] Rui Hu, Alicia A. McDonough, and Anita T. Layton. Functional implications of the sex differences in transporter abundance along the rat nephron: modeling and analysis. *American Journal of Physiology-Renal Physiology*, 317(6):F1462–F1474, 2019.

[61] Rui Hu, Alicia A. McDonough, and Anita T. Layton. Sex differences in solute transport along the nephrons: effects of Na^+ transport inhibition. *American Journal of Physiology-Renal Physiology*, 319(3):F487–F505, 2020.

[62] S. G. Iams and B. C. Wexler. Retardation in the development of spontaneous hypertension in SH rats by gonadectomy. *The Journal of Laboratory and Clinical Medicine*, 90(6):997–1003, 1977.

[63] Kazuo Itoh, Yasuhisa Izumi, Toshiyuki Inoue, Hiroki Inoue, Yosuke Nakayama, Takahiro Uematsu, Toshihiro Fukuyama, Takeshi Yamazaki, Yoshiyuki Yasuoka, Tetsuya Makino, Yoshinori Nagaba, Katsuyuki Tomita, Norio Kobayashi, Kazuhiro Kawahara, Masashi Mukoyama, and Hiroshi Nonoguchi. Expression of three isoforms of Na-K-2Cl cotransporter (NKCC2) in the kidney and regulation by dehydration. *Biochemical and Biophysical Research Communications*, 453(3):356–361, October 2014.

[64] Sandra L. Jackson, Mary E. Cogswell, Lixia Zhao, Ana L. Terry, Chia-Yih Wang, Jacqueline Wright, Sallyann M. Coleman King, Barbara Bowman, Te-Ching Chen, Robert Merritt, and Catherine M. Loria. Association between urinary sodium and potassium excretion and blood pressure among adults in the united states: National health and nutrition examination survey, 2014. *Circulation*, 137(3):237–246, 2018.

[65] Hong Ji, Wei Zheng, Xie Wu, Jun Liu, Carolyn M. Ecelbarger, Rebecca Watkins, Arthur P. Arnold, and Kathryn Sandberg. Sex chromosome effects unmasked in angiotensin II–induced hypertension. *Hypertension*, 55(5):1275–1282, 2010.

[66] Jermaine G. Johnston, Joshua S. Speed, Bryan K. Becker, Malgorzata Kasztan, Reham H. Soliman, Megan K. Rhoads, Binli Tao, Chunhua Jin, Aron M. Geurts, Kelly A. Hyndman, Jennifer S. Pollock, and David M. Pollock. Diurnal control of blood pressure is uncoupled from sodium excretion. *Hypertension*, 75(6):1624–1634, 2020.

[67] Alexandria Juffre and Michelle L. Gumz. Recent advances in understanding the kidney circadian clock mechanism. *American Journal of Physiology-Renal Physiology*, 326(3):F382–F393, 2024.

[68] Aharon Katchalsky and Peter F Curran. *Nonequilibrium thermodynamics in biophysics*. Harvard University Press, 1965.

[69] Mark A Knepper, Tae-Hwan Kwon, and Soren Nielsen. Molecular physiology of water balance. *New England Journal of Medicine*, 372(14):1349–1358, 2015.

[70] Benjamin Ko, Abinash Mistry, Lauren Hanson, Rickta Mallick, and Robert S Hoover. Mechanisms of angiotensin ii stimulation of ncc are time-dependent in mdct15 cells. *American Journal of Physiology-Renal Physiology*, 308(7):F720–F727, 2015.

[71] Benjamin Ko, Abinash C Mistry, Lauren Hanson, Rickta Mallick, Brandi M Wynne, Tiffany L Thai, James L Bailey, Janet D Klein, and Robert S Hoover. Aldosterone acutely stimulates ncc activity via a spak-mediated pathway. *American Journal of Physiology-Renal Physiology*, 305(5):F645–F652, 2013.

[72] Birgit C.P. Koch, J. Elsbeth Nagtegaal, E. Christiaan Hagen, Pieter M. Ter Wee, and Gerard A. Kerkhof. Different melatonin rhythms and sleep–wake rhythms in patients on peritoneal dialysis, daytime hemodialysis and nocturnal hemodialysis. *Sleep Medicine*, 11(3):242–246, 2010.

[73] Kimiaki Komukai, Seibu Mochizuki, and Michihiro Yoshimura. Gender and the renin–angiotensin–aldosterone system. *Fundamental & Clinical Pharmacology*, 24(6):687–698, 2010.

[74] Halla Krid, Aude Dorison, Amel Salhi, Lydie Cheval, and Gilles Crambert. Expression profile of nuclear receptors along male mouse nephron segments reveals a link between ERR and thick ascending limb function. *PLoS ONE*, 7(3):e34223, 2012.

[75] Ivana Y Kuo and Barbara E Ehrlich. Ion channels in renal disease. *Chemical reviews*, 112(12):6353–6372, 2012.

[76] Lucas Lauder, Felix Mahfoud, Michel Azizi, Deepak L Bhatt, Sebastian Ewen, Kazuomi Kario, Gianfranco Parati, Patrick Rossignol, Markus P Schlaich, Koon K Teo, Raymond R Townsend, Costas Tsioufis, Michael A Weber, Thomas Weber, and Michael Böhm. Hypertension management in patients with cardiovascular comorbidities. *European Heart Journal*, 44(23):2066–2077, 2023.

[77] Anita T Layton. A complete set of equations for a computational model of electrolyte and water transport along the nephrons in a mammalian kidney. *bioRxiv*, 2022.

[78] Anita T Layton and Aurélie Edwards. *Mathematical modeling in renal physiology*, volume 862. Springer, 2014.

[79] Anita T. Layton and Michelle L. Gumz. Sex differences in circadian regulation of kidney function of the mouse. *American Journal of Physiology-Renal Physiology*, 323(6):F675–F685, 2022.

[80] Anita T. Layton, Kamel Laghmani, Volker Vallon, and Aurélie Edwards. Solute transport and oxygen consumption along the nephrons: effects of Na $^+$ transport inhibitors. *American Journal of Physiology-Renal Physiology*, 311(6):F1217–F1229, 2016.

[81] Anita T Layton and Harold E Layton. A computational model of epithelial solute and water transport along a human nephron. *PLoS computational biology*, 15(2):e1006108, 2019.

[82] Anita T. Layton, Volker Vallon, and Aurélie Edwards. Modeling oxygen consumption in the proximal tubule: effects of NHE and SGLT2 inhibition. *American Journal of Physiology-Renal Physiology*, 308(12):F1343–F1357, 2015.

[83] Anita T. Layton, Volker Vallon, and Aurélie Edwards. A computational model for simulating solute transport and oxygen consumption along the nephrons. *American Journal of Physiology-Renal Physiology*, 311(6):F1378–F1390, 2016.

[84] David BN Lee, Edmund Huang, and Harry J Ward. Tight junction biology and kidney dysfunction. *American Journal of Physiology-Renal Physiology*, 290(1):F20–F34, 2006.

[85] Jessica Leete and Anita T. Layton. Sex-specific long-term blood pressure regulation: Modeling and analysis. *Computers in Biology and Medicine*, 104:139–148, 2019.

[86] Jean-Christophe Leloup and Albert Goldbeter. Toward a detailed computational model for the mammalian circadian clock. *Proceedings of the National Academy of Sciences*, 100(12):7051–7056, 2003.

[87] Lilach O Lerman, Theodore W Kurtz, Rhian M Touyz, David H Ellison, Alejandro R Chade, Steven D Crowley, David L Mattson, John J Mullins, Jeffrey Osborn, Alfonso Eirin, et al. Animal models of hypertension: a scientific statement from the american heart association. *Hypertension*, 73(6):e87–e120, 2019.

[88] Franziska Limmer, Elisabeth Schinner, Hayo Castrop, Helga Vitzthum, Franz Hofmann, and Jens Schlossmann. Regulation of the Na+-K+-2Cl- cotransporter by c gmp/c gmp-dependent protein kinase i after furosemide administration. *The FEBS Journal*, 282(19):3786–3798, 2015.

[89] Johannes Loffing and Christoph Korbmacher. Regulated sodium transport in the renal connecting tubule (CNT) via the epithelial sodium channel (ENaC). *Pflügers Archiv - European Journal of Physiology*, 458(1):111–135, 2009.

[90] Yiyun Lou, Fan Zhang, Yuqin Luo, Liya Wang, Shisi Huang, and Fan Jin. Serum and glucocorticoid regulated kinase 1 in sodium homeostasis. *International journal of molecular sciences*, 17(8):1307, 2016.

[91] David Makanjuola and Marta Lapsley. The kidneys, renal function and kidney disease. In *Clinical Biochemistry: Metabolic and Clinical Aspects*, pages 124–151. Churchill Livingstone, 2014.

[92] Mariano Marcano, Hun-Mo Yang, Aniel Nieves-González, Chris Clausen, and Leon C Moore. Parameter estimation for mathematical models of NKCC2 cotransporter isoforms. *American Journal of Physiology-Renal Physiology*, 296(2):F369–F381, 2009.

[93] A. A. Marcoux, L. E. Tremblay, S. Slimani, M. J. Fiola, F. Mac-Way, A. P. Garneau, and P. Isenring. Molecular characteristics and physiological roles of Na^+-K^+-Cl^- cotransporter 2. *Journal of Cellular Physiology*, 236(3):1712–1729, March 2021.

[94] Christine Maric-Bilkan and Michaele B. Manigrasso. Sex differences in hypertension: Contribution of the renin–angiotensin system. *Gender Medicine*, 9(4):287–291, 2012.

[95] Vítor M. Martins, Patrícia K. Ziegelmann, Filipe Ferrari, Leonardo G. Bottino, Marcelo B. Lucca, Henrique L. Ruchaud Corrêa, Gabriela B. Blum, Lucas Helal, Sandra C. Fuchs, and Flávio D. Fuchs. Thiazide diuretics alone or combined with potassium-sparing diuretics to treat hypertension: a systematic review and network

meta-analysis of randomized controlled trials. *Journal of Hypertension*, 41(7):1108–1116, 2023.

[96] Alicia A. McDonough, Autumn N. Harris, Lingyun Xiong, and Anita T. Layton. Sex differences in renal transporters: assessment and functional consequences. *Nature Reviews Nephrology*, 2023.

[97] Alicia A. McDONOUGH, Patrick K. K. Leong, and Li E. Yang. Mechanisms of pressure natriuresis: How blood pressure regulates renal sodium transport. *Annals of the New York Academy of Sciences*, 986(1):669–677, 2003.

[98] Robert S McMahon, Dana Penfold, and Khalid Bashir. Anatomy, abdomen and pelvis: kidney collecting ducts. In *StatPearls [Internet]*. StatPearls publishing, 2024.

[99] RS McMahon, D Penfold, and K Bashir. *Anatomy, Abdomen and Pelvis: Kidney Collecting Ducts*. StatPearls Publishing, Treasure Island (FL), 2024. [Updated 2024 May 1].

[100] Joseph Meltzer. Chapter 32 - renal physiology. In Hugh C. Hemmings and Talmage D. Egan, editors, *Pharmacology and Physiology for Anesthesia*, pages 561–573. W.B. Saunders, 2013.

[101] Andrew Mente, Martin J. O'Donnell, Sumathy Rangarajan, Matthew J. McQueen, Paul Poirier, Andreas Wielgosz, Howard Morrison, Wei Li, Xingyu Wang, Chen Di, Prem Mony, Anitha Devanath, Annika Rosengren, Aytekin Oguz, Katarzyna Zatonska, Afzal Hussein Yusufali, Patricio Lopez-Jaramillo, Alvaro Avezum, Noorhassim Ismail, Fernando Lanas, Thandi Puoane, Rafael Diaz, Roya Kelishadi, Romaina Iqbal, Rita Yusuf, Jephat Chifamba, Rasha Khatib, Koon Teo, and Salim Yusuf. Association of urinary sodium and potassium excretion with blood pressure. *New England Journal of Medicine*, 371(7):601–611, 2014.

[102] D B Morgan and C Davidson. Hypokalaemia and diuretics: an analysis of publications. *BMJ*, 280(6218):905–908, 1980.

[103] K.M. Moritz, J.S.M. Cuffe, L.B. Wilson, H. Dickinson, M.E. Wlodek, D.G. Simmons, and K.M. Denton. Review: Sex specific programming: A critical role for the renal renin–angiotensin system. *Placenta*, 31:S40–S46, 2010.

[104] Mien T. X. Nguyen, Jiyang Han, Donna L. Ralph, Luciana C. Veiras, and Alicia A. McDonough. Short-term nonpressor angiotensin II infusion stimulates sodium transporters in proximal tubule and distal nephron. *Physiological Reports*, 3(9):e12496, 2015.

[105] Mien T. X. Nguyen, Donna H. Lee, Eric Delpire, and Alicia A. McDonough. Differential regulation of Na^+ transporters along nephron during ANG II-dependent hypertension: distal stimulation counteracted by proximal inhibition. *American Journal of Physiology-Renal Physiology*, 305(4):F510–F519, 2013.

[106] Sarah M Nwia, Xiao Chun Li, Ana Paula de Oliveira Leite, Rumana Hassan, and Jia Long Zhuo. The Na+/H+ exchanger 3 in the intestines and the proximal tubule of the kidney: localization, physiological function, and key roles in angiotensin ii-induced hypertension. *Frontiers in Physiology*, 13:861659, 2022.

[107] Yukino Ogawa, Nobuya Koike, Gen Kurosawa, Tomoyoshi Soga, Masaru Tomita, and Hajime Tei. Positive autoregulation delays the expression phase of mammalian clock gene per2. *PLoS ONE*, 6(4):e18663, 2011.

[108] Akira Onishi, Yiling Fu, Rohit Patel, Manjula Darshi, Maria Crespo-Masip, Winnie Huang, Panai Song, Brent Freeman, Young Chul Kim, Manoocher Soleimani, Kumar Sharma, Scott Culver Thomson, and Volker Vallon. A role for tubular Na^+ /h $^+$ exchanger NHE3 in the natriuretic effect of the SGLT2 inhibitor empagliflozin. *American Journal of Physiology-Renal Physiology*, 319(4):F712–F728, 2020.

[109] Y Ouchi, L Share, J T Crofton, K Iitake, and D P Brooks. Sex difference in the development of deoxycorticosterone-salt hypertension in the rat. *Hypertension*, 9(2):172–177, 1987.

[110] Maricica Pacurari, Ramzi Kafoury, Paul B. Tchounwou, and Kenneth Ndebele. The renin-angiotensin-aldosterone system in vascular inflammation and remodeling. *International Journal of Inflammation*, 2014:1–13, 2014.

[111] Seema Patel, Abdur Rauf, Haroon Khan, and Tareq Abu-Izneid. Renin-angiotensin-aldosterone (RAAS): The ubiquitous system for homeostasis and pathologies. *Biomedicine & Pharmacotherapy*, 94:317–325, 2017.

[112] R Daniel Peluffo and Julio A Hernández. The Na+, K+-ATPase and its stoichiometric ratio: some thermodynamic speculations. *Biophysical Reviews*, 15(4):539–552, 2023.

[113] Yasaman Pirahanchi, Rishita Jessu, and Narothama R Aeddula. Physiology, sodium potassium pump. In *StatPearls [Internet]*. StatPearls Publishing, 2023.

[114] Angel Pizarro, Katharina Hayer, Nicholas F. Lahens, and John B. Hogenesch. CircaDB: a database of mammalian circadian gene expression profiles. *Nucleic Acids Research*, 41:D1009–D1013, 2012.

[115] Martin R Pollak, Susan E Quaggin, Melanie P Hoenig, and Lance D Dworkin. The glomerulus: the sphere of influence. *Clinical Journal of the American Society of Nephrology*, 9(8):1461–1469, 2014.

[116] Richard A. Preston, David Afshartous, Evelyn V. Caizapanta, Barry J. Materson, Rolando Rodco, Eileen Alonso, and Alberto B. Alonso. Thiazide-sensitive NCC (sodium-chloride cotransporter) in human metabolic syndrome: Sodium sensitivity and potassium-induced natriuresis. *Hypertension*, 77(2):447–460, 2021.

[117] L. E. Ramsay, W. W. Yeo, and P. R. Jackson. Thiazide diuretics: first-line therapy for hypertension. *Journal of Hypertension. Supplement: Official Journal of the International Society of Hypertension*, 10(3):S29–32; discussion S32–33, 1992.

[118] Lawrence E. Ramsay. Thiazide diuretics in hypertension. *Clinical and Experimental Hypertension*, 21(5):805–814, 1999.

[119] Anne M. Ramsey, Adam Stowie, Atlantis Hill, Ivory Ellis, Megan K. Rhodes, David M. Pollock, and Alec J. Davidson. Long-term circadian disruption shortens life span and dampens blood pressure diurnal rhythms in stroke-prone spontaneously hypertensive rats. *American Journal of Physiology-Heart and Circulatory Physiology*, 325(1):H106–H112, 2023.

[120] Jane F. Reckelhoff, Huimin Zhang, Kumud Srivastava, L. Jackson Roberts, Jason D. Morrow, and J. Carlos Romero. Subpressor doses of angiotensin II increase plasma f $_2$ -isoprostanes in rats. *Hypertension*, 35(1):476–479, 2000.

[121] A. J. Reyes. Effects of diuretics on renal excretory function. *European Heart Journal*, 13:15–21, 1992.

[122] Jacob Richards, Benjamin Ko, Sean All, Kit-Yan Cheng, Robert S. Hoover, and Michelle L. Gumz. A role for the circadian clock protein per1 in the regulation of the NaCl co-transporter (NCC) and the with-no-lysine kinase (WNK) cascade in mouse distal convoluted tubule cells. *Journal of Biological Chemistry*, 289(17):11791–11806, 2014.

[123] M. Robert, J. O. Roux, F. Bourelly, A. M. Boularan, J. Guiter, and L. Monnier. Circadian variations in the risk of urinary calcium oxalte stone formation. *British Journal of Urology*, 74(3):294–297, 1994.

[124] Esther M. Rodenburg, Bruno H. Stricker, and Linda E. Visser. Sex-related differences in hospital admissions attributed to adverse drug reactions in the netherlands. *British Journal of Clinical Pharmacology*, 71(1):95–104, Jan 2011.

[125] Marije Russcher, Inês Chaves, Karolina Lech, Birgit C. P. Koch, J. Elsbeth Nagtegaal, Kira F. Dorsman, Anke't Jong, Manfred Kayser, H. (Martijn) J. R. Van Faassen, Ido P. Kema, Gijsbertus T. J. Van Der Horst, and Carlo A. J. M. Gaillard. An observational study on disturbed peripheral circadian rhythms in hemodialysis patients. *Chronobiology International*, 32(6):848–857, 2015.

[126] Mohammad Saifur Rohman, Noriaki Emoto, Hidemi Nonaka, Ryusuke Okura, Masataka Nishimura, Kazuhiro Yagita, Gijsbertus T.J. Van Der Horst, Masafumi Matsuo, Hitoshi Okamura, and Mitsuhiro Yokoyama. Circadian clock genes directly regulate expression of the Na+/H+ exchanger NHE3 in the kidney. *Kidney International*, 67(4):1410–1419, 2005.

[127] Kathryn Sandberg and Hong Ji. Sex differences in primary hypertension. *Biology of Sex Differences*, 3(1):7, 2012.

[128] J. M. Sands, H. Nonoguchi, and M. A. Knepper. Vasopressin effects on urea and h2o transport in inner medullary collecting duct subsegments. *American Journal of Physiology-Renal Physiology*, 253(5):F823–F832, 1987.

[129] Ueli Schibler, Ivana Gotic, Camille Saini, Pascal Gos, Thomas Curie, Yann Emmenegger, Flore Sinturel, Pauline Gosselin, Alan Gerber, Fabienne Fleury-Olela, Gianpaolo Rando, Maud Demarque, and Paul Franken. Clock-talk: Interactions between central and peripheral circadian oscillators in mammals. *Cold Spring Harbor Symposia on Quantitative Biology*, 80:223–232, 2015.

[130] John Curtis Seely, Gordon C. Hard, and Brad Blankenship. Chapter 11 - kidney. In Andrew W. Suttie, editor, *Boorman's Pathology of the Rat (Second Edition)*, pages 125–166. Academic Press, 2018.

[131] Yehuda Sharabi, Roy Illan, Yehuda Kamari, Haim Cohen, Moshe Nadler, Franz H. Messerli, and Ehud Grossman. Diuretic induced hyponatraemia in elderly hypertensive women. *Journal of Human Hypertension*, 16(9):631–635, Sep 2002.

[132] David B. Simon, Fiona E. Karet, Jahed M. Hamdan, Antonio Di Pietro, Sami A. Sanjad, and Richard P. Lifton. Bartter's syndrome, hypokalaemic alkalosis with hypercalciuria, is caused by mutations in the Na–K–2CI cotransporter NKCC2. *Nature Genetics*, 13(2):183–188, 1996.

[133] R. K. Singh, A. Bansal, S. K. Bansal, and S. P. Rai. Circadian variations of blood and urinary constituents in renal stone formers. *Progress in Clinical and Biological Research*, 341B:551–557, 1990.

[134] Kristen Solocinski, Jacob Richards, Sean All, Kit-Yan Cheng, Syed J. Khundmiri, and Michelle L. Gumz. Transcriptional regulation of NHE3 and SGLT1 by the circadian clock protein per1 in proximal tubule cells. *American Journal of Physiology-Renal Physiology*, 309(11):F933–F942, 2015.

[135] Roberto M Soriano, Dana Penfold, and Stephen W Leslie. Anatomy, abdomen and pelvis, kidneys. 2018.

[136] Melissa M. Stadt, Stephanie Abo, and Anita T. Layton. Circadian regulation of electrolyte and water transport in the rat kidney. *SIAM Journal on Applied Mathematics*, pages S1–S16, 2022.

[137] Melissa M. Stadt, Stephanie Abo, and Anita T. Layton. Circadian regulation of electrolyte and water transport in the rat kidney. *SIAM Journal on Applied Mathematics*, 84(3):S1–S16, 2024.

[138] Melissa M. Stadt and Anita T. Layton. Adaptive changes in single-nephron GFR, tubular morphology, and transport in a pregnant rat nephron: modeling and analysis. *American Journal of Physiology-Renal Physiology*, 322(2):F121–F137, 2022.

[139] Melissa M. Stadt, Crystal A. West, and Anita T. Layton. Effect of pregnancy and hypertension on kidney function in female rats: Modeling and functional implications. *PLOS ONE*, 18(5):e0279785, 2023.

[140] Matthew Stevenson, Cyrus Mowdawalla, Bokey Wong, Alexander Chu, Louis Ragolia, Volker Vallon, and M.Mahmood Hussain. Clock and bmal1 inhibit expression of sglt1 in mouse kidneys and glucose reabsorption. *Physiology*, 39:1756, 2024.

[141] Lisa R. Stow and Michelle L. Gumz. The circadian clock in the kidney. *Journal of the American Society of Nephrology*, 22(4):598–604, 2011.

[142] Whitney Sussman, Matthew Stevenson, Cyrus Mowdawalla, Samantha Mota, Louis Ragolia, and Xiaoyue Pan. BMAL1 controls glucose uptake through paired-homeodomain transcription factor 4 in differentiated caco-2 cells. *American Journal of Physiology. Cell Physiology*, 317(3):C492–C501, 2019.

[143] Sangita Swapnasrita, Aurélie Carlier, and Anita T. Layton. Sex-specific computational models of kidney function in patients with diabetes. *Frontiers in Physiology*, 13:741121, 2022.

[144] Daiei Takahashi, Takayasu Mori, Naohiro Nomura, Muhammad Zakir Hossain Khan, Yuya Araki, Moko Zeniya, Eisei Sohara, Tatemitsu Rai, Sei Sasaki, and Shinichi Uchida. WNK4 is the major WNK positively regulating NCC in the mouse kidney. *Bioscience Reports*, 34(3):e00107, 2014.

[145] Nobuyuki Takahashi, Daniel R. Chernavvsky, R. Ariel Gomez, Peter Igarashi, Hillel J. Gitelman, and Oliver Smithies. Uncompensated polyuria in a mouse model of bartter's syndrome. *Proceedings of the National Academy of Sciences*, 97(10):5434–5439, 2000.

[146] Tsjitske J. Toering, Anne Marijn Van Der Graaf, Folkert W. Visser, Hendrik Buikema, Gerjan Navis, Marijke M. Faas, and A. Titia Lely. Gender differences in response to acute and chronic angiotensin II infusion: a translational approach. *Physiological Reports*, 3(7):e12434, 2015.

[147] Marco A. Valdez-Flores, Rosa Vargas-Poussou, Sjoerd Verkaart, Omar A. Z. Tutakhel, Angel Valdez-Ortiz, Anne Blanchard, Cyrielle Treard, Joost G. J. Hoenderop, René J. M. Bindels, and Sabina Jeleń. Functionomics of NCC mutations in gitelman syndrome using a novel mammalian cell-based activity assay. *American Journal of Physiology-Renal Physiology*, 311(6):F1159–F1167, 2016.

[148] Rosa Vargas-Poussou, Delphine Feldmann, Martin Vollmer, Martin Konrad, Lisa Kelly, Lambertus PWJ van den Heuvel, Lamia Tebourbi, Matthias Brandis, Lothar Karolyi, Steven C Hebert, et al. Novel molecular variants of the Na-K-2Cl cotransporter gene are responsible for antenatal bartter syndrome. *The American Journal of Human Genetics*, 62(6):1332–1340, 1998.

[149] Luciana C. Veiras, Adriana C.C. Girardi, Joshua Curry, Lei Pei, Donna L. Ralph, An Tran, Regiane C. Castelo-Branco, Nuria Pastor-Soler, Cristina T. Arranz, Alan S.L. Yu, and Alicia A. McDonough. Sexual dimorphic pattern of renal transporters and electrolyte homeostasis. *Journal of the American Society of Nephrology*, 28(12):3504–3517, 2017.

[150] Luciana C Veiras, Brandon E McFarlin, Donna L Ralph, Vadym Buncha, Jessica Prescott, Borna S Shirvani, Jillian C McDonough, Darren Ha, Jorge Giani, Susan B Gurley, et al. Electrolyte and transporter responses to angiotensin ii induced hypertension in female and male rats and mice. *Acta Physiologica*, 229(1):e13448, 2020.

[151] P Verdecchia, G Schillaci, M Guerrieri, C Gatteschi, G Benemio, F Boldrini, and C Porcellati. Circadian blood pressure changes and left ventricular hypertrophy in essential hypertension. *Circulation*, 81(2):528–536, 1990.

[152] Jean-Frédéric Vodoz, Vincent Cottin, Jean-Charles Glérant, Geneviève Derumeaux, Chahéra Khouatra, Anne-Sophie Blanchet, Bénédicte Mastroïanni, Jean-Yves Bayle, Jean-François Mornex, and Jean-François Cordier. Right-to-left shunt with hypoxemia in pulmonary hypertension. *BMC Cardiovascular Disorders*, 9(1):15, 2009.

[153] Bangchen Wang, Donghai Wen, Huaqing Li, Jun Wang-France, and Steven C. Sansom. Net K+ secretion in the thick ascending limb of mice on a low-Na, high-K diet. *Kidney International*, 92(4):864–875, 2017.

[154] Chi-Tarng Wang, L Gabriel Navar, and Kenneth D Mitchell. Proximal tubular fluid angiotensin II levels in angiotensin II-induced hypertensive rats:. *Journal of Hypertension*, 21(2):353–360, 2003.

[155] H Wang, K Ikeda, M Kihara, Y Nara, R Horie, and Y Yamori. Sodium preference and excretion in spontaneously hypertensive rats on various diets. *Clinical and experimental pharmacology and physiology*, 12(2):139–144, 1985.

[156] Ning Wei, Michelle L. Gumz, and Anita T. Layton. Predicted effect of circadian clock modulation of nhe3 of a proximal tubule cell on sodium transport. *American Journal of Physiology-Renal Physiology*, 315(3):F665–F676, September 2018.

[157] Alan M Weinstein. A kinetically defined Na+/H+ antiporter within a mathematical model of the rat proximal tubule. *The Journal of general physiology*, 105(5):617–641, 1995.

[158] Alan M Weinstein, Sheldon Weinbaum, Yi Duan, Zhaopeng Du, QingShang Yan, and Tong Wang. Flow-dependent transport in a mathematical model of rat proximal tubule. *American Journal of Physiology-Renal Physiology*, 292(4):F1164–F1181, 2007.

[159] Crystal A West, Paul A Welling, David A West Jr, Richard A Coleman, Kit-Yan Cheng, Chao Chen, Thomas D DuBose Jr, Jill W Verlander, Chris Baylis, and

Michelle L Gumz. Renal and colonic potassium transporters in the pregnant rat. *American Journal of Physiology-Renal Physiology*, 314(2):F251–F259, 2018.

[160] Caroline N. White, Gemma A. Figtree, Chia-Chi Liu, Alvaro Garcia, Elisha J. Hamilton, Karin K. M. Chia, and Helge H. Rasmussen. Angiotensin II inhibits the Na^+ -k $^+$ pump via PKC-dependent activation of NADPH oxidase. *American Journal of Physiology-Cell Physiology*, 296(4):C693–C700, 2009.

[161] Niels Wiinberg, Asbjørn Høegholm, Hanne R. Christensen, Lia E. Bang, Kim L. Mikkelsen, Poul Ebbe Nielsen, Tage L. Svendsen, Jens P. Kampmann, Niels H. Madsen, and Michael W. Bentzon. 24-h ambulatory blood pressure in 352 normal danish subjects, related to age and gender*. *American Journal of Hypertension*, 8(10):978–986, 1995.

[162] Aurore Woller, Hélène Duez, Bart Staels, and Marc Lefranc. A mathematical model of the liver circadian clock linking feeding and fasting cycles to clock function. *Cell Reports*, 17(4):1087–1097, 2016.

[163] B. Xue, A.K. Johnson, and M. Hay. Sex differences in angiotensin II- induced hypertension. *Brazilian Journal of Medical and Biological Research*, 40(5):727–734, 2007.

[164] Baojian Xue, Alan Kim Johnson, and Meredith Hay. Sex differences in angiotensin II- and aldosterone-induced hypertension: the central protective effects of estrogen. *American Journal of Physiology-Regulatory, Integrative and Comparative Physiology*, 305(5):R459–R463, 2013.

[165] Baojian Xue, Jaya Pamidimukkala, and Meredith Hay. Sex differences in the development of angiotensin II-induced hypertension in conscious mice. *American Journal of Physiology-Heart and Circulatory Physiology*, 288(5):H2177–H2184, 2005.

[166] M. Zhang, Y. Mao, S.H. Ramirez, R.F. Tuma, and T. Chabrashvili. Angiotensin II induced cerebral microvascular inflammation and increased blood–brain barrier permeability via oxidative stress. *Neuroscience*, 171(3):852–858, 2010.

[167] Ray Zhang, Nicholas F. Lahens, Heather I. Ballance, Michael E. Hughes, and John B. Hogenesch. A circadian gene expression atlas in mammals: Implications for biology and medicine. *Proceedings of the National Academy of Sciences*, 111(45):16219–16224, 2014.

[168] Rui-Yu Zhang, Li-Jun Mou, Xue-Mei Li, Xue-Wang Li, and Yan Qin. [temporally relationship between renal local clock system and circadian rhythm of the water electrolyte excretion]. *Zhongguo Yi Xue Ke Xue Yuan Xue Bao. Acta Academiae Medicinae Sinicae*, 37(6):698–704, 2015.

[169] Long Zhao, Guoqi Li, Fanyu Meng, Zhonghua Sun, and Jiayi Liu. Cortical and medullary oxygenation evaluation of kidneys with renal artery stenosis by BOLD-MRI. *PLOS ONE*, 17(3):e0264630, 2022.

[170] Yongxiang Zhao, Heidi Schubert, Alan Blakely, Biff Forbush, Micholas Dean Smith, Jesse Rinehart, and Erhu Cao. Structural bases for Na+-Cl- cotransporter inhibition by thiazide diuretic drugs and activation by kinases. *Nature Communications*, 15(1):7006, 2024.

[171] Kaixin Zheng and Anita T Layton. Predicting sex differences in the effects of diuretics in renal epithelial transport during angiotensin ii-induced hypertension. *American Journal of Physiology-Renal Physiology*, 326(5):F737–F750, 2024.

[172] Jia Long Zhuo, Manoocher Soleimani, and Xiao Chun Li. New insights into the critical importance of intratubular Na+/H+ exchanger 3 and its potential therapeutic implications in hypertension. *Current hypertension reports*, 23(6):34, 2021.

[173] Adrian Zietara, Denisha R Spires, Alexandria Juffre, Hannah M Costello, G Ryan Crislip, Lauren G Douma, Vladislav Levchenko, Lashodya V Dissanayake, Christine A Klemens, Oksana Nikolaienko, et al. Knockout of the circadian clock protein per1 (period1) exacerbates hypertension and increases kidney injury in dahl salt-sensitive rats. *Hypertension*, 79(11):2519–2529, 2022.

Appendix A

Equations and Parameters of Clock Gene and Transporter Expression

A1 Governing Equations Overview

Eq. A1-A21 are 25 governing equations of 12 mRNAs: Per1, Per2, Cry1, Cry2, Rev-Erb, Ror, Bmal1, NHE3, NKCC2, SGLT1,NCC, and ENaC; 7 proteins: PER1, PER2, CRY1, CRY2, REV-ERB, ROR, and BMAL1; and 5 protein complexes: PER1-CRY1, PER2-CRY1, PER1-CRY2, PER2-CRY2, and CLOCK-BMAL1. Because in our formulation all mRNA are regualted by 5 protein complexes in an analogous pattern, we unify the formulation by defining a regulation factor F_X (Eq. A13) where X is the name of mRNA. All parameters are listed with description in Section A4.

A2 mRNA equations

$$\frac{d[\text{Per1}]}{dt} = -\text{dm_Per1} \cdot [\text{Per1}] + \text{V_Per1} \cdot F_{\text{Per1}} \tag{A1}$$

$$\frac{d[\text{Per2}]}{dt} = -\text{dm_Per2} \cdot [\text{Per2}] + \text{V_Per2} \cdot F_{\text{Per2}} \tag{A2}$$

$$\frac{d[\text{Cry1}]}{dt} = -\text{dm_Cry1} \cdot [\text{Cry1}] + \frac{\text{V_Cry1} \cdot F_{\text{Cry1}}}{(1 + (\frac{\text{REV_ERB}}{\text{Ki_Cry1_rev}})^{\text{hill_Cry1_REV}})} \tag{A3}$$

$$\frac{\mathrm{d}[\mathrm{Cry2}]}{\mathrm{dt}} = -\mathrm{dm_Cry2} \cdot [\mathrm{Cry2}] + \frac{\mathrm{V_Cry2} \cdot \mathrm{F_{Cry2}}}{(1 + (\frac{\mathrm{REV_ERB}}{\mathrm{Ki_Cry2_rev}})^{\mathrm{hill_Cry2_REV}})} \tag{A4}$$

$$\frac{\mathrm{d}[\mathrm{Rev\text{-}Erb}]}{\mathrm{dt}} = -\mathrm{dm_rev} \cdot [\mathrm{Rev\text{-}Erb}] + \mathrm{V_Rev} \cdot \mathrm{F_{rev}} \tag{A5}$$

$$\frac{\mathrm{d}[\mathrm{Ror}]}{\mathrm{dt}} = -\mathrm{dm_Ror} \cdot [\mathrm{Ror}] + \mathrm{V_Ror} \cdot \mathrm{F_{Ror}} \tag{A6}$$

$$\frac{\mathrm{d}[\mathrm{Bmal1}]}{\mathrm{dt}} = -\mathrm{dm_Bmal1} \cdot [\mathrm{Bmal1}] + \frac{\mathrm{V_Bmal1} \cdot (1 + \mathrm{fold_Bmal1} \cdot (\frac{[\mathrm{ROR}]}{\mathrm{Ka_Bmal1_Ror}})^{\mathrm{hill_Bmal1_ROR}})}{1 + (\frac{[\mathrm{REV\text{-}ERB}]}{\mathrm{Ki_Bmal1_rev}})^{\mathrm{hill_Bmal1_REV}} + (\frac{[\mathrm{ROR}]}{\mathrm{Ka_Bmal1_Ror}})^{\mathrm{hill_Bmal1_ROR}}} \tag{A7}$$

$$\begin{aligned}\frac{\mathrm{d}[\mathrm{NHE3}]}{\mathrm{dt}} &= -\mathrm{dm_NHE3} \cdot [\mathrm{NHE3}] + \mathrm{V_NHE3} \cdot (1 + \mathrm{fold_NHE3} \cdot (\frac{[\mathrm{CLOCK-BMAL1}]}{\mathrm{Ka_NHE3_cb}})^{\mathrm{hill_NHE3_cb}} \cdot (1 \\ &+ (\frac{[\mathrm{PER1-CRY2}]}{\mathrm{Ka_NHE3_P1C2}})^{\mathrm{hill_NHE3_p1c2}}))/(1 + (\frac{[\mathrm{CLOCK-BMAL1}]}{\mathrm{Ka_NHE3_cb}})^{\mathrm{hill_NHE3_cb}} \cdot (1 + (\frac{[\mathrm{PER1-CRY2}]}{\mathrm{Ka_NHE3_P1C2}})^{\mathrm{hill_NHE3_p1c2}}) \\ &\cdot (1 + (\frac{[\mathrm{PER2_CRY1}]}{\mathrm{Ki_NHE3_p2c1}})^{\mathrm{hill_NHE3_p2c1}}) \cdot (1 + (\frac{[\mathrm{PER2_CRY2}]}{\mathrm{Ki_NHE3_p2c2}})^{\mathrm{hill_NHE3_p2c2}}) \cdot (1 + \frac{[\mathrm{PER1-CRY1}]}{\mathrm{Ki_NHE3_p1c1}} +)^{\mathrm{hill_NHE3_p1c1}})\end{aligned} \tag{A8}$$

$$\frac{\mathrm{d}[\mathrm{NKCC2}]}{\mathrm{dt}} = -\mathrm{dm_NKCC2} \cdot [\mathrm{NKCC2}] + \mathrm{V_NKCC2} \cdot \mathrm{F_{NKCC2}} \tag{A9}$$

$$\begin{aligned}\frac{\mathrm{d}[\mathrm{SGLT1}]}{\mathrm{dt}} =& -\mathrm{dm_SGLT1} \cdot [\mathrm{SGLT1}] \\ &+ \frac{\mathrm{V_SGLT1}(1 + \mathrm{fold_SGLT1} \cdot (\frac{[\mathrm{PER1-CRY1}]}{\mathrm{Ka_SGLT1_p1c1}} + \frac{[\mathrm{PER1-CRY2}]}{\mathrm{Ka_SGLT1_p1c2}})^{\mathrm{hill_NCC_p1c}})}{1 + (\frac{[\mathrm{CLOCK-BMAL1}]}{\mathrm{Ki_SGLT1_cb}})^{\mathrm{hill_SGLT1_cb}} + (\frac{[\mathrm{PER1-CRY1}]}{\mathrm{Ka_SGLT1_p1c1}} + \frac{[\mathrm{PER1-CRY2}]}{\mathrm{Ka_SGLT1_p1c2}})^{\mathrm{hill_NCC_p1c}}}\end{aligned} \tag{A10}$$

$$\begin{aligned}\frac{\mathrm{d}[\mathrm{NCC}]}{\mathrm{dt}} =& -\mathrm{dm_NCC} \cdot [\mathrm{NCC}] \\ &+ \frac{\mathrm{V_NCC}(1 + \mathrm{fold_NCC} \cdot (\frac{[\mathrm{PER1-CRY1}]}{\mathrm{Ka_NCC_p1c1}} + \frac{[\mathrm{PER1-CRY2}]}{\mathrm{Ka_NCC_p1c2}})^{\mathrm{hill_NCC_p1c}})}{1 + (\frac{[\mathrm{CLOCK-BMAL1}]}{\mathrm{Ki_NCC_cb}})^{\mathrm{hill_NCC_cb}} + (\frac{[\mathrm{PER1-CRY1}]}{\mathrm{Ka_NCC_p1c1}} + \frac{[\mathrm{PER1-CRY2}]}{\mathrm{Ka_NCC_p1c2}})^{\mathrm{hill_NCC_p1c}}}\end{aligned} \tag{A11}$$

$$\frac{\mathrm{d}[\mathrm{ENaC}]}{\mathrm{dt}} = -\mathrm{dm_ENaC} \cdot [\mathrm{ENaC}] + \frac{\mathrm{V_ENaC}(1 + \mathrm{fold_ENaC} \cdot (\frac{[\mathrm{CLOCK-BMAL1}]}{\mathrm{Ka_ENaC_cb}})^{\mathrm{hill_ENaC_cb}}(1 + (\frac{[\mathrm{PER1-CRY1}]}{\mathrm{Ka_ENaC_p1c1}} + \frac{[\mathrm{PER1-CRY2}]}{\mathrm{Ka_ENaC_p1c2}})^{\mathrm{hill_ENaC_p1c}})}{1 + (\frac{[\mathrm{CLOCK-BMAL1}]}{\mathrm{Ka_ENaC_cb}})^{\mathrm{hill_ENaC_cb}}(1 + (\frac{[\mathrm{PER1-CRY1}]}{\mathrm{Ka_ENaC_p1c1}} + \frac{[\mathrm{PER1-CRY2}]}{\mathrm{Ka_ENaC_p1c2}})^{\mathrm{hill_ENaC_p1c}})} \tag{A12}$$

$$\begin{aligned} \mathrm{F_X} = (1 + \mathrm{fold_X} \cdot (\frac{[\mathrm{CLOCK_BMAL1}]}{\mathrm{Ka_X_cb}})^{\mathrm{hill_X_cb}}))/(1 + (\frac{[\mathrm{CLOCK_BMAL1}]}{\mathrm{Ka_X_cb}})^{\mathrm{hill_X_cb}} \\ \cdot(1 + (\frac{[\mathrm{PER1_CRY1}]}{\mathrm{Ki_X_p1c1}})^{\mathrm{hill_X_p1c1}}) \cdot (1 + (\frac{[\mathrm{PER1_CRY2}]}{\mathrm{Ki_X_p1c2}})^{\mathrm{hill_X_p1c2}}) \cdot \\ (1 + (\frac{[\mathrm{PER2_CRY1}]}{\mathrm{Ki_X_p2c1}})^{\mathrm{hill_X_p2c1}}) \cdot (1 + (\frac{[\mathrm{PER2_CRY2}]}{\mathrm{Ki_X_p2c2}})^{\mathrm{hill_X_p2c2}})) \end{aligned} \tag{A13}$$

A3 Protein Equations

$$\begin{aligned} \frac{\mathrm{d}[\mathrm{PER1}]}{\mathrm{dt}} = -\mathrm{dp_PER1} \cdot [\mathrm{PER1}] + \mathrm{kp_PER1} \cdot [\mathrm{Per1}] - \mathrm{kass_p1c1} \cdot [\mathrm{PER1}] \cdot [\mathrm{CRY1}] \\ -\mathrm{kass_p1c2} \cdot [\mathrm{PER1}] \cdot [\mathrm{CRY2}] + \mathrm{kdiss_p1c1} \cdot [\mathrm{PER1\text{-}CRY1}] + \mathrm{kdiss_p1c2} \cdot [\mathrm{PER1\text{-}CRY2}] \end{aligned} \tag{A14}$$

$$\begin{aligned} \frac{\mathrm{d}[\mathrm{PER2}]}{\mathrm{dt}} = -\mathrm{dp_PER2} \cdot [\mathrm{PER2}] + \mathrm{kp_PER2} \cdot [\mathrm{Per2}] - \mathrm{kass_p2c1} \cdot [\mathrm{PER2}] \cdot [\mathrm{CRY1}] \\ -\mathrm{kass_p2c2} \cdot [\mathrm{PER2}] \cdot [\mathrm{CRY2}] + \mathrm{kdiss_p2c1} \cdot [\mathrm{PER2\text{-}CRY1}] + \mathrm{kdiss_p2c2} \cdot [\mathrm{PER2\text{-}CRY2}] \end{aligned} \tag{A15}$$

$$\begin{aligned} \frac{\mathrm{d}[\mathrm{CRY1}]}{\mathrm{dt}} = -\mathrm{dp_CRY1} \cdot [\mathrm{CRY1}] + \mathrm{kp_CRY1} \cdot [\mathrm{Cry1}] - \mathrm{kass_p1c1} \cdot [\mathrm{PER1}] \cdot [\mathrm{CRY1}] \\ -\mathrm{kass_p2c1} \cdot [\mathrm{PER2}] \cdot [\mathrm{CRY1}] + \mathrm{kdiss_p1c1} \cdot [\mathrm{PER1\text{-}CRY1}] + \mathrm{kdiss_p2c1} \cdot [\mathrm{PER2\text{-}CRY1}] \end{aligned} \tag{A16}$$

$$\frac{\mathrm{d}[\mathrm{CRY2}]}{\mathrm{dt}} = -\mathrm{dp_CRY2} \cdot [\mathrm{CRY2}] + \mathrm{kp_CRY2} \cdot [\mathrm{Cry2}] - \mathrm{kass_p1c2} \cdot [\mathrm{PER1}] \cdot [\mathrm{CRY2}]$$
$$-\mathrm{kass_p2c2} \cdot [\mathrm{PER2}] \cdot [\mathrm{CRY2}] + \mathrm{kdiss_p1c2} \cdot [\mathrm{PER1\text{-}CRY2}] + \mathrm{kdiss_p2c2} \cdot [\mathrm{PER2\text{-}CRY2}] \tag{A17}$$

$$\frac{\mathrm{d}[\mathrm{PER1\text{-}CRY1}]}{\mathrm{dt}} = \mathrm{kass_p1c1} \cdot [\mathrm{PER1}] \cdot [\mathrm{CRY1}] - \mathrm{kdiss_p1c1} \cdot [\mathrm{PER1\text{-}CRY1}] - \mathrm{d_p1c1} \cdot [\mathrm{PER1\text{-}CRY1}] \tag{A18}$$

$$\frac{\mathrm{d}[\mathrm{PER2\text{-}CRY1}]}{\mathrm{dt}} = \mathrm{kass_p2c1} \cdot [\mathrm{PER2}] \cdot [\mathrm{CRY1}] - \mathrm{kdiss_p2c1} \cdot [\mathrm{PER2\text{-}CRY1}] - \mathrm{d_p2c1} \cdot [\mathrm{PER2\text{-}CRY1}] \tag{A19}$$

$$\frac{\mathrm{d}[\mathrm{PER1\text{-}CRY2}]}{\mathrm{dt}} = \mathrm{kass_p1c2} \cdot [\mathrm{PER1}] \cdot [\mathrm{CRY2}] - \mathrm{kdiss_p1c2} \cdot [\mathrm{PER1\text{-}CRY2}] - \mathrm{d_p1c2} \cdot [\mathrm{PER1\text{-}CRY2}] \tag{A20}$$

$$\frac{\mathrm{d}[\mathrm{PER2\text{-}CRY2}]}{\mathrm{dt}} = \mathrm{kass_p2c2} \cdot [\mathrm{PER2}] \cdot [\mathrm{CRY2}] - \mathrm{kdiss_p2c2} \cdot [\mathrm{PER2\text{-}CRY2}] - \mathrm{d_p2c2} \cdot [\mathrm{PER2\text{-}CRY2}] \tag{A21}$$

$$\frac{\mathrm{d}[\mathrm{REV\text{-}ERB}]}{\mathrm{dt}} = -\mathrm{dp_REV} \cdot [\mathrm{REV\text{-}ERB}] + \mathrm{kp_REV} \cdot [\mathrm{Rev\text{-}Erb}] \tag{A22}$$

$$\frac{\mathrm{d}[\mathrm{ROR}]}{\mathrm{dt}} = -\mathrm{dp_ROR} \cdot [\mathrm{ROR}] + \mathrm{kp_ROR} \cdot [\mathrm{Ror}] \tag{A23}$$

$$\frac{\mathrm{d}[\mathrm{BMAL1}]}{\mathrm{dt}} = -\mathrm{dp_BMAL1} \cdot [\mathrm{BMAL1}] + \mathrm{kp_BMAL1} \cdot [\mathrm{Bmal1}] - \mathrm{kass_cb} \cdot [\mathrm{BMAL1}] \tag{A24}$$

$$+\mathrm{kdiss_cb} \cdot [\mathrm{CLOCK\text{-}BMAL1}] \tag{A25}$$

$$\frac{\mathrm{d}[\mathrm{CLOCK\text{-}BMAL1}]}{\mathrm{dt}} = -\mathrm{d_cb} \cdot [\mathrm{CLOCK\text{-}BMAL1}] + \mathrm{kass_cb} \cdot [\mathrm{BMAL1}] \tag{A26}$$

$$-\mathrm{kdiss_cb} \cdot [\mathrm{CLOCK\text{-}BMAL1}] \tag{A27}$$

A4 Baseline parameters

Table A1: Degradation rates (in hour^{-1}) of protein complexes, mRNAs, and proteins .

Parameter	**Value**	**Description**
d_cb	0.098775151	CLOCK-BMAL1 complex degradation rate
d_p1c1	2.747914868	PER1-CRY1 protein complex degradation rate
d_p1c2	3.857884688	PER1-CRY2 protein complex degradation rate
d_p2c1	1.98150769	PER2-CRY1 protein complex degradation rate
d_p2c2	0.009962143	PER2-CRY2 protein complex degradation rate
dm_Bmal1	10.29999143	Bmal1 mRNA degradation rate
dm_Cry1	1.680357077	Cry1 mRNA degradation rate
dm_Cry2	1.102297307	Cry2 mRNA degradation rate
dm_Per1	0.393284589	Per1 mRNA degradation rate
dm_Per2	0.199538876	Per2 mRNA degradation rate
dm_Rev	0.202152455	Rev mRNA degradation rate
dm_Ror	0.733726737	Ror mRNA degradation rate
dm_NHE3	2.6212974828	NHE3 mRNA degradation rate
dm_NKCC2	0.147706095	NKCC2 mRNA degradation rate
dm_SGLT1	0.9719928901	SGLT1 mRNA degradation rate
dm_NCC	0.11428499820	NCC mRNA degradation rate
dm_ENaC	1.4666546516	ENaC mRNA degradation rate
dp_BMAL1	0.1223564	BMAL1 protein degradation rate
dp_CRY1	0.07170199	CRY1 protein degradation rate
dp_CRY2	0.063886143	CRY2 protein degradation rate
dp_PER1	2.118148503	PER1 protein degradation rate
dp_PER2	1.092137167	PER2 protein degradation rate
dp_REV	1.54249893	REV-ERB protein degradation rate
dp_ROR	0.110251246	ROR protein degradation rate

Table A2: Activation ratios (dimensionless).

Parameter	Value	Description
fold_Bmal1	29.23079974	Activation ratio of Bmal1 by ROR
fold_Cry1	17.45987491	Activation ratio of Cry1 by CLOCK-BMAL1
fold_Cry2	13.21473162	Activation ratio of Cry2 by CLOCK-BMAL1
fold_Per1	2.431717595	Activation ratio of Per1 by CLOCK-BMAL1
fold_Per2	3.308354134	Activation ratio of Per2 by CLOCK-BMAL1
fold_Rev	118.5947203	Activation ratio of Rev by CLOCK-BMAL1
fold_Ror	5.603448203	Activation ratio of Ror by CLOCK-BMAL1
fold_NHE3	5.63209402975596	Activation ratio of NHE3 by CLOCK-BMAL1 and PER1-CRY2
fold_NKCC2	0.385311524	Activation ratio of NKCC2 by CLOCK-BMAL1
fold_SGLT1	2.36457412221910	Activation ratio of SGLT1 by CLOCK-BMAL1
fold_NCC	1.026401864136	Activation ratio of NCC by PER1-CRY1 and PER1-CRY2
fold_ENaC	6.2735611435	Activation ratio of ENaC by CLOCK-BMAL1

Table A3: Hill coefficients (dimensionless).

Parameter	Value	Description
hill_Bmal1_REV	6.315290784	Hill coefficient regulation of Bmal1 by REV-ERB
hill_Bmal1_ROR	10.19219221	Hill coefficient regulation of Bmal1 by ROR
hill_Cry1_cb	4.565210968	Hill coefficient regulation of Cry1 by CLOCK-BMAL1
hill_Cry1_p1c1	1.768766266	Hill coefficient regulation of Cry1 by PER1-CRY1
hill_Cry1_p1c2	1.438000996	Hill coefficient regulation of Cry1 by PER1-CRY2
hill_Cry1_p2c1	1.589908884	Hill coefficient regulation of Cry1 by PER2-CRY1
hill_Cry1_p2c2	1.830362004	Hill coefficient regulation of Cry1 by PER2-CRY2
hill_Cry1_Rev	4.820086463	Hill coefficient regulation of Cry1 by REV-ERB
hill_Cry2_cb	1.367823416	Hill coefficient regulation of Cry2 by CLOCK-BMAL1
hill_Cry2_p1c1	2.1098479	Hill coefficient regulation of Cry2 by PER1-CRY1
hill_Cry2_p1c2	2.026033401	Hill coefficient regulation of Cry2 by PER1-CRY2
hill_Cry2_p2c1	1.602187775	Hill coefficient regulation of Cry2 by PER2-CRY1
hill_Cry2_p2c2	1.655287085	Hill coefficient regulation of Cry2 by PER2-CRY2
hill_Cry2_rev	1.032736435	Hill coefficient regulation of Cry2 by REV-ERB
hill_Per1_cb	4.096754782	Hill coefficient regulation of Per1 by CLOCK-BMAL1
hill_Per1_p1c1	4.137208965	Hill coefficient regulation of Per1 by PER1-CRY1
hill_Per1_p1c2	4.352895626	Hill coefficient regulation of Per1 by PER1-CRY2
hill_Per1_p2c1	4.556232531	Hill coefficient regulation of Per1 by PER2-CRY1
hill_Per1_p2c2	3.006414519	Hill coefficient regulation of Per1 by PER2-CRY2
hill_Per2_cb	5.973526978	Hill coefficient regulation of Per2 by CLOCK-BMAL1
hill_Per2_p1c1	4.917946201	Hill coefficient regulation of Per2 by PER1-CRY1
hill_Per2_p1c2	4.094774755	Hill coefficient regulation of Per2 by PER1-CRY2
hill_Per2_p2c1	4.287994314	Hill coefficient regulation of Per2 by PER2-CRY1
hill_Per2_p2c2	5.627510726	Hill coefficient regulation of Per2 by PER2-CRY2
hill_Rev_cb	13.59046465	Hill coefficient regulation of Rev-Erb by CLOCK-BMAL1
hill_Rev_p1c1	4.593824878	Hill coefficient regulation of Rev-Erb by PER1-CRY1
hill_Rev_p1c2	4.473939935	Hill coefficient regulation of Rev-Erb by PER1-CRY2
hill_Rev_p2c1	4.502871061	Hill coefficient regulation of Rev-Erb by PER2-CRY1
hill_Rev_p2c2	4.474437607	Hill coefficient regulation of Rev-Erb by PER2-CRY2
hill_Ror_cb	11.23225359	Hill coefficient regulation of Ror by CLOCK-BMAL1
hill_Ror_p1c1	3.346138809	Hill coefficient regulation of Ror by PER1-CRY1
hill_Ror_p1c2	4.279505041	Hill coefficient regulation of Ror by PER1-CRY2
hill_Ror_p2c1	3.213895403	Hill coefficient regulation of Ror by PER2-CRY1
hill_Ror_p2c2	4.047251298	Hill coefficient regulation of Ror by PER2-CRY2
hill_NHE3_cb	2.2098682284	Hill coefficient regulation of NHE3 by CLOCK-BMAL1
hill_NHE3_p1c1	4.0457153929	Hill coefficient regulation of NHE3 by PER1-CRY1
hill_NHE3_p1c2	5.8872697770	Hill coefficient regulation of NHE3 by PER1-CRY2
hill_NHE3_p2c1	5.1885742129	Hill coefficient regulation of NHE3 by PER2-CRY1
hill_NHE3_p2c2	1.7481499102	Hill coefficient regulation of NHE3 by PER2-CRY2
hill_NKCC2_cb	21.63335325	Hill coefficient regulation of NKCC2 by CLOCK-BMAL1
hill_NKCC2_p1c1	10.57552098	Hill coefficient regulation of NKCC2 by PER1-CRY1
hill_NKCC2_p1c2	11.3012353	Hill coefficient regulation of NKCC2 by PER1-CRY2
hill_NKCC2_p2c1	11.0258738	Hill coefficient regulation of NKCC2 by PER2-CRY1
hill_NKCC2_p2c2	15.74026414	Hill coefficient regulation of NKCC2 by PER2-CRY2
hill_SGLT1_cb	1.8701185743	Hill coefficient regulation of SGLT1 by CLOCK-BMAL1
hill_SGLT1_p1c	5.86981584935250	Hill coefficient regulation of SGLT1 by PER1-CRY1 and PER1-CRY2
hill_NCC_cb	2.1869392091	Hill coefficient regulation of NCC by CLOCK-BMAL1
hill_NCC_p1c	4.8511288196	Hill coefficient regulation of NCC by PER1-CRY1 and PER1-CRY2
hill_ENaC_cb	6.4999347889	Hill coefficient regulation of ENaC by CLOCK-BMAL1
hill_ENaC_p1c	10.4928793515923	Hill coefficient regulation of ENaC by PER1-CRY1 and PER1-CRY2

Table A4: Regulation thresholds (dimensionless).

Parameter	Value	Description
Ka_Bmal1_ror	0.788134198	Regulation threshold of Bmal1 by ROR
Ka_Cry1_cb	2.965895772	Regulation threshold of Cry1 by CLOCK-BMAL1
Ka_Cry2_cb	9.818058078	Regulation threshold of Cry2 by CLOCK-BMAL1
Ka_Per1_cb	3.045974034	Regulation threshold of Per1 by CLOCK-BMAL1
Ka_Per2_cb	0.996030215	Regulation threshold of Per2 by CLOCK-BMAL1
Ka_Rev_cb	2.407381652	Regulation threshold of Rev-Erb by CLOCK-BMAL1
Ka_Ror_cb	2.531369156	Regulation threshold of Ror by CLOCK-BMAL1
Ka_NHE3_cb	3.0427238397	Regulation threshold of NHE3 by CLOCK-BMAL1
Ka_NKCC2_cb	1.238599283	Regulation threshold of NKCC2 by CLOCK-BMAL1
Ki_SGLT1_cb	5.414004356	Regulation threshold of SGLT1 by CLOCK-BMAL1
Ki_NCC_cb	0.5108645898	Regulation threshold of NCC by CLOCK-BMAL1
Ka_ENaC_cb	3.2433974568	Regulation threshold of ENaC by CLOCK-BMAL1
Ki_Bmal1_rev	0.000960248	Regulation threshold of Bmal1 by REV-ERB
Ki_Cry1_p1c1	2.559548048	Regulation threshold of Cry1 by PER1-CRY1
Ki_Cry1_p1c2	2.536630442	Regulation threshold of Cry1 by PER1-CRY2
Ki_Cry1_p2c1	2.455448644	Regulation threshold of Cry1 by PER2-CRY1
Ki_Cry1_p2c2	3.054560489	Regulation threshold of Cry1 by PER2-CRY2
Ki_Cry1_rev	3.597110237	Regulation threshold of Cry1 by REV-ERB
Ki_Cry2_p1c1	2.852145929	Regulation threshold of Cry2 by PER1-CRY1
Ki_Cry2_p1c2	3.094816119	Regulation threshold of Cry2 by PER1-CRY2
Ki_Cry2_p2c1	2.709023574	Regulation threshold of Cry2 by PER2-CRY1
Ki_Cry2_p2c2	2.309457939	Regulation threshold of Cry2 by PER2-CRY2
Ki_Cry2_rev	0.378297016	Regulation threshold of Cry2 by REV-ERB
Ki_Per1_p1c1	1.010242998	Regulation threshold of Per1 by PER1-CRY1
Ki_Per1_p1c2	1.721720548	Regulation threshold of Per1 by PER1-CRY2
Ki_Per1_p2c1	1.624880971	Regulation threshold of Per1 by PER2-CRY1
Ki_Per1_p2c2	0.368879768	Regulation threshold of Per1 by PER2-CRY2
Ki_Per2_p1c1	1.063344333	Regulation threshold of Per2 by PER1-CRY1
Ki_Per2_p1c2	0.568083313	Regulation threshold of Per2 by PER1-CRY2
Ki_Per2_p2c1	0.86599114	Regulation threshold of Per2 by PER2-CRY1
Ki_Per2_p2c2	0.467627765	Regulation threshold of Per2 by PER2-CRY2
Ki_Rev_p1c1	84.46016203	Regulation threshold of Rev-Erb by PER1-CRY1
Ki_Rev_p1c2	83.99580669	Regulation threshold of Rev-Erb by PER1-CRY2
Ki_Rev_p2c1	84.00271945	Regulation threshold of Rev-Erb by PER2-CRY1
Ki_Rev_p2c2	83.99582755	Regulation threshold of Rev-Erb by PER2-CRY2
Ki_Ror_p1c1	1.094009455	Regulation threshold of Ror by PER1-CRY1
Ki_Ror_p1c2	2.291802041	Regulation threshold of Ror by PER1-CRY2
Ki_Ror_p2c1	0.17734771	Regulation threshold of Ror by PER2-CRY1
Ki_Ror_p2c2	3.087808611	Regulation threshold of Ror by PER2-CRY2
Ki_NHE3_p1c1	0.5248622142	Regulation threshold of NHE3 by PER1-CRY1
Ka_NHE3_p1c2	0.51148790424	Regulation threshold of NHE3 by PER1-CRY2
Ki_NHE3_p2c1	0.04273092406	Regulation threshold of NHE3 by PER2-CRY1
Ki_NHE3_p2c2	0.50842406780	Regulation threshold of NHE3 by PER2-CRY2
Ki_NKCC2_p1c1	7.111624431	Regulation threshold of NKCC2 by PER1-CRY1
Ki_NKCC2_p1c2	6.374145136	Regulation threshold of NKCC2 by PER1-CRY2
Ki_NKCC2_p2c1	6.328221462	Regulation threshold of NKCC2 by PER2-CRY1
Ki_NKCC2_p2c2	0.944237431	Regulation threshold of NKCC2 by PER2-CRY2
Ka_SGLT1_p1c1	5.579866217	Regulation threshold of SGLT1 by PER1-CRY1
Ka_SGLT1_p1c2	0.3368079674	Regulation threshold of SGLT1 by PER1-CRY2
Ka_NCC_p1c1	0.61559096740	Regulation threshold of NCC by PER1-CRY1
Ka_NCC_p1c2	0.17552314947	Regulation threshold of NCC by PER1-CRY2
Ka_ENaC_p1c1	1.0303132234	Regulation threshold of ENaC by PER1-CRY1
Ka_ENaC_p1c2	0.22547393780	Regulation threshold of ENaC by PER1-CRY2

Table A5: Association and dissociation rates (in hour^{-1}) for the protein complexes.

Parameter	Value	Description
kass_cb	0.008965832	CLOCK-BMAL1 association rate
kass_p1c1	0.614435343	PER1-CRY1 association rate
kass_p1c2	3.17074452	PER1-CRY2 association rate
kass_p2c1	0.011242223	PER2-CRY1 association rate
kass_p2c2	0.323930911	PER2-CRY2 association rate
kdiss_cb	0.000499612	CLOCK-BMAL1 dissociation rate
kdiss_p1c1	1.079660064	PER1-CRY1 dissociation rate
kdiss_p1c2	0.016210814	PER1-CRY2 dissociation rate
kdiss_p2c1	1.493335258	PER2-CRY1 dissociation rate
kdiss_p2c2	0.146751896	PER2-CRY2 dissociation rate

Table A6: Translation rates (in hour^{-1}).

Parameter	Value	Description
kp_BMAL1	3.271143875	Bmal1 translation rate
kp_CRY1	0.738295688	Cry1 translation rate
kp_CRY2	0.829860113	Cry2 translation rate
kp_PER1	3.798692975	Per1 translation rate
kp_PER2	1.980575626	Per2 translation rate
kp_REV	0.206633966	Rev-Erb translation rate
kp_ROR	1.875730412	Ror translation rate

Table A7: Maximal transcription rates (in hour^{-1}).

Parameter	Value	Description
V_Bmal1	0.646614483	Bmal1 maximal transcription rates
V_Cry1	0.401023403	Cry1 maximal transcription rates
V_Cry2	0.65185826	Cry2 maximal transcription rates
V_Per1	1.109303016	Per1 maximal transcription rates
V_Per2	1.671549554	Per2 maximal transcription rates
V_Rev	0.006423385	Rev-Erb maximal transcription rates
V_Ror	0.373099089	Ror maximal transcription rates
V_NHE3	2.0096808453	NHE3 maximal transcription rates
V_NKCC2	0.521355199	NKCC2 maximal transcription rates
V_SGLT1	1.0020169907	SGLT1 maximal transcription rates
V_NCC	0.36248470731	NCC maximal transcription rates
V_ENaC	0.52277652371	ENaC maximal transcription rates